Computational Studies in Actinide Chemistry

Infante, I.A.C.

2006

VRIJE UNIVERSITEIT

Computational Studies in Actinide Chemistry

ACADEMISCH PROEFSCHRIFT

ter verkrijging van de graad Doctor aan
de Vrije Universiteit Amsterdam,
op gezag van de rector magnificus
prof.dr. L. M. Bouter,
in het openbaar te verdedigen
ten overstaan van de promotiecommissie
van de faculteit der Exacte Wetenschappen
op dinsdag 3 oktober 2006 om 13.45 uur
in het auditorium van de universiteit,
De Boelelaan 1105

door

Ivan Antonio Carlo Infante

geboren te Clusone, Italië

promotor: prof.dr. E.J. Baerends
copromotor: dr. L. Visscher

CONTENTS

CHAPTER 1

Relativistic Quantum Chemistry

If I understand Dirac correctly, his meaning is this: there is no God, and Dirac is his Prophet.

Wolfgang Pauli

1.1 Introduction

In the phenomena that occur in everyday life we intuitively apply a series of notions which are at the base of the Newtonian physics. When, for example, we cross a street and the traffic light is on red, we can quickly estimate the speed of the car that is coming on our direction, provided that does not suddenly accelerate. If the measured time to reach our position is long enough, then we can safely cross the road. Our guess is based on a certain description of the dynamics of the car that turns out to be the same for us and for the car's driver. The laws that describe this motion are said to be invariant under a Galilei transformation over all the inertial frames. The theory that explains the movement of these macroscopic objects is known as *classical mechanics*.

Macroscopic objects can be pushed to move at very high speed, and if their velocities come close to the speed of light, then classical mechanics is no longer capable of

predicting their trajectories. Einstein developed a new theory where space and time are not two distinct entities, like we intuitively expect, but are closely linked. The equations of motion in this new domain are not invariant under a Galilei transformation, but under a Lorentz transformation. We can explain what happens to these very fast objects making paradoxical examples. One of these is the well known twins paradox, in which one of two brothers is an astronaut who travels on a spaceship at speed of light and the other, less adventurous brother, prefers to live in a slow moving object, i.e. the earth. At the end of his trip, the first brother is younger than his brother, because of the phenomenon of time contraction [1]. A fast-moving person ages more slowly due to the relation that connects the coordinates of two different frames: $t' = \frac{t-(xv/c^2)}{\sqrt{1-v^2/c^2}}$ (in the approximation we move along the x axis). The dynamics that explains the behavior of fast moving objects is called the *special theory of relativity*.

At microscopic scale, it is more difficult to predict trajectories because of the dual wave-particle nature that each object intrinsically possesses. The Heisenberg principle teaches us that speed and position cannot be known exactly at the same time, the more accurately one is measured, the bigger is the uncertainty on the measurement of the other. The equations of motion of microscopic objects can be deduced from the Schrödinger equation and the theory that explains their behavior is called *quantum mechanics*. In the last forty years, the evolution of computer power has helped in finding an approximate solution to the Schrödinger equation for microscopic systems of increasing complexity. In particular, the movement of electrons can be decoupled from the much slower nuclei (Born-Oppenheimer approximation), in order to predict the properties of molecular systems, by looking, for example, at their atomic vibrations, at the electronic energy levels, or at the features of the valence electrons. In the beginning, it was important to assess the validity of the quantum mechanical formulae in order to interpret or match experimental data. Currently, quantum chemistry has achieved a degree of precision so high that it can be used as a powerful tool to predict the behavior of a chemical system, and anticipate the outcome of an experiment, which is the ultimate goal.

A very small object can also move at velocities close to the speed of light. For example, an electron moving in the vicinity of a "heavy" nucleus can increase its speed so much that its mass can change significantly and the volume (orbital) in which it moves deforms. This can affect certain properties of a system. It has been shown that very precise calculations on the H_2 molecule demand a relativistic description.

[1] The twins paradox is more complicated than it looks. For simplicity, we considered the "standard" explanation, in which we suppose that the spaceship motion is not accelerated.

The combination of quantum mechanics and the special theory of relativity is known as *relativistic quantum mechanics*. Usually, the relativistic contribution is observed for elements with high atomic number, because its magnitude increases as Z^2. For heavier elements the radial distribution of the s and p orbitals shows a contraction and the d and f orbitals are more diffuse. Furthermore, at these velocities, the orbital angular momentum l and the spin momentum s cannot be separated, but are coupled into a single quantity, the total angular momentum $j = l + s$. Under the influence of this coupling, the energy levels of an electron in an atom depend on the main quantum number n *and* the total angular momentum j.

In many ordinary cases relativity does not manifest itself to a great extent and can be safely neglected (especially for light atoms), but in other situations relativistic corrections must be included for a satisfactory description of a system.

Ionization potentials, electron affinities, bond lengths, activation energies can all be described in the relativistic framework depending on the desired accuracy. There are many situations in which relativistic effects play a major role, and in this thesis I want to focus on two different cases: the spectroscopy of small molecules containing an actinide element and the analysis of the interaction between a solute molecule - which includes an heavy element - and a solvent.

1.2 The spectroscopy of small molecules

Actinide molecules contain one (or more) heavy atoms, with atomic number ranging from 90 to 103. The spectroscopy of these molecules remains a challenge for computational chemists because the manifold of accessible states is so dense, that an accurate description can be achieved only by describing on equal footing both the dominant relativistic effects and the electron correlation. Nowadays, relativity can be taken into account at a very high accuracy by solving the 4-component Dirac equation or by using a pseudo-relativistic one-component (scalar) or two-component (spin-orbit) equation. The reliability of molecular property calculations, depends, thus, on the description of the electron correlation. The correlation energy is defined as the difference between the exact energy of the system and the Hartree-Fock energy, in which the electron-electron interaction is included in a mean-field approximation (MFA). Correlation energy is divided into dynamic correlation, generated from the mutual repulsion of electrons as deviation from the MFA, and non-dynamic correlation, arising from the inadequacy of a single reference determinant to describe a molecular state.

Till this moment, the most widely used approach that accurately describes these

two contributions has proven to be CASSCF/CASPT2. The reliability of this method, however, is limited by the heavy computational costs that are requested when active spaces including more than 20 orbitals are chosen. It is thus necessary to explore new methods that remove this bottleneck by keeping the same or even increasing the level of precision in the calculation.

In the last ten years a new method is emerging in atomic physics as the most powerful tool to evaluate with very high precision the excited spectrum of atomic systems: the multi-reference Fock-Space Coupled Cluster method (FSCC) [1]. The attraction for this method is multiple: 1) it is a Coupled Cluster wave function model, which is considered the most accurate way to compute dynamic correlation energy; 2) it describes on the same ground the non-dynamic correlation energy; 3) it scales like N^6 (in case of CCSD), that is a relatively cheap scaling factor for a post Hartree Fock method. The drawback is that FSCC suffers of convergence problems for the presence of intruder states. To overcome this problem, the novel Intermediate Hamiltonian FSCC (IHFSCC), a variant of the FSCC method, has been recently developed. Despite being very promising tools, a significant disadvantage of FSCC and IHFSCC is that until this day only few results are available for molecular systems.

In this thesis, one of the goals is to test the validity of single reference and multi-reference Coupled Cluster methods by analyzing actinide systems of different complexity. The choice has fallen on linear triatomic molecules as start, because they are small systems with high symmetry. In particular, the UO_2 and CUO molecules have been selected. The infrared spectrum of these systems in argon matrix shows low energies that were assigned to the U-O asymmetric stretch (and C-U stretch in the case of CUO). In neon matrix, the same asymmetric stretch lies at much higher value, shifted of about 130 cm^{-1}. The experimentalists [2], puzzled by this behavior, suggested a change on the ground state of the trapped molecule, thus implying an interaction of the actinide molecule with the noble gases. This would be unexpected as the noble gases are known to have a very small reactivity. These two molecules have been object of experimental and theoretical debate for years and an indisputable interpretation of their behavior has not been found until today. This thesis aims to provide an explanation using novel advanced computational models.

1.3 The treatment of nuclear waste

The chemistry of the actinides is attractive mainly because it is used in the production of energy by controlled nuclear fission chain reactions. The process from the extraction

to the preparation of the enriched fissile element used in a nuclear reactor is called the *nuclear fuel cycle* [3]. There are different nuclear cycles, one for each actinide used as a fission element for the production of energy. I will focus on the uranium fuel nuclear cycle, because of the uranium abundance in nature.

In the first step, U^{235} is extracted as uranium ore, consisting of about 0.3% of uranium oxide U_3O_8. In the refining step, the uranium ore is processed and the uranium oxide separated in the form of a white-yellow powder, called "yellowcake". In the conversion step, the U_3O_8 is transformed into uranium hexafluoride, UF_6, which is the form commonly used to enrich uranium to U^{236}. The radioactive decay of the uranium is accelerated in a controlled chain reaction and yields heat which is used to boil water and produce steam. The steam is employed in a turbine to generate electricity [4]. Nowadays, nuclear energy sustains about 7% of the total consumed energy in the world, and about 17% of the total electricity. Besides these positive aspects, nuclear power is still seen with skepticism because of the drawbacks of treating the nuclear waste and the possibility of nuclear weapons proliferation. Since the latter problem is well beyond the scope of this thesis - we leave it in the capable hands of our politicians, hoping they know what they are doing -, I can shift our attention to the former obstacle.

During the production of nuclear energy, some of the spent fuel is not used but finishes as nuclear waste, which is a mixture of uranium, plutonium, minor actinides, lanthanides and other transition metals used during the nuclear fuel cycle. The goal is to reprocess the spent fuel to separate the fission products from the other secondary elements, and then use them again to produce nuclear energy. There are several ways to carry out these separations: Plutonium URanium EXtraction process (PUREX) [5], in which uranium and plutonium are selectively extracted from the aqueous solution into an organic phase using tri-butyl phospate (TBP); TRans Uranic Extraction (TRUEX) [6] which is used to remove the minor actinides, Am and Cm, from the nuclear waste; DIAMide EXtraction (DIAMEX) [7], which is similar to the TRUEX process, but uses the malondiamide as extractant agent; Selective ActiNide EXtraction (SANEX) [8], which is used after TRUEX or DIAMEX to separate minor actinides from the very similar lanthanides.

From these processes we can identify some common characteristics. The separation is always carried out in aqueous solution and comes from the interaction of an organic extractant agent, like TBP or malonamide, with one of the actinides, which has more affinity than the others with the the organic compound. Moreover, the water molecules are not simply spectators, but can enhance or lower the selectivity

by acting as co-ligands, and the acidity conditions of the solution also can contribute to the separation. These circumstances make understanding the process of separation very complicated. For example, to this day, the mechanism with which TBP extracts uranium and plutonium is not known. A theoretical analysis of these processes can give some insights in the chemistry involved in these separations, suggesting the possible extractants in advance, because handling of radioactive materials is delicate and dangerous.

Unfortunately, relativistic quantum chemistry is still at an early stage of development and before achieving such an ambitious objective, a lot of research must be done. At the moment, there are few applications to study the interaction of water with molecules containing an actinide atom. The main works are focused on the uranyl cation UO_2^{2+} [9–11], which is the form in which uranium is extracted in the PUREX process. The choice of this molecule is motivated by the fact that it has a closed-shell configuration, making it computationally relatively easy. The coordination of the uranyl in water has been studied using wavefunction based and DFT approaches, that focus on a coordination in the first shell of five water molecules, all of which are placed in the equatorial plane. Nonetheless, these approaches have some drawbacks. The static methods have the advantage of using many explicit water molecules, but the time-dependent behavior, which is critical in studying the reaction on the interface liquid-solvent in the separation process, is lost. The Car-Parrinello molecular dynamics (CPMD) approaches, on the other hand, have the advantage of simulating the movement of water molecules over time, but the maximum box size allowed needed for the CPMD simulations is too small to describe the correct behavior of the water. QM/MM based MD methods may help, but at the moment none of the computer programs available to us support this.

Although an accurate description of the mechanism of separation that is behind the nuclear waste reprocessing is out of reach at this time, we can test the reliability of some theoretical approaches by studying the properties of some actinide compounds in water solution. One of these methods is the mixed QM/MM scheme, in which one part of the system is treated quantum mechanically (QM), and the other with molecular mechanics (MM). This method has not been used much for studying actinide systems, and the idea here is to check its validity by studying the structure and the coordination number of molecules for which experimental data are available, like the Extended X-ray Absorption Fine Structure (EXAFS). EXAFS is an experimental technique in solution that can ascertain with fair accuracy the coordination number and bond lengths of molecules with an heavy atom.

The coordination number has always been a difficult property to analyze theoretically, because it strongly depends on the more flexible outer shells of water molecules. The goal in this thesis is to see whether the QM/MM method is capable of describing the structure of the first-shell and its coordination, but also to analyze the short-range effects between the solute and the surrounding water. To study these characteristics, two systems have been chosen: the tetrafluorouranylate $UO_2F_4^{2-}$ and the terahydroxouranylate, $UO_2(OH)_4^{2-}$. The former has a coordination number of seven, with one water molecule pushed into the first shell by the surrounding water, which represents a good benchmark for testing the method; the second molecule seems to have a coordination of six, but the EXAFS experiment is not completely clear for this molecule, giving an uncertainty of ± 1. My purpose is to see whether the QM/MM scheme produces trustworthy results for theses two systems.

1.4 This thesis

This thesis is divided into two parts: the first deals with very accurate calculations of the excitation energies of small actinide molecules using a multi-reference Coupled Cluster approach; the second deals with a qualitative understanding of the interaction between a solute, which includes an actinide atom, and the solvent using Density Functional Theory (DFT) methods.

In Chapter 2, an overview of the theory and methods used in this thesis is provided. Two important contributions are outlined: the relativistic corrections and the electron correlation. The former is described using relativistic quantum theory beginning with the origin of the 4-component Dirac equation and ending with the solution of many electron systems. The electron correlation is treated in general, but with particular stress placed on the novel Fock-Space Coupled Cluster method. Details on how this approach is used in practical calculations are also given.

Chapters from 3 to 5 are devoted to the study of the spectroscopy of small actinide molecules. In Chapter 3, the CUO molecule is analyzed using single-reference Coupled Cluster with singles and doubles excitations, CCSD, and the perturbative inclusion of the triples, CCSD(T). A first attempt at using the Fock-Space method is carried out, but only with very small P model spaces. Chapter 4 is dedicated to the analysis of the excitation spectrum of the UO_2 molecule. The Intermediate Hamiltonian Fock-Space Coupled Cluster (IHFSCC) is used extensively. A deep analysis of the composition of the excited states is carried out, and a new interpretation of the experimental data has been given. In Chapter 5, the excitation energies of the NpO_2^+ and PuO_2^{2+} ions,

isoelectronic with the UO_2, are computed using IHFSCC. A comparison with previous calculated data and with available experimental spectra is also performed.

Chapter 6 and 7 are devoted to the study of the effect of explicit water molecules on the coordination and on the electronic structure of two actinide molecules. Chapter 6 is based on the computation of uranyl tetrafluorouranylate coordination number. Chapter 7 is dedicated to the analysis of the tetrahydroxouranylate compound, which is more challenging due to the presence of the hydroxyl groups that give rise to several more configurations in the first shell.

CHAPTER 2

Theory and Methodology

Bobby: Two hundred and ninety nine million, seven hundred and ninety two thousand, four hundred and fifty eight metres per second! This is the original measurement for the speed of light.
Lucas: And you know that?
Bobby: It's the basic principal of physics
Lucas: Along with "shit happens"?

from the movie Mindhunters (2004)

2.1 The origin of the Dirac equation

In this thesis, the focus is on light particles (electrons) moving in the field of *heavy* nuclei. A correct description of these systems should be based on relativistic quantum chemistry, which introduces in a natural way the spin of the electrons, and takes into account the effects that occur when particles move at velocities close to the speed of light.

This theory is based on the Dirac equation, which combines together quantum mechanics and the principles of the special relativity. The Dirac equation is invariant under Lorentz transformations [12], which arise from the following two postulates,

1. Physical laws are the same in all inertial frames

2. The speed of light c is the same in all inertial frames .

In deriving this equation, one must start with the idea of preserving the relativistic equivalence between space and time coordinates. The Schrödinger equation [13] does not conform to this requirement because it is first order in time derivatives and second order in space derivatives. To find an expression that is invariant under Lorentz transformation, it is possible to start from the classical relativistic energy of a free-particle

$$E = \sqrt{p^2c^2 + m^2c^4} \tag{2.1}$$

Quantization of equation (2.1) is done by performing the following operator substitution

$$\widehat{E} = ih\frac{\partial}{\partial t}, \quad \widehat{\mathbf{p}} = \frac{\hbar}{i}\nabla \tag{2.2}$$

In this domain, space and time coordinate do not appear symmetrically, thus to solve this problem, Klein and Gordon [14, 14–16] proposed to square equation (2.1), and then to employ the operator substitution in (2.2),

$$\left(\nabla^2 - \frac{1}{c^2}\frac{\partial^2}{\partial t^2} - \frac{m^2c^2}{\hbar}\right)\psi(\boldsymbol{r}, t) = 0 \tag{2.3}$$

In this formula the second derivative with respect to the time appears, which means that the probability to find a particle somewhere in the space is time-dependent. Furthermore, this equation does not account for spin and can not be used to describe the motion of an electron.

Dirac argued that it is necessary for the time coordinate to appear as a first derivative, and, in order to preserve this condition, the space coordinate should appear as first derivative as well. The equation that Dirac proposed has the following form, which results in one of the forms of the Dirac equation [17–19]

$$i\hbar\frac{\partial}{\partial t}\psi(\mathbf{r}, t) = (c\tilde{\boldsymbol{\alpha}} \cdot \widehat{\boldsymbol{p}} + \tilde{\beta}mc^2)\psi(\mathbf{r}, t) \tag{2.4}$$

To maintain space and time on the same order α and β have to be respectively a vector and a scalar. Under this condition, the following properties have to be satisfied

$$\alpha_x^2 = \alpha_y^2 = \alpha_z^2 = \beta^2 = 1 \tag{2.5}$$

$$\boldsymbol{\alpha}\beta + \beta\boldsymbol{\alpha} = 0 \tag{2.6}$$

$$\alpha_x\alpha_y + \alpha_y\alpha_x = \alpha_y\alpha_z + \alpha_z\alpha_y = \alpha_x\alpha_z + \alpha_z\alpha_x = 0 \tag{2.7}$$

which means that the α components anticommute with each other and α also anti-commutes with β. To obey these requirements at the same time α and β have to

be 4×4 times matrices. Since the square of these matrices have to be equal to the identity operator, we can assume that the matrix elements have to be equal to zero, one or i

$$\alpha_x = \begin{pmatrix} 0 & 0 & 0 & 1 \\ 0 & 0 & 1 & 0 \\ 0 & 1 & 0 & 0 \\ 1 & 0 & 0 & 0 \end{pmatrix}, \alpha_y = \begin{pmatrix} 0 & 0 & 0 & -i \\ 0 & 0 & i & 0 \\ 0 & -i & 0 & 0 \\ i & 0 & 0 & 0 \end{pmatrix}, \alpha_z = \begin{pmatrix} 0 & 0 & 1 & 0 \\ 0 & 0 & 0 & -1 \\ 1 & 0 & 0 & 0 \\ 0 & -1 & 0 & 0 \end{pmatrix} \tag{2.8}$$

$$\beta = \begin{pmatrix} 1 & 0 & 0 & 0 \\ 0 & 1 & 0 & 0 \\ 0 & 0 & -1 & 0 \\ 0 & 0 & 0 & -1 \end{pmatrix} \tag{2.9}$$

α and β matrices can be written more compactly in 2-component form:

$$\alpha_x = \begin{pmatrix} 0_2 & \sigma_x \\ \sigma_x & 0_2 \end{pmatrix}, \alpha_y = \begin{pmatrix} 0_2 & \sigma_y \\ \sigma_y & 0_2 \end{pmatrix}, \alpha_z = \begin{pmatrix} 0_2 & \sigma_z \\ \sigma_z & 0_2 \end{pmatrix} \tag{2.10}$$

$$\beta = \begin{pmatrix} 1_2 & 0_2 \\ 0_2 & -1_2 \end{pmatrix} \tag{2.11}$$

in which 0_2 and 1_2 are the 2-dimensional identity and null matrices, respectively, and σ_x, σ_y and σ_z are the Pauli matrices,

$$\sigma_x = \begin{pmatrix} 0 & 1 \\ 1 & 0 \end{pmatrix}, \sigma_y = \begin{pmatrix} 0 & -i \\ i & 0 \end{pmatrix}, \sigma_z = \begin{pmatrix} 1 & 0 \\ 0 & -1 \end{pmatrix} \tag{2.12}$$

2.2 The properties of the Dirac Equation

The time-dependent equation (2.4) is Lorentz invariant and its wavefunction Ψ is not a scalar quantity, but rather a 4-component vector, referred as a spinor

$$\Psi(\boldsymbol{r}, t) = \begin{pmatrix} \psi^L_\uparrow(\boldsymbol{r}, t) \\ \psi^L_\downarrow(\boldsymbol{r}, t) \\ \psi^S_\uparrow(\boldsymbol{r}, t) \\ \psi^S_\downarrow(\boldsymbol{r}, t) \end{pmatrix} \tag{2.13}$$

in this case $\uparrow$ and $\downarrow$ represent the degree of freedom of the electron spin; L and S are respectively the large and small components of the wavefunction.

Most of the properties we are interested in can be assumed as a collection of time-independent set of states, therefore the Dirac equation can be written as the product of a spatial and a temporal part

$$\Psi(\boldsymbol{r}, t) = \Psi(\boldsymbol{r})\Theta(t) \tag{2.14}$$

the solution of the temporal form is a simple exponential, whereas the solution of the time-independent free-particle Dirac equation can be found by solving the following matrix equation

$$\begin{pmatrix} mc^2 - E & c(\boldsymbol{\sigma} \cdot \boldsymbol{p}) \\ c(\boldsymbol{\sigma} \cdot \boldsymbol{p}) & -mc^2 - E \end{pmatrix} \begin{pmatrix} \psi^L \\ \psi^S \end{pmatrix} = 0 \tag{2.15}$$

which is expressed in compact form using the 2-component Pauli matrices defined in (2.12). For convenience we can shift the axis of the energy by a constant value $-mc^2$, which is the rest mass energy. This is equivalent to a change of gauge, and it does not affect the result.

The first important difference with the non-relativistic case is that the spectrum of eigenvalues is unbounded from above and below (see Figure 2.1 on the left). In other words, the *positive* solutions lie above 0 and describe the *electronic* continuum, which is the same as found by solving the non-relativistic Schrödinger equation; the *negative* solutions lie below $-2mc^2$ and describe the positronic continuum. However, this picture shows some incongruities. For example, the electronic states are not bounded from below, which means that, in principle, the lowest positive solution may not be the ground state, and one electron could fall from the positive into the negative energy continuum.

This odd situation was solved by Dirac [20] by defining a new vacuum, which is the configuration in which all the negative states are filled and all the positive states are unoccupied. All other non-vacuum configurations are formed by adding electrons to the positive states. An electron cannot fall into the negative continuum because of the Pauli exclusion principle, therefore the lowest positive solution can be effectively considered a bound state. Conceptually interesting is that an electron can be excited from the negative continuum to the positive, leaving a charged positive hole called *positron*. The energy barrier for the creation of an electron-positron pair is $2mc^2$, which is much higher than the energies commonly involved in molecular chemistry and for our purposes these excitations may not be taken into consideration. However, the solution of the Dirac equation leaves open the possibility of an electron interacting with an infinitely negative charged continuum, which means even the simplest system needs to be treated as a infinitely many-body problem. These difficulties can be

Figure 2.1: The spectrum of a free particle solution (on the left) and of a hydrgen-like system (on the right).

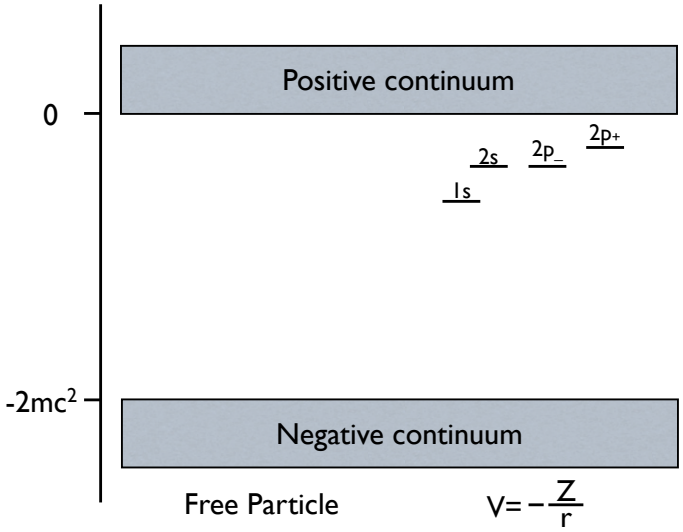

overcome if one bases the quantum mechanical description of the system on quantum electrodynamics (QED) [21,22], where the interaction between a charged particle and an electromagnetic field can be expressed in a single term. QED can be considered as a further generalization of the Dirac problem, but it goes beyond the scope of this thesis to discuss this theory.

2.3 The Solution of the One-Electron Dirac Equation in the field of a Nucleus

The Dirac equation can be formulated by considering systems of increasing complexity. In the previous section we have studied the free-particle case, now we can consider an electron subjected to a Coulomb-like potential, such as $V = -\frac{Z}{r}$, of a fixed nucleus. The time-independent Dirac equation (2.15) becomes then:

$$\begin{pmatrix} -E+V & c(\boldsymbol{\sigma}\cdot\boldsymbol{p}) \\ c(\boldsymbol{\sigma}\cdot\boldsymbol{p}) & -2mc^2-E+V \end{pmatrix} \begin{pmatrix} \psi^L \\ \psi^S \end{pmatrix} = 0 \tag{2.16}$$

It is common practice in non-relativistic quantum theory to approximate the nucleus to a point charge. However, this can create problems [23] when we deal with heavy nuclei. These are better approximated by the finite-size nuclei [24].

The solutions of equation (2.16) can be found exactly and can be expanded for small values of Z/c:

$$E = -\frac{Z^2}{n^2} + \frac{3Z^4}{8n^4c^2} - \frac{nZ^4}{2n^4c^2(j+\frac{1}{2})} + ... \tag{2.17}$$

where n is the main quantum number, Z is the charge of the nucleus and j is the total angular momentum. The first term on the right hand side is the binding energy; the second term appears only in the relativistic case, it weakens the electron-nucleus interaction and grows rapidly with nuclear charge mainly for the inner core electrons; the third term is related to the spin orbit coupling. In non-relativistic theory, the total energy depends only on the main quantum number n (first term in equation (2.17)), therefore orbitals with same angular momentum have the same energy. In relativistic theory, orbitals with same main quantum number *and* total angular momentum j have the same energy. For example, the non-relativistic $2p$'s with $l = 1$ are split in two levels of different energies, the $2p_{1/2}$ and $2p_{3/2}$. The orbital $2s_{1/2}$ is degenerate with $2p_{1/2}$, because they have the same n and j (see Figure 2.1 for more details).

2.4 The Many-Electron Dirac Equation

In all our calculations we will consider the Born-Oppenheimer (BO) approximation [25], in which the electrons are considered to be moving in the field of *fixed* nuclei. Within this approximation the many-electron Hamiltonian has the following form,

$$\widehat{H} = \sum_{i=1}^{N} \widehat{h}_i + \sum_{i<j} g_{ij} \tag{2.18}$$

where N is the total number of electrons. Here $\widehat{h}_i$ is the one-electron Hamiltonian

$$\widehat{H}_i = c\boldsymbol{\alpha}_i \cdot \widehat{\boldsymbol{p}}_i + \beta_i m_i c^2 + V(\boldsymbol{r}_i), \tag{2.19}$$

with $V(\boldsymbol{r}_i)$ the effect of the electron-nuclei interaction and any applied potentials felt by the electron i at position $\boldsymbol{r}_i$. The last term in Eq. (2.19) represents the electron-electron interaction. The leading term of this interaction can be thought to be the simple Coulombic interaction $1/r_{ij}$, but this term is not Lorentz invariant. The corrections to the Coulomb interaction can be rigorously obtained from quantum

electrodynamics at any order of accuracy, however in practice one can obtain the approximate correction,

$$g_{ij}^{breit} = -\frac{1}{2r_{ij}}\left[\boldsymbol{\alpha_i}\cdot\boldsymbol{\alpha_j} + \frac{(\boldsymbol{\alpha_j}\times\boldsymbol{r_{ij}})(\boldsymbol{\alpha_i}\times\boldsymbol{r_{ij}})}{r_{ij}^2}\right], \tag{2.20}$$

which is known as Breit interaction. The first term in brackets on the right-hand side of Eq. (2.20) is known as the Gaunt interaction [26], $\widehat{g}^{gaunt}$, which contains spin-spin, orbit-orbit and spin-orbit contributions, whreas the second term is the gauge interaction, which represents the retardation effects induced by the choice of a finite speed of light. For our purposes we will consider only the Coulomb term, and thus the resulting many-electron Hamiltonian will be referred to as *Dirac-Coulomb* Hamiltonian.

2.5 The Dirac-Coulomb-Hartree-Fock approach

The Dirac-Coulomb eigenvalue equation can be written in compact form as:

$$\widehat{H}|\Psi\rangle = E|\Psi\rangle \tag{2.21}$$

where $\widehat{H}$ is the many-electron Hamiltonian, and Ψ is the N-electron wavefunction, that spans all the possible Slater-determinants of orthonormal orbitals. At this level of theory, we consider the Dirac-Coulomb-Hartree-Fock approximation (DC-HF), that, like the non-relativistic theory, makes use of only one Slater determinant.

The structure of equation (2.21) is very similar to the non-relativistic case, but with the difference that the orbitals are not scalar but 4-component vectors. We anticipated previously that the Dirac equation is not bounded from below, therefore the electronic ground-state is an excited state in the spectrum defined by the Dirac-Coulomb Hamiltonian. However, the variational theorem can be employed for stationary states and not necessary for only minima . The minimax procedure [27–29] is used, it minimizes the energies with respect to the electronic variational parameters and maximizes the energy with respect to the corresponding positronic parameters. Based on the Roothaan equations [30], the Dirac-Coulomb-Hartree-Fock (DC-HF) pseudoeigenvalue equation can then be written analogously to the non-relativistic case:

$$\boldsymbol{FC} = \boldsymbol{SC\epsilon} \tag{2.22}$$

where the overlap matrix $\boldsymbol{S}$ is real and block-diagonal; $\boldsymbol{C}$ is the matrix of the complex expansion coefficients; $\boldsymbol{F}$ is the Fock matrix and can be split in the one- and two-

electron terms. The elements of the $\boldsymbol{F}$ matrices can be computed in different ways [31–34].

For the goals of this thesis, the expectation value of the Dirac-Coulomb Hamiltonian for a one-determinantal wavefunction can be generalized to include open-shell electrons by means of average of configurations formalism [32, 35, 36] yielding,

$$\begin{aligned} E &= \langle\Psi|H|\Psi\rangle = \sum_{i=1}^{N_c}\langle\phi_i|\widehat{h}|\phi_i\rangle + \frac{1}{2}\sum_{i,j=1}^{N_c}[(ii|jj) - (ij|ji)] + f\Bigg[\sum_{k=1}^{N_o}\langle\phi_i|\widehat{h}|\phi_i\rangle \\ &\quad + \frac{1}{2}\,a\cdot f\sum_{k,l=1}^{N_o}[(kk|ll) - (kl|lk)] + \sum_{i,k=1}^{N_c,N_o}[(ii|kk) - (ik|ki)]\Bigg] \end{aligned} \tag{2.23}$$

where N_c is the number of closed-shell electrons, N_o is the number of open-shell electrons, $\langle\phi_i|\widehat{h}|\phi_i\rangle$ is the diagonal matrix element of the one-electron Dirac operator; the $(\lambda\mu|\nu\omega)$ is a compact form for the 2-electron integrals defined in Mulliken notation. More precisely, these integrals are written in the following way,

$$(\lambda\mu|\nu\omega) = \iint \psi_\lambda^\ddagger(\boldsymbol{r}_1)\psi_\mu(\boldsymbol{r}_1)\frac{1}{r_{12}}\psi_\nu^\ddagger(\boldsymbol{r}_2)\psi_\omega(\boldsymbol{r}_2) \tag{2.24}$$

in equation(2.23), $(\lambda\lambda|\mu\mu)$ and $(\lambda\mu|\mu\lambda)$ are respectively the Coulomb and Exchange integrals. Furthermore, f is the fractional occupation number and a is the coupling constant,

$$f = \frac{n}{m}, \qquad a = \frac{m(n-1)}{n(m-1)} \tag{2.25}$$

in which n and m are respectively the number of open shell electrons and m the number of open-shell spinors.

2.6 Symmetry

The computational cost of calculating the energy and properties of any molecular system can be greatly reduced by considering the point group symmetry of the molecule in question. The symmetry depends on the spatial position of the atoms; therefore, any Hamiltonian that describe the physical state of the system (within the Born-Oppheneimer approximation [25]) has to be invariant under the symmetry operations of the point group to which the molecule belongs. The non-relativistic Schrödinger equation conforms to this requirement because it depends only on the spatial coordinates. The Dirac-Coluomb Hamiltonian, on the other hand, is not invariant because it depends on both the spatial and spin coordinates of the atoms in the molecule.

Therefore, a more general point group has to be defined. This new group [37, 38] is called double group, since it possesses twice the number of symmetry operations of a spatial point-group. In this domain, the irreducible representations (irreps) related to spatial symmetry are called boson irreps, whereas the extra irreps, which cover the whole double group are called fermion irreps [39].

The symmetry requirements of a double group are more strict and less computational favorable than the non-relativistic case. For example, a molecule that has D_{2h} symmetry has only two fermion irreps and six boson irreps. If we consider a molecule with this symmetry that has only "light" elements (i.e. the spin-orbit coupling effect is negligible), but its energy is computed by solving the Dirac-Couloumb equation, the calculations are much slower, because many of the two-electron integrals computed are nearly zero.

2.7 Basis set considerations

Another factor that affects the computational cost and the accuracy of a calculation is the basis-set. The choice of the appropriate basis set depends on the system and on the properties that have to be calculated. However, one should always check the convergence of the results with respect to the size of the basis. However, in relativistic quantum theory, the molecular spinors are 4-component vectors, therefore the expansion in finite real basis functions has to span both the large and the small components [40],

$$\psi_i = \begin{pmatrix} \sum_\mu c_{\mu i}^{L\alpha} \phi_\mu^L \\ \sum_\mu c_{\mu i}^{S\alpha} \phi_\mu^S \\ \sum_\mu c_{\mu i}^{L\beta} \phi_\mu^L \\ \sum_\mu c_{\mu i}^{S\beta} \phi_\mu^S \end{pmatrix} \tag{2.26}$$

where the ϕ_i are the vectors of the basis functions for the large and small components and c_i's are the complex expansion coefficients. The upper and lower components of a 4-component spinor are written more explicitly as a linear combination of primitive cartesian Gaussian type of orbitals:

$$\phi_i^L = N_i^L x^{k_i^L} y^{m_i^L} z^{o_i^L} e^{-\alpha_i^L r^2}, \quad \phi_i^S = N_i^S x^{k_i^S} y^{m_i^S} z^{o_i^S} e^{-\alpha_i^S r^2} \tag{2.27}$$

where N is a normalization constant and k, m and o are such that their sum gives the angular momentum l: $k + m + o = l$. The Gaussian basis functions that describe the small component space are coupled to the ones that span the large component space, because from the DC-HF equation they can always be written as a function of the

other. However, an approximation is necessary to build basis sets that are common for both the components.

The small component functions of the molecular spinor can be written as dependent of the large component functions, in such a way that in the non-relativistic limit for c $\rightarrow \infty$, the ϕ^S disappears:

$$\phi^S = -\frac{1}{2mc}(\boldsymbol{\sigma} \cdot \boldsymbol{p})\phi^L \tag{2.28}$$

This condition is called *kinetic balance* [41,42] and it is nowadays used for building relativistic small component basis-sets, starting from the large component counterparts. From equation (2.28), we can see that the small component functions depend on the operator $\boldsymbol{\sigma} \cdot \boldsymbol{p}$, which is a partial derivative along the x,y,z coordinates. Applying this derivative to equation (2.27), we obtain a dependence of the small component on $l-1$ and $l+1$, which means that in the design of the basis-sets higher angular momenta are included, increasing the number of primitive small-component functions with respect to the number of primitives of the large component. This already indicates that solving a DC-HF problem can be quite expensive when compared to the non-relativistic counterpart. For the construction of the Fock-matrix the two electron integrals can be divided in more subclasses: $(LL|LL)$, $(LL|SS)$ and $(SS|SS)$. Dyall and Faegri [43] estimated that while the number of integrals in the non-relativistic approximation is approximately equal to the number of $(LL|LL)$ integrals, the number of $(LL|SS)$ is about 13 times larger than the $(LL|LL)$ and the $(SS|SS)$ is 39 times larger. Overall, the computational cost for a Dirac-Fock calculation with an *uncontracted* basis-set is about 53 times larger than the non-relativistic counterpart. Usually, the effect of the $(SS|SS)$ integrals is negligible and the number of integrals can be strongly reduced by adopting simple coulombic corrections [44] or the one-center approximation [45].

2.8 Transformed Hamiltonians

In quantum chemistry it is common to analyze data from several points of view. For example, in many situations, it is convenient to look at the effect of spin orbit coupling starting from a spin free wave function. Since the 4-component approach is used in this thesis, the spin orbit term is included from the outset. It is necessary to find a way to isolate this contribution, and this is achieved using Dyall's method, in which the spin orbit term is projected out via a reformulation of the Dirac equation [46]. It is also possible to go further within the same framework and remove the relativistic corrections themselves by adopting the Levy-Leblond approximation [47].

Only recently computer programs have been developed to solve the 4-component Dirac equations for molecules, extending to less than 15 years (see for example DIRAC [48]), that is used extensively in this thesis. This is because the algorithms are complicated and time consuming. However, relativistic corrections can be employed when starting from a non-relativistic ansatz by using different kinds of approximations, as will be explained briefly here.

Perhaps, the most common approach is to use Relativistic Effective Core Potentials [49] (RECP), in which a set of parameters that take into account the the inner-core electrons contributions, such as electron interactions and spin-orbit coupling effects, is optimized and used to build core potentials thanks to *a priori* relativistic atomic calculations. On top of it a standard Hartree-Fock (or DFT) approximation is employed in the valence region. This approach is based on the idea that most of the molecular properties like geometrical structure and reaction paths depend mainly on the interaction between valence electrons, which do not suffer from strong relativistic effects. The drawbacks of this method are that properties depending on core electrons like EFG's and NMR parameters are not well reproduced.

An approximation, which is formally more rigorous is the Douglas-Kroll-Hess (DKH) approximation [50–52] . This method decouples large and small components in successive unitary transformations and reduces a 4-component problem to a scalar one- or to a spin-orbit two-components.

In this thesis, we do not make use of any of these approximations, but we employ the Zeroth Order Regular Approximation (ZORA) [53–57], in which the effective 2-component Hamiltonian is based on the elimination of the small component by expressing it in terms of the large component. A more rigorous way to achieve the same result is to generate an effective 2-component Hamiltonian from the Foldy-Wouthuysen transformation [58]. One can find the appropriate unitary transformation which reduces the 4-component Hamiltonian in a diagonal-block form by expressing the small component in term of the large component. The upper left block of the transformed Hamiltonian is the 2-component Foldy–Wouthuysen Hamiltonian. Of course the transformed Hamiltonian is not completely diagonal. In the zeroth order regular approximation the Foldy–Wouthuysen Hamiltonian is as follows,

$$(\boldsymbol{\sigma}\cdot\boldsymbol{p}\frac{c^2}{2c^2-V}\boldsymbol{\sigma}\cdot\boldsymbol{p}+V)\psi_i=\epsilon_i^{zora}\psi_i \tag{2.29}$$

An improved version includes some higher order terms as well and is called the scaled-ZORA equation,

$$\frac{\boldsymbol{\sigma}\cdot\boldsymbol{p}\frac{c^2}{2c^2-V}\boldsymbol{\sigma}\cdot\boldsymbol{p}+V}{1+\langle\psi_i|\boldsymbol{\sigma}\cdot\boldsymbol{p}\frac{c^2}{2c^2-V}\boldsymbol{\sigma}\cdot\boldsymbol{p}|\psi_i\rangle}\psi_i=\epsilon_i^{scaled}\psi_i \tag{2.30}$$

which differs from the ZORA equation only on the denominator:

The scaled ZORA values can be considered as corrected ZORA energies, in particular for the core orbitals. In the valence region, ZORA and scaled-ZORA give the same accuracy, which is also close to the Dirac energies. Already at the zeroth order the ZORA equation contains the dominant relativistic effects: the mass-velocity term, the Darwin term, and the spin-orbit coupling.

In quantum chemistry calculations, the energies can be computed using the one-component scalar relativistic ZORA (SR-ZORA) when spin-orbit coupling is not very important, or with the two-component ZORA, when spin-orbit effects are crucial [57].

2.9 Electron correlation

In the Hartree-Fock approximation [27,35,59] the electron-electron interaction is considered to rise from one single Slater determinant. Generally, this solution recovers more than 95% of the total energy, but for many applications the remainder is crucial to have an accurate description of the properties of the system. In the Hartree-Fock ansatz, the motion of the electrons is said to be uncorrelated and the state corresponding to this configuration is called vacuum. For simplicity, we will consider in the following a nonrelativistic regime, since the treatment of the electron correlation is equivalent for relativistic system.

In the real system, electrons interact with the field generated by other electrons through the manifestation of instantaneous excitations from occupied to unoccupied spin orbitals. The correlation energy E_{corr} is then defined as the difference between the total exact non-relativistic energy E_{tot} of the system considered and the vacuum (Hartree-Fock) energy E_{HF} in a complete basis-set expansion [59]:

$$E_{corr}=E_{tot}-H_{HF} \tag{2.31}$$

The total energy is more negative than the HF energy. To evaluate the correlation energy, the total wavefunction that describes the real system has to contain all the possible excitations arising from the vacuum configuration. One way to describe this is to write the total wavefunction as a linear combination of all the excited Slater determinants. This method is called full configuration interaction (FCI) and in second

quantized form it can be written as [27]:

$$|FCI\rangle = \big(1 + \sum_{ai} c_i^a a_a^\dagger a_i + \sum_{a>b,i>j} c_{ij}^{ab} a_a^\dagger a_b^\dagger a_i a_j \dots\big)|HF\rangle \tag{2.32}$$

in which an intermediate normalization of the $|FCI\rangle$ has been employed because the $|HF\rangle$ determinant is assumed the dominant reference state of the total wavefunction. The second and the third term within the brackets are the single and double excitations, respectively, expressed in terms of creation ($a^\dagger$) and annihilation (a) operators. The expansion in equation (2.32) is carried out for all the excitations. The coefficients are optimized by a variational procedure and the expectation value of the energy is obtained by solving the following eigenvalue equation

$$\boldsymbol{HC} = E_{CI}\boldsymbol{C} \tag{2.33}$$

where $\boldsymbol{C}$ is the matrix of the expansion coefficients. The diagonalization of the Hamiltonian $\boldsymbol{H}$ matrix gives the spectrum of exact eigenvalues for the system for a given basis set.

The correlation energy is a direct function of the doubly excited configurations, because they are the only ones that interact directly with the vacuum determinant. However, the doubly excited coefficients are themselves function of single, triple and higher excitations, which make the approach to be exact only by considering the complete expansion of Slater determinants. Because of this, the memory requirements asked for storing a huge number of determinants grows rapidly with the size of the system and the full CI approach becomes unfeasible even for small molecules. It is essential to choose only a small subset of determinants which carries most of the correlation energies and this is generally done by truncating the CI expansion.

Usually, the singly and doubly excited configurations are retained and the truncated CI is called CISD, where S and D stand for single and double excitations. In general, this method can recover more than 90% of the *dynamic* correlation energy [60]. We introduced the term *dynamic*, because it is referred to the correlation energy that arises from exciting a single determinant (in this case the Hartree-Fock determinant). In many situations, however, the quasi degeneracies of a few states make the single-reference approach less sound and a multi-reference approach is needed to evaluate the amount of *non-dynamic* (static) correlation energy, which arises from the simultaneous excitation of more determinants. The multi-reference CI (MRCI) wavefunction is constructed by including all the few determinants that describe that particular point of the energy surface and by adding on top of each reference configuration all the excitations up to the desired truncation of the CI expansion. If we

consider only single and double, the MR-CISD wave function [61] is obtained. To summarize, the non-dynamic correlation energy requires only those few determinants that contribute to the multi-reference character of that particular state; the dynamic correlation energy is the energy that comes from the ability of electrons to "avoid" each other and needs a much larger number of determinants to be described .

However, all the truncated forms of CI expansion suffer of lack of size-extensivity and make these methods unreliable for computing large systems or bond-breakings. There are different approximations that can be used to account of all the correlation energy of a system and we can summarize briefly here:

1. *Perturbation theory.* The exact solution is approximated by an order-by-order expansion of the wave-function and its energy. The most common approach that is used is MP2 [62, 63], which is a second-order expansion. This approach is non-variational, and the accuracy depends on the type of system but it can be sufficiently good to approximate most of the molecular properties [64, 65]. Unfortunately, it is a single-reference approach and only dynamic correlation energy can be retrieved, but, on the other hand, it is size-extensive;

2.*CASSCF.* The Complete Active Space method [66] is based on the concept that in the active orbital space all the possible configurations are obtained by distributing the electrons amongst all the possible active orbitals. Both the expansion coefficients and the orbitals are optimized, giving a highly flexible wave-function that can be used to accurately describe quasi-degenerate states , where non-dynamic correlation is important. However, the size of the active space is limited and not all the dynamic correlation energy is recovered. Usually, this method is used for qualitative purposes and is coupled with other methods that can compute also the dynamic contribution.

3. *RAS-CI.* The Restricted Active Space approach [67] can obtain the MR-CISD wavefunction we have mentioned before and recovers both dynamic and non-dynamic correlation energy. The active orbital space is divided in three different subspaces RAS1, RAS2 and RAS3. RAS1 is the *occupied* space in which at the most two electron holes are created; RAS3 is the *unoccupied* space that receives at most two electrons from RAS1 and eventually from RAS2; RAS2 is the CAS space in which all the possible excitations are considered and is formed by both occupied and unoccupied orbitals. The results can be very accurate but the approach is not size-extensive.

4.*CASPT2.* With this method [68, 69] the non-dynamic correlation energy is retrieved by considering all the excitations within the CAS space. The multiconfigurational CASSCF wavefunctions are then used as the zeroth-order states to apply second-order perturbation theory, to recover the rest of the dynamic correlation en-

ergy. This method, which is not variational, is very accurate and satisfies the size-extensivity requirement.

In this thesis none of these methods have been used to treat correlation energy. When very high accuracy is not needed, we have performed calculations using density functional theory; when the systems critically depend on very small energy differences, we employed more precise methods like multi-reference coupled cluster. These schemes will be discussed with more details later.

2.10 Coupled-cluster theory

In the previous section we stressed that any approximation used to compute the energy of a system has to satisfy the size-extensitivity condition. All the methods that involve truncated CI are not size-extensive, whereas the methods that obey this condition are mainly non-variational, so the total energy can be lower than the true total energy. This does not pose a problem because we are always interested in differences of energies and not absolute values.

One of the most successful non-variational approaches used to recover the *dynamic* correlation energy is based on Coupled Cluster theory. We have seen in equation (2.32) that the total wavefunction depends on the expansion coefficients of double, triple, quadruple excitations and so forth. A way to reduce the complexity of this expression is, for example, to approximate the coefficients of the quadruple as products of the coefficients of the doubles. This is the so-called coupled-pair approximation [59]. Using second quantization, the Coupled Cluster wavefunction is written in the following way [27]:

$$|CC\rangle = e^{\widehat{T}}|HF\rangle \tag{2.34}$$

where $\widehat{T} = \widehat{T}_1 + \widehat{T}_2 + \widehat{T}_3 + \dots$ is called the cluster operator. For simplicity we can restrict our terms to $\widehat{T}_2$ only. Thus, we obtain the CCD wavefunction:

$$|CCD\rangle = e^{\widehat{T}_2}|HF\rangle \tag{2.35}$$

where T_2 is defined as:

$$\widehat{T}_2 = \sum_{a>b\ i>j} \tau_{ij}^{ab} a_a^\dagger a_b^\dagger a_i a_j \tag{2.36}$$

Equation (2.35) can be expanded as a series of power

$$|CCD\rangle = \big(1 + \sum_{a>b,i>j} \tau_{ij}^{ab} a_a^\dagger a_b^\dagger a_i a_j + \sum_{a>b,i>j,c>d,k>l} \tau_{ij}^{ab}\tau_{kl}^{cd} a_a^\dagger a_b^\dagger a_i a_j a_c^\dagger a_d^\dagger a_k a_l + \dots\big)|HF\rangle \tag{2.37}$$

This form of the wavefunction has the same structure as a full CI expansion and ensures that all the higher order excitations are products of double excitations. In (2.37) the $\tau_{ij}^{ab}\tau_{kl}^{cd}$ are called *disconnected* cluster amplitudes, whereas τ_{ijkl}^{abcd} are the *connected* cluster amplitudes. Including also the T_1 excitation operator, the CCSD wavefunction is obtained. It is apparent that whatever is the truncation of the CC wavefunction, the expansion has always a full CI structure, that assures the size-extenistivity of the approximation. However, the quadruple excitations cannot be simply considered as the product of doubles excitations:

$$\tau_{ijkl}^{abcd} \cong \tau_{ij}^{ab} \cdot \tau_{kl}^{cd} \tag{2.38}$$

because also excitation from $i \rightarrow c$, $j \rightarrow l$, and so on have to be considered. There are 18 distinct ways a quadruple excitation from disconnected double excitations can be recovered and the third term in the brackets of equation (2.37) shows only one of them. The CC wavefunction is not linear in terms of the expansion coefficients and the variational theorem is not applicable to obtain the total energy.

The Coupled-Cluster energy is recovered starting from the the Schrödinger eigenvalue equation:

$$\widehat{H}|CC\rangle = E_{CC}|CC\rangle \rightarrow \widehat{H}e^{\widehat{T}}|HF\rangle = E_{CC}e^{\widehat{T}}|HF\rangle \tag{2.39}$$

Multiplication of both sides of (2.39) by $\langle HF|e^{-\widehat{T}}$ gives,

$$E_{CC} = \langle HF|e^{-\widehat{T}}\widehat{H}e^{\widehat{T}}|HF\rangle \tag{2.40}$$

The amplitudes are obtained by projecting equation (2.39) onto an excited manifold $|\Phi\rangle$ of determinants:

$$\langle\Phi|\widehat{H}e^{\widehat{T}}|HF\rangle = E_{CC}\langle\Phi|\widehat{H}e^{\widehat{T}}|HF\rangle \tag{2.41}$$

From equation (2.40), the CC energy is computed starting from a single-reference determinant and depends directly on the single and double amplitudes, with the highest excitations contributing indirectly. From equation (2.41), the amplitudes themselves depend from the CC energy making the procedure iterative.

The integrals in the CC equations are expressed in MO-basis because the AO integrals make the approach too combersome. Therefore, a 4-index AO $\rightarrow$ MO basis-transformation step is employed just before the start of the CC procedure [70–72]. In some occasions, this can be the bottleneck of the calculation, but is the prize that has to be paid to make the CC algorithm more efficient. A further improvement of the CCSD approximation is the CCSD(T) [70], which includes the triples excitations

in a perturbative fashion. In this thesis, this can be considered the most accurate approach to calculate the dynamic correlation energy. The relativistic extension of the Coupled Cluster equations have been developed by Visscher et al. [73–75] .

2.11 Fock-space Coupled Cluster

The Fock–Space Coupled–Cluster (FSCC) method [1] is a multireference approach that has proven to be very successful in computing with very high accuracy the excitation energies of atoms and molecules [76–78]. While the atomic energies were computed for basically all the elements, molecular calculations have been carried out only for few systems, mainly containing light atoms. The basic features of the Fock-space method are that the full electronic spectrum can be computed of any molecule in one single-run and that the method scales like a normal CCSD calculation (N^6), which makes this approach suitable to analyze larger systems, provided a reasonable amount of memory is used.

In the treatment of the FSCC theory, we assume a reference state which is usually a closed-shell single-determinant [79]. After correlating this state, we define a subspace of the correlated space as the *model space* P [80] that recovers some of the eigenfunctions of the Hamiltonian H. The remaining part of the functional space is called *orthogonal space* Q. $\widehat{P}$ and $\widehat{Q}$ are projection operators that project out any component that lies in the model and orthogonal space, respectively (see Figure 2.2 on the left for more details). They are connected by the following relation:

$$\widehat{P} + \widehat{Q} = \widehat{1} \tag{2.42}$$

In the FSCC method, we add/remove electrons to/from the P space and recorrelate all the system at each step. To see the properties of the model space, we can multiply on the left both sides of the Schrödinger equation by $\widehat{P}$

$$\widehat{P}\widehat{H}\widehat{\Omega}|\Psi_0\rangle = E\widehat{P}|\Psi\rangle \tag{2.43}$$

where $\widehat{\Omega}$ is the wave operator, Ψ is the wavefunction that describes the Hamiltonian $\widehat{H}$ and Ψ_0 is the projected wavefunction into the model space. Equation (2.43) becomes then:

$$\widehat{P}\widehat{H}\widehat{\Omega}|\Psi_0\rangle = E|\Psi_0\rangle \tag{2.44}$$

The operator that emerges from (2.44), $\widehat{H}_{eff} = \widehat{P}\widehat{H}\widehat{\Omega}\widehat{P}$, is called effective Hamiltonian and implies that its eigenvectors represent the model functions and its eigenvalues are the exact energies of the corresponding true states of the Hamiltonian $\widehat{H}$.

The Fock-space excitation operator $\widehat{T}$ can be decomposed according to the number of valence holes, m, the number valence particles, n, and the usual total number of excited electrons, l [79]:

$$\widehat{T} = \sum_{m\geq 0}\sum_{n\geq 0}\left(\sum_{l}\widehat{T}_{l}^{(m,n)}\right) \tag{2.45}$$

In Figure 2.2 a schematic view of the FSCC approach is depicted. A particle is denoted as a full circle, an electron hole as an empty circle and an excitation as an arrow connecting a particle with a hole. The FSCC method works as follow: firstly, the CC correlation energy, is computed for the closed-shell reference determinant, which is called sector (0,0), and it is described by the arrows a, b, e and f on the left-side of Figure 2.2. Afterwards, two possible paths can be chosen: in sector (1,0), one electron - denoted as an empty circle on the top of arrow c - is removed from the occupied region of the P model space, which is now referred as the active occupied space. In the second path, one electron - a full circle at the base of arrow g - is added to unoccupied region of the model space P, referred to as active virtual space, forming the corresponding active particle defined as sector (0,1).

All the l excitations of this removed/added electron in the inactive Q space are generated using equation (2.45) to account for the rest of the dynamic correlation energy (arrows c and h). A full diagonalization of the H_{eff} is carried out in the space P to obtain the exact spectrum of electronic ionization potentials, for sector (1,0) - arrow d - , or electronic affinities, for sector (0,1) - arrow g - . These non-dynamic correlation energy contributions are added to the CC energy of the reference state to obtain the spectrum of the singly ionized molecules.

To explain better, if we start from a closed shell reference molecule Mol^{2+} and we are interested for sector (1,0) energies, we obtain the spectrum of the Mol^{3+}, whereas if we are interested for sector (0,1) energies, we obtain the states for the Mol^{+} ion. In the case we remove(add) a second electron from the active occupied(active virtual) space, we recover the electronic spectrum of Mol^{4+} for sector (2,0) or the spectrum of Mol for sector (0,2). In some situations we could also choose to remove and add one electron at the same time, sector (1,1), in order to obtain the excitation energies of the reference Mol^{2+} molecule.

The advantage of this method over standard CC methods is twofold. It is possible to have a full set of excited states in one run, instead of computing CC energies for each reference determinant and the FSCC takes into account also the multireference character of a state, whereas the standard CC can only describe states dominated by one single determinant. The drawback is that using single and double excitations

(l=2), only singlet and triplets states can be retrieved. For other multiplet states, higher excitations have to be considered, but this make the algorithm more complicated and computationally intensive. In this thesis, we only employed the FSCCSD approximation.

2.12 The Intermediate Hamiltonian Fock-space Coupled Cluster

To fully appreciate the high-accuracy of the FSCC method, it is necessary to choose appropriate P and Q subspaces. Usually, the model space P should include all those determinants that contribute to the state (ground or excited) of interest. If this is not accomplished the accuracy is lowered and problems of convergence can arise, because the separation between Q and P is not large enough. In the FSCC equations there are some terms on the denominator that depend on the difference in energy between two states, one in P and the other in Q. If this difference is small, these terms become too large and the calculation diverges. To avoid problems of this kind, the intermediate Hamiltonian coupled cluster approach (IH-FSCC) was developed [81,82] and allowed the choice of more flexible P spaces, without major problems of convergence.

In this framework, the model space P is itself divided in two subspace P_m and P_i (see Figure 2.2 on the right), with dimension N_m and N_i, whose operators satisfy the following condition:

$$\widehat{P}_i + \widehat{P}_m = \widehat{P} \tag{2.46}$$

Two sets of wavelike operators are defined and expanded in coupled cluster ansatz. One of them is called $\widehat{\Omega}$ and operates in P_m:

$$\widehat{\Omega}\widehat{P}_m|\Psi_m\rangle = \{e^{\widehat{S}}\}\widehat{P}_m|\Psi_m\rangle = |\Psi_m\rangle \tag{2.47}$$

where $|\Psi_m\rangle$ is the projected wavefunction of the Hamiltonian $\widehat{H}$ in P_m. The second operator acts in P and satisfies the following condition:

$$\widehat{R}\widehat{P}|\Psi_m\rangle = \{e^{\widehat{T}}\}\widehat{P}|\Psi_m\rangle = |\Psi_m\rangle \tag{2.48}$$

It is important to notice that we did not put any restrictions on P_i and the previous equations are only valid for eigenstates in P_m. $\widehat{T}$ and $\widehat{S}$ are excitation operators. An intermediate Hamiltonian $\widehat{H}_I$ can then be constructed:

$$\widehat{H}_I = \widehat{P}\widehat{H}\widehat{R}\widehat{P} \tag{2.49}$$

Figure 2.2: A schematic view of the excitations involved in the FSCC(left) and IHF-SCC(right) approaches. Both sector (1,0) and sector (0,1) are depicted for the FSCC. For simplicity, on the right side, only sector (0,1) is considered. The empty circles indicate a hole, the full circles an electron and the arrows an excitation.

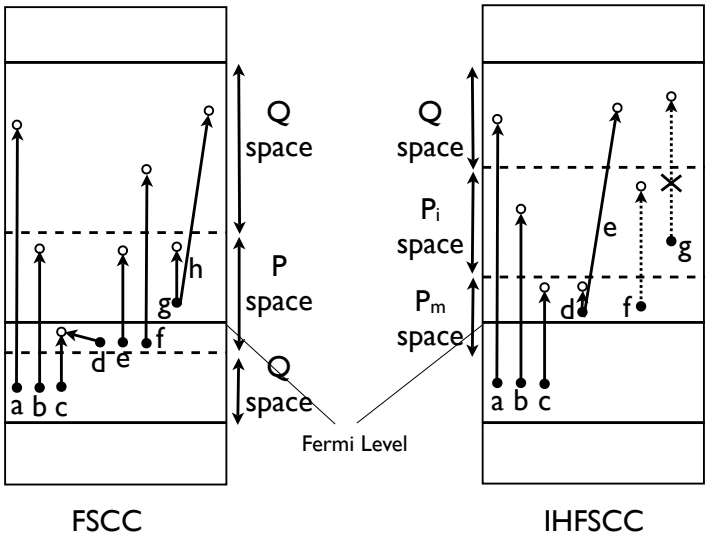

which after diagonalization gives exact solutions of the Schrödinger equation in P_m - arrow d in Figure 2.2 on the right - , but not in P_i - dotted arrow f - :

$$\widehat{H}_I\widehat{P}|\Psi_m\rangle = E_m\widehat{P}|\Psi_m\rangle \tag{2.50}$$

The IH-FSCC equations are derived for $\widehat{S}$ and $\widehat{T}$ and are valid under the condition $\widehat{Q}\widehat{S}\widehat{P}_m = \widehat{Q}\widehat{T}\widehat{P}_m$. These expressions depend on some terms that in the denominator are based on the energy difference between a state in P_m and a state in Q, which means that some of the excitations from the P_i space are removed - see dotted arrow g in Figure 2.2 -. P_i space acts as a buffer between P_m and Q subspaces. If P_i is sufficiently large the presence of intruder states is minimized and the calculation suffers less for problems of convergence [83–85].

The choice of the P_m space is not arbitrary, but is based upon the physical process we want to describe. For example, the calculation of sector (0,2) for the Mol^{2+} ion (described in the previous section) implies the selection on the P_m space of those orbitals that are important for an accurate description of the excited states of interest for the *Mol* molecule. If this does not happen, the results carry a bias that can be

removed only by choosing a more appropriate P_m space. The selection of the corresponding P_i space is also critical, because in the intermediate Hamiltonian approach the possibility of the occurrence of intruder states is reduced, but not totally removed. If the P_i is not large enough, it cannot acts as an efficient buffer and the difference in energy of two states, one in P_m and one in Q, may be still small enough that the calculation can diverge.

A rule of thumb for the choice of the P_i space can be given for each sector:

$$
\begin{aligned}
Sector(0,1) \quad & a. \quad E_{Q^{min}} > E_{P_m^{max}} && (2.51)\\
& b. \quad 2E_{P^{min}} - E_{HOMO} > E_{P_m^{max}} && (2.52)\\
Sector(1,0) \quad & a. \quad E_{P_m^{min}} > E_{Q^{max}} && (2.53)\\
& b. \quad 2E_{P_m^{max}} - E_{LUMO} < E_{P_m^{min}} && (2.54)\\
Sector(0,2) \quad & \quad E_{Q^{min}} > 2E_{P_m^{max}} - E_{P_m^{min}} && (2.55)\\
Sector(2,0) \quad & \quad E_{Q^{max}} < 2E_{P_m^{min}} - E_{P_m^{max}} && (2.56)
\end{aligned}
$$

where P_m^{max} and P_m^{min} are the energies of the lowest and highest orbitals in the P_m space, and Q^{min} is the energy of the lowest orbital in the Q space. It is important to say that the use of the Mol^{2+} orbitals, which are not optimal for the neutral Mol molecule, requires a large basis set and correlated space, in order that a sufficient orbital relaxation is achieved. While more experience is gained in using the IHFSCC method, it is thus prudent to carry out systematic enlargements of basis sets and/or active spaces, to ensure that reliable results are obtaned. In some of the applications of this thesis, the IH-FSCCSD method was used extensively.

2.13 Density functional theory

We have mentioned that to describe a system of N interacting particles in quantum mechanics one has to solve the Schrödinger equation (Dirac equation for a relativistic system). However, due to the electron-electron interaction term in the Hamiltonian, the equation is in practice unsolvable and approximate solutions have to be found. Density functional theory moves the attention from the many-body electronic wavefunction of the system, which depends on 3N spatial variables to the electron density, which depends on only three variables.

Hohenberg and Kohn [86] postulated and proved in 1964 that there is a one-to-one mapping, up to an arbitrary uniform constant, between the density of a system in a non-degenerate ground state and the external potential applied to the system.

In other words the density ρ uniquely defines the potential of the system, which parametrizes the Hamiltonian and thus the wavefunction. It follows that the many-body wavefunction is a functional of the density, and hence all the properties of the system, in particular, the total energy, can be expressed as a functional of the electron density. The exact ground-state density minimizes the ground-state total energy functional. One can prove a relativistic version of the Hohenberg-Kohn theorem [87,88], based on the mapping between the external 4-component potential and the 4-component current. However, a principle of minimum energy has not been rigorously proven [89] since the Dirac equation admits negative solutions.

DFT is in principle exact, but in practice needs approximations for the universal functional $F_{HK}[\rho] = \langle\Psi[\rho]|\hat{T} + \hat{W}|\Psi[\rho]\rangle$, with $\hat{T}$ and $\hat{W}$ the kinetic and electron-electron interaction operators of the system. Kohn and Sham [90] make the density functional approach practical by introducing a non-interacting system moving in an effective potential V_s which produces the same density as in the real interacting system. One has to solve, then, the one-electron Kohn-Sham equations,

$$\left(-\frac{1}{2}\nabla^2 + V_S(\boldsymbol{r}) \right)\psi_i(\boldsymbol{r}) = \epsilon_i\psi_i(\boldsymbol{r}) \tag{2.57}$$

where the Kohn-Sham potential $V_s(\mathbf{r})$ is given as,

$$V_s(\mathbf{r}) = V(\mathbf{r}) + \int \frac{\rho(\mathbf{r}')}{|\mathbf{r} - \mathbf{r}'|} d\mathbf{r}' + V_{xc}(\mathbf{r}). \tag{2.58}$$

Here the terms on the right-hand side are, from left to right, the external potential, the Hartree potential, and the exchange-correlation (xc) potential, respectively. The expectation value for the energy of the full-interacting system is

$$E[\rho] = T_s[\rho] + \int \rho(\boldsymbol{r})V(\boldsymbol{r})d^3\boldsymbol{r} + \frac{1}{2}\iint \frac{\rho(\boldsymbol{r_1})\rho(\boldsymbol{r_2})}{r_{12}} d^3\boldsymbol{r_1}d^3\boldsymbol{r_2} + E_{XC}[\rho] \tag{2.59}$$

T_s is the kinetic energy of the non-interacting system; the second term is the nuclear attraction energy and the third is the classical Coulomb self-energy; the last term is the xc energy and is that part of the energy that contains the difference between the interacting and non-interacting kinetic energy term, the exchange energy and dynamic correlation contributions.

Unfortunately, the exchange correlation functional is not known exactly and has to be approximated. The quality of a DFT calculation is strictly related to how well the exchange-correlation term is described for a particular system. Nowadays there are plenty of xc functionals and each of them can be used to analyze particular properties of a system. The most common are the local-density approximation (LDA)

[91] and the generalized gradient approximations (GGA) like BLYP [92, 93], BP86 [94, 95] or PBE [96]. One functional that has wide success is the B3LYP [97], which mixes the exact exchange term from Hartree-Fock theory and the GGA xc functional BLYP. These kind of xc functionals are called hybrid functionals and are also widely spread in literature. In this thesis we will make use of DFT when we are interested in the qualitative understanding of a particular system. When we are concerned on quantitative and more accurate results, we turn our attention on more specific methods, like intermediate Fock-space coupled cluster theory.

2.14 The QM/MM approach

In some of the applications of this thesis, it is important to study the effects of the solvent on molecules containing an actinide element. The computational modeling of conditions in solution demands in principle a high level quantum mechanical approach because it is crucial to analyze with reasonable accuracy charge transfers, coordination numbers and bond breakings that occur when the solute interacts with the solvent or with other molecules in solution. However, the treatment of molecular systems including a large number of solvent molecules is beyond the limits of the current computer technology, and full quantum mechanical methods can not be employed in a short-range period.

There are different ways to handle the effect of the environment and two general approaches can be defined. One in which the solvent is treated like a continuum of dielectric constant ϵ, in which the solute is placed in a cavity [98–100]. The other is a discrete approach in which the solvent molecules are added explicitly to the solute. To study the time-dependent behavior of a whole solute/solvent system, it is essential to provide all the possible configurations that sample a given statistical ensemble. Based on the finite temperature ensemble averages, the free energy profile of a system can be computed, and associated to all the thermodynamic properties that are identified in an experiment. This sampling can be performed probabilistically using Monte Carlo (MC) simulations or deterministically, using the so-called molecular dynamics(MD), in which Newton's equations of motion are integrated. The latter method can be done using full QM approaches like the Car-Parrinello dynamics [101] or, if a good parametrization is achieved, using classical molecular dynamics. In other situations, the properties of a molecule in solution can be probed using static methods. In these calculations, which are performed at zero temperature limit, the properties of the solute/solvent system are described by scanning the potential energy surface to find

stationary points. Each of these minima or saddle points provides starting points for analysis, or new optimizations.

However, in these frameworks, the number of explicit solvent molecules is still so large that a full quantum mechanical approach is computationally not affordable, and approximations have to be found in order to maintain high accuracy and low computational needs.

In this thesis, we are interested in applying a static method, therefore from now on we focus mainly on this approach. In this domain, it is usually common to divide the whole system in different layers, each of them computed at different level of approximations. An example of this is the frozen-density embedded scheme, developed recently [102], in which the solvent effect can be described by an embedded potential. This scheme has been successfully applied to model electronic absorption spectra of small organic molecules [103–105].

A more traditional way to treat the solute/solvent interaction is based on the mixing of classical and quantum mechanical methods. The so-called QM/MM approach treats the total system by dividing it in two regions: the active site, which contains the properties of interest, is computed at full QM level, and the reminder of the system using classical methods, like molecular mechanics (MM) [106]. Molecular mechanics is a totally different approach than quantum mechanical methods. While these last ones are based on *a priori* interpretation of a molecular systems, which is described by solving the Dirac equation (in the relativistic framework), molecular mechanics can be considered as *a posteriori* method, in which the potential energy surface of a molecular system is divided in a set of simple mathematical functions that are fit to reproduce the experiment. In MM the molecules are usually described as balls connected together by springs. For example, Hooke‘s law is applied to describe bonds and angles, a simple Coulomb potential is employed for the interaction between charges, and the van der Waals equation is considered for weak interactions. This simplistic approach shows some clear limits, but it can be successfully used when it is interfaced to more accurate methods, and is used to describe parts of a system which are not directly involved in the properties to be analyzed.

The total QM/MM energy can be expressed in the following way:

$$E_{TOT} = E^{I}_{QM} + E^{II}_{MM} + E^{I-II}_{MM} \tag{2.60}$$

For the purposes of this thesis, the QM region is computed using DFT. The second term is the classical contribution that is computed using the AMBER95 force-field

[107], which describes the potential energy as

$$E_{MM}^{II} = \sum_{r}^{bonds} K_b(r-r_0)^2 + \sum_{\theta}^{angles} K_\theta(\theta-\theta_0)^2 + \sum_{n}^{dihedrals} V_n(1+\cos(n\phi-\gamma)) + \\ + \sum_{i<j}^{atoms} \epsilon\left[\left(\frac{R^*}{r_{ij}}\right)^{12} - 2\left(\frac{R^*}{r_{ij}}\right)^{6}\right] + \sum_{i<j}^{atoms} \frac{q_i q_j}{r_{ij}} \tag{2.61}$$

where K_b and K_θ represent the bond stretching and the bending force constants; V_n is the rotational potential; ϵ is the well depth, with R^* the van der Waals radius and q_i is the charge on atom i. In this approach, polarization effects are neglected, because the separation between the QM and MM regions is made on the second water shell, where these terms are less important.

In this thesis, the parametrization of bond and angle force constants involving an heavy atom is not very critical because they all belong to the QM region and are computed explicitly. However, for sake of comparison, one can be interested in finding a parametrization of the MM region using the tools that are commonly employed in classical methods, and check how well they perform when compared to the full QM results. One of these tools are the Badger's rules [108], which are commonly used to evaluate bond stretching and bending angle force constants. As regards the bond parameters, Badger assumed that two atoms connected to each other have an effective charge and they are attracted by a Coulombic force and repelled by the Pauli repulsion, which is approximated as linear:

$$E_b = E_{ob} - Fr_{ij} - G\frac{q_i q_j}{r_{ij}^2} \tag{2.62}$$

where E_{ob} is the unperturbed bonding energy, F and G are two constants to be defined and r_{ij} is the distance between atom i and atom j. At the equilibrium bond distance, the force constant is,

$$K_b = \left(\frac{\partial^2 E_b}{\partial r_{ij}^2}\right) = 2G\frac{q_i q_j}{r_{ij}^3} \tag{2.63}$$

where $2G = 664.12$ is computed based on a set of empirical data. The charges and the bond distances are determined from reference systems calculations at full QM level.

Based on the same assumption, the angle bend force constants between the atoms i, j and k can be determined starting from,

$$E_\theta = E_{o\theta} - F\theta - M\frac{q_i q_j}{r_{ik}^2} \tag{2.64}$$

where,

$$r_{ik}^2 = r_{ij}^2 + r_{jk}^2 - 2r_{ij}r_{jk}\cos\theta \tag{2.65}$$

At the equilibrium configuration, the force constant is,

$$K_\theta = 664.12 \frac{q_i q_j}{r_{ik}^5} \left[3 r_{ij} r_{jk} (1 - \cos^2 \theta) - r_{ik}^2 \cos \theta \right] \tag{2.66}$$

also in this case the bond distance and the angle are computed at high accuracy on QM model systems.

The most relevant MM parameters are the charges (q) used in the evaluation of the E_{MM}^{I-II} interaction term that is mainly electrostatic. We decided for the multipole derived charges [109], that are obtained in a self-consistent manner during the QM/MM geometry optimizations on the QM region of the complex under study. The QM/MM scheme does not allow for polarization of the QM part, but it exerts only a mechanical coupling between the two regions. This relaxation can be interpreted as a correction for the changes induced by the change of geometry in the QM part.

Part I

Spectroscopy of Small Molecules

CHAPTER 3

The importance of spin-orbit coupling and electron correlation in the rationalization of the ground state of the CUO molecule

Jules: But I'm tryin', Ringo. I'm tryin' real hard...

from the movie Pulp Fiction (1994)

3.1 Abstract

We present calculations at the relativistic coupled cluster theory that predict the $^1\Sigma_0^+$ ground state of CUO to lie 58.2 kJ/mol below the first excited state, $^3\Phi_2$. This can be contrasted with the outcome of earlier DFT and CASPT2 calculations that both predicted a $^3\Phi_2$ ground state upon inclusion of spin-orbit coupling in the calculations. Our result gives further justification to the interpretation of the measured frequency shifts of this species in various noble gas matrices as being caused by significant interaction between the uranium and the heavier noble gas atoms.

3.2 Introduction

Many new small actinide molecules have been synthesized and characterized in recent years via laser ablation matrix infrared experiments [110,111]. Of the new species the small CUO molecule has attracted much attention due to its remarkable behavior in different rare gas matrices [112,113]. Bringing laser ablated uranium atoms in contact with CO, the strong triple bond of the carbon monoxide is broken leaving CUO as the primary product of a reaction that also gives other secondary components like OUCCO [110]. Upon trapping the CUO molecule in different solid noble-gas (Ng) matrices Andrews and coworkers [114, 115] found a large vibration frequency shift that could be explained by assuming that the ground state of the molecule is changed due to the interaction with the noble gas matrix: in neon the interaction is weak and the same singlet ground state is found as in the gasphase, whereas the stronger interaction with argon or krypton is sufficient to make the lowest lying triplet state the groundstate. Since the two states differ by occupation of either a bonding (in case of the singlet) or of a nonbonding uranium $5f$-orbital (in case of the triplet states) a large frequency shift in the C-U stretching vibration is observed.

The simple intuitive picture sketched above was initially supported by DFT calculations of Bursten et al [116] that indicated that the interaction with a single argon atom is already enough to overcome the energy difference of only a few kJ/mol between the $^1\Sigma^+$ and the $^3\Phi$ states. They furthermore showed that the experimental infrared spectra of CUO in CUO-Ne and in CUO-Ar matrices match precisely the vibrational frequencies computed by DFT theory for the gasphase species. Experimentally, the normal modes have frequencies of 1047.3 and 872.2 cm^{-1} (CUO-Ne matrix) and 852.5 and 804.3 cm^{-1} (CUO-Ar), while the theoretical frequencies are 1049 and 874 cm^{-1} ($^1\Sigma^+$) and 943 and 902 cm^{-1} ($^3\Phi$), respectively. The DFT calculations of Bursten were, however, done without considering spin-orbit coupling (SOC) effects that can easily overcome such small energy differences between singlet and triplet states. Roos, Widmark and Gagliardi [117] performed accurate CASPT2 calculations and found that already without including SOC the triplet state is the lowest in the gasphase. With SOC the triplet state is found to lie about 50 kJ/mol below the singlet. This is in contradiction with the later experiments of Andrews and coworkers that indicate that more than one rare gas atom is bound to the CUO [114]. With more interacting Ng atoms the energy difference between the singlet and triplet (with the singlet being lower) should be larger in order to prevent that also the weak interaction with neon would change the ground state. Both sides agree that the experimental evidence for an inversion of ground state relative to the gasphase or weakly bound Ne

atoms is overwhelming, but the question remains how this trend can be reproduced in a theoretical description.

In this work we intend to look at the effect of SOC in a DFT approach and to check how much the choice of functional influences the computed energy difference. To give an independent verification of the ab initio results we have performed calculations with the Dirac-Coulomb Coupled Cluster with Single and Double excitations with perturbative treatment of triples [DC-CCSD(T)] method [73] to allow for a very precise treatment of both relativistic and electron correlation effects. Also in this method it is possible to isolate SOC effects from other relativistic effects, which makes the analysis of results easier. With the two schemes we can study all four aspects of the stabilization of one state over the other: the difference in bond lengths, the relativistic approximation, the SOC correction and the correlation energy. Since several multiplet states arise from the low-lying unoccupied $5f$-orbitals from the uranium, the use of single reference method like DC-CCSD(T) or DFT may not be appropriate. We therefore also performed a number of calculations using the multireference (Fock space [118]) CCSD approaches to verify the consistency of the computed results. We will divide the discussion of the different theoretical results that we achieved into three parts. First, we vary the structure (bond lengths) and see how this affects the energies of the two states of interest. We then approximate the Hamiltonian to get information about the SOC effect; and finally we compare how the different methods (DFT, CCSD, MR-CCSD, CASPT2) treat the correlation energy. Furthermore, other contributions that are analyzed in more detail are the choice of the basis sets (for all methods), the exchange-correlation functional (for DFT) and the active space (for CC and MR-CC).

Before continuing, we remember that in the presence of a spin-orbit (SO) term, the $^3\Phi$ state is decomposed in three different states labeled by the Ω value (with Ω the projection of the total electronic angular momentum on the molecular axis). The $^3\Phi_2$ and $^3\Phi_4$ states may be described by the single determinant wave functions $|\sigma_{-1/2}\phi_{7/2}|$ and $|\sigma_{-1/2}\phi_{7/2}|$, respectively; but the $^3\Phi_3$ interacts with the $^1\Phi_3$ and needs to be described by a two determinant reference function including both $|\sigma_{-1/2}\phi_{7/2}|$ and $|\sigma_{1/2}\phi_{5/2}|$. This makes this state less accessible for CC and DFT approaches, and we therefore chose to focus only on the lowest $^3\Phi_2$ component. In conventional approaches, in which SOC is considered as a perturbation, one also finds a significant mixing of this state with the $^3\Phi_2$ state due to the occurrence of SOC matrix elements between the almost degenerate $\phi_{5/2}$ and $\delta_{5/2}$ orbitals. This mixing need not be considered in variational SOC calculations because these matrix elements are close to

zero according to Brillouins theorem which makes the single reference CC approach possible. To shorten the notation we define ΔE_Ω as the energy gap between the components of the triplet state $^3\Phi_\Omega$ (with Ω=2, 3, 4) and the singlet $^1\Sigma_0^+$. In spinfree calculations we will simply use the notation ΔE.

3.3 Methodology

All-electron DFT calculations were done using the scalar and spin-orbit Zeroth Order Regular Approximation (ZORA) [54–57] as implemented in the ADF2003 package [119, 120]. ADF offers a wide choice of functionals that will be indicated by the acronym used in the program. The primary reference can easily be found in the documentation of the program and will not be listed unless explicitly discussed in the text.

The all-electron CCSD(T) calculations were done using the full 4-component Dirac-Coulomb (DC) Hamiltonian, as implemented in the DIRAC program [48]. For purpose of analysis we have also made use of the transformed Dirac-Coulomb (DC) equation [121], which can be approximated to the scalar relativistic Spin-Free (SFDC) Hamiltonian [46]. For computational efficiency only the $(LL|LL)$ and $(SS|LL)$ two-electron integrals were included. Test calculations that included the more numerous but numerically insignificant $(SS|SS)$ integrals showed that that associated error is marginal, only 0.4% in ΔE_Ω. Geometry optimizations have been performed at DFT/ZORA level applying a convergence on the gradient at 10^{-4} with accuracy on the integration grid of 10^{-10}. In these ZORA/DFT calculations we used a triple-ζ basis augmented by two polarization functions on all the atoms (TZ2P). The 1s core of C and O atoms and all orbitals up to the 5d shell for U have been kept frozen based on relativistic atomic calculations. Single point ab initio calculations were carried out using fully uncontracted basis sets taking the exponents from the cc-pVTZ sets [122–124] for the carbon and oxygen atoms, and either the 26s21p17d12f basis set of de Jong [125] or the 33s29p21d15f3g1h basis set of Faegri [126].

The computed correlation energy in CCSD(T) will depend on the choice of the active space. The important orbitals for the C and O atoms are the subvalence $2s$ and the valence $2p$ orbitals. Correlation of the core $1s$ electrons may be considered unimportant at the level of accuracy that we try to achieve. For uranium the situation is more complicated and different partitionings of the valence shell are possible. The minimal choice for an active space is to consider only the 6 electrons in the $5f$, $6d$ and $7s$ orbitals. This gives a total minimum number of electrons to be correlated

of 12. Taking also the subvalence uranium $6p$ and carbon and oxygen $2s$ electrons into consideration increases this number to 22 electrons. Core-valence correlations due to interaction with the deeper lying $5d$ and $6s$ electrons may also be important and are treated with the largest active space used in this work: 34 electrons. Besides choosing the number of electrons to be correlated we also restricted the full set of virtual orbitals to the set relevant for valence and subvalence correlation. We did so by deleting virtuals with an orbital energy above 10 au.

3.4 Results and Discussion

3.4.1 Geometry

The $^1\Sigma_0^+$ and $^3\Phi_2$ states have a rather different C-U bond length since one electron less contributes to C-U bonding in the triplet state. This gives an elongation of about 0.10 Å of the C-U bond and 0.02 Å of the U-O bond in the triplet state. To avoid large errors in the computation of the relative energies it is therefore important to compute the adiabatic energy differences rather than employing a common geometry. This point was already mentioned by Roos et al. [117] and is confirmed by our DC-CCSD(T) calculations. For example, at the DC-CCSD(T) level of theory, we compute $\Delta E_2 = 15.1$ kJ/mol using the $^1\Sigma_0^+$ geometry and $\Delta E_2 = 40.6$ kJ/mol, with two separate geometries. Since DC-CCSD(T) calculations are computational intensive, full geometry optimization were not feasible at this level of theory. We therefore had to choose geometries optimized at a different level of theory. The question then arises whether it is better to use either the ECP-CASPT2 or DKH-CASPT2 structures reported by Roos et al. [117] or to use the ZORA-DFT structures. The ECP-CASPT2 geometries differ most from the DFT ones so that a comparison of the difference between the two structures serves to give some indication about the sensitivity of the computed ΔE_2 to the optimization procedure.

As shown in Table 3.1, all bond distances optimized at ECP-CASPT2 level are slightly larger (about 0.01-0.03 Å) than those optimized with ZORA-DFT, with as exception the C-U bond in the singlet state that is nearly identical in the two methods. Table 3.1 shows that there is some influence of the choice of structure, about 8 kJ/mol on the ΔE_2, but this difference is small enough to not affect the conclusions drawn in this work. For the DC-CCSD core correlation calculations reported below we used the ECP-CASPT2 geometries.

Table 3.1: Adiabatic $\Delta E_2 = E(^3\Phi_2) - E(^1\Sigma_0^+)$ energies (kJ/mol) computed at different level of theory. The geometries labeled DFT are obtained by optimization of $^1\Sigma_0$ and $^3\Phi_2$ states at DFT/BPW91 level [127]; the ECP-CASPT2 geometries are taken from ref. [117]

Hamiltonian	SF-ZORA	DC	DC	DC	DC
method	DFT/BPW91	HF	CCSD	CCSD(T)	MRCCSD
ΔE_2 // DFT[a]	-2.9	-24.7	46.4	52.7	
ΔE_2 // CASPT2[b]	2.5	-36.8	34.3	40.6	34.3

[a]The bond lengths in the singlet geometry: O–U 1.808 Å and C-U 1.760 Å
The bond lengths in the triplet geometry: O–U 1.833 Å and C-U 1.865 Å
[b]The bond lengths in the singlet geometry: O–U 1.808 Å and C-U 1.772 Å
The bond lengths in the triplet geometry: O–U 1.842 Å and C-U 1.889 Å

3.4.2 Spin-Orbit coupling

In order to study the effect of SOC we first need to look closer at the electronic configuration of the CUO molecule. In Table 3.2 we list the DFT orbital energies obtained at DFT/BPW91 [127] and DFT/BPW91+SO level of theory for the singlet state. The orbital energy difference between a virtual orbital and the HOMO gives a first indication of the excitation energy [128]. We find a non-aufbau configuration with the ϕ LUMO lying lower than the HOMO. This does already indicate the near-degeneracy of the singlet and triplet states. Apart from the ϕ LUMO we find a δ orbital at low energy that is also largely a uranium $5f$-orbital, but with some $6d$ character. The antibonding σ and π orbitals lie at higher energy. Due to SOC all but the σ orbital energies are split into two levels and we find that the splitting between the $\phi_{5/2}$ and $\phi_{7/2}$ is large enough to influence the order of states.

We first performed DFT calculations similar to the work of Bursten et al. [110, 116, 129], to see whether use of the more accurate relativistic approximation, ZORA, instead of the quasi-relativistic Pauli approach would make any difference. This is not the case: the scalar results shown in Table 3.2 are consistent with the ones obtained by Andrews, giving a higher stabilization of the $^1\Sigma_0^+$ states over the $^3\Phi$ state of ΔE=12.6 kJ/mol. The $^3\Delta$ state formed by occupying the δ orbital lies also close in energy (ΔE=40.6 kJ/mol) while the other states ($^3\Sigma$ and $^3\Pi$) lie at much higher in energy, as expected. SOC is now considered by computing the energy of the lowest Ω states of a given multiplet. Since ADF cannot optimize structures when the SOC option is activated, we performed single point runs on the geometries obtained at the spinfree level assuming the SOC-induced structural effects are small. We see that

SOC indeed has a significant effect on the relative energies ranging from 1.5 kJ/mol for the $^3\Delta$ to 15.5 kJ/mol for ΔE_2. The latter shift brings the $^3\Phi_2$ below the $^1\Sigma_0^+$ state (ΔE_2=2.9 kJ/mol), which is in contradiction to the picture sketched to explain the experimental findings. However, the SOC-DFT calculations do not include spin-polarization, and their results have to be treated with caution.

Given this failure of the DFT approach to confirm the experimental picture we now examine the CUO molecule using ab initio methods. At the SFDC-HF level of theory (four component Hamiltonian, excluding SOC) we find the $^1\Sigma^+$ and $^3\Phi$ at approximately the same energy with ΔE=2.9 kJ/mol. With SOC the $^3\Phi_2$ state falls below the $^1\Sigma_0^+$ with ΔE_2=36.8 kJ/mol. From analysis of the orbitals from the SOC calculations we furthermore deduce that the $\delta_{5/2}$ orbital acquires 10% $\phi_{5/2}$ character, which is reasonable agreement with the 14% admixture of $^3\Delta_2$ state in the $^3\Phi_2$ state found in the multi-state CASPT2 calculations by Roos et al. [117].

The splitting between the $^1\Sigma_0^+$ and $^3\Phi$ states is larger than the 15.5 kJ/mol found at DFT level but both methods give the same qualitative picture. Inclusion of electron correlation effects is thus required to reach agreement with the experimental findings. We chose to use the DC-CCSD(T) approach, correlating initially 22 electrons and fixing the virtual orbital threshold at 10 au. At SFDC-CCSD(T) level of theory correlation lowers $^1\Sigma^+$ state relative to the $^3\Phi$ giving ΔE =79.9 kJ/mol. SOC again stabilizes the $^3\Phi_2$ but due to the larger initial difference the computed energy difference ΔE_2 remains now positive at 40.6 kJ/mol. The SOC splitting of 39.3 kJ/mol itself is almost identical to the 39.7 kJ/mol found in absence of correlation (Table 3.3). This tells us that the main difference between DFT and ab initio approach lies in the description of the correlation energy. The somewhat larger spin-orbit splitting found in the ab initio calculation may be due to the more compact ϕ spinor determined by the HF procedure, but is not decisive in explaining the observed difference. Decisive is the fact that the $^1\Sigma^+$ state is more stabilized by electron correlation that the $^3\Phi$ state.

A somewhat uncertain factor in the $^3\Phi$ CCSD calculation is the fact that, for technical reasons, we needed to use noncanonical orbitals that are optimized for the average energy expression of the four determinants describing both the singlet and the triplet coupled Φ states arising from the configuration $\sigma^1\phi^1$. In order to check possible artifacts arising from this approach we also carried out calculations at MR-CCSD level. This technique, based on the Fock-space method, allows us to compute electron affinities by adding one electron to a set of active virtual spinors. We can then compute ΔE_2 directly as the difference between the first and second electron of

Table 3.2: Composition and orbital energy eigenvalues (kJ/mol) of orbitals computed at the scalar and SOC ZORA-DFT level of theory. Only the most important contributions are listed.

		Composition (SF)			
	Symmetry	(%)	Type	Energy(SF)	Energy(SO)
LUMO+6	$\pi_{3/2}$	43	$5f_{z^2y}$(U)	-127.4	-107.1
		24	$7p_y$(U)		
		11	$2p_y$(C)		
		11	$2p_y$(O)		
LUMO+5	$\pi_{1/2}$	43	$5f_{z^2x}$(U)	-127.4	-145.7
		24	$7p_x$(U)		
		11	$2p_x$(C)		
		11	$2p_x$(O)		
LUMO+4	$\sigma_{1/2}$	55	$7s$(U)	-297.2	-298.2
		14	$2p_z$(C)		
		12	$6d_{z^2}$(U		
		6	$2p_z$(O)		
LUMO+3	$\delta_{5/2}$	91	$5f_{xyz}$(U)	-349.3	-321.3
		9	$6d_{xy}$(U)		
LUMO+2	$\delta_{3/2}$	91	$5f_z$(U)	-349.3	-365.7
		9	$6d_{x^2-y^2}$(U)		
LUMO+1	$\phi_{7/2}$	100	$5f_y$(U)	-417.8	-384.0
LUMO	$\phi_{5/2}$	100	$5f_x$(U)	-417.8	-446.7
HOMO	$\sigma_{1/2}$	39	$5f_{z^3}$(U)	-398.5	-396.6
		24	$2p_z$(C)		
		15	$7s$(U)		
		9	$6d_{z^2}$(O)		
HOMO-1	$\pi_{3/2}$	44	$2p_y$(C)	-482.5	-479.6
		34	$5f_{z^2y}$(U)		
		21	$6d_{yz}$(U)		
HOMO-2	$\pi_{1/2}$	44	$2p_x$(C)	-482.5	-492.1
		34	$5f_{z^2x}$(U)		
		21	$6d_{xz}$(U)		
HOMO-3	$\sigma_{1/2}$	32	$2p_z$(O)	-710.2	-709.2
		26	$5f_{z^3}$(U)		
		23	$2s$(C)		
		8	$6p_z$(U)		

Table 3.3: Comparison of computed energy differences (kJ/mol) relative to the $^3\Sigma_0^+$ energy for various GGA xc functionals [96,127,130–133]. In the SOC case we have chosen the triplet state with lowest value of Ω as indicated. The SOC values for the open-shell are unpolarized, thus they may be in error.

	BPW91 $^3\Sigma_0^+$	BPW91 $^3\Pi_0$	BPW91 $^3\Delta_1$	BPW91 $^3\Phi_2$	BLYP $^3\Phi_2$	PBE $^3\Phi_2$	RPBE $^3\Phi_2$	revPBE $^3\Phi_2$
SF	81.6	236.4	40.6	12.6	13.8	12.6	6.3	5.4
SOC	77.8	226.8	38.9	-2.9	-2.2	-2.4	-8.5	-9.2

CUO^+, where we take CUO^+ in its $^2\Sigma^+$ ground state that has one unpaired electron in the $\sigma_{1/2}$ spinor. Choosing as active virtuals: $\sigma_{1/2}$ and $\phi_{5/2}$, we obtain three electron affinities of CUO^+, relating to respectively the: $^1\Sigma_0^+$, $^3\Phi_2$ and $^3\Phi_3$ states. The advantage of this alternative Fock-space approach lies now in the fact that a more balanced description of the singlet and the triplet states is achieved, one cannot speak of true multireference CC as symmetry prohibits mixing of the three excited states. The MRCC results confirm the trend found in the single reference calculations giving a ΔE_2=34.3 kJ/mol.

3.4.3 Verification of the computed values

Since we are interested in a small energy gap we need to carefully examine all factors that may influence the outcome of the calculations. For the ab initio correlated calculations the finite size of the single particle basis set and the choice of active space are likely to be the most important sources of errors. For a DFT approach basis set truncation errors are usually marginal but the choice of the exchange-correlation functional may be crucial. We will examine the errors in both methods in the next section.

DFT method

xc functionals

We already looked at the choice of the Hamiltonian and saw that the ZORA approach gives values in agreement with a Pauli Hamiltonian. To verify that the choice of functional does not influence the qualitative picture drawn from the DFT calculations we computed ΔE at SOC-free level of theory using the various xc-functionals available in ADF (Table 3.3). All modern functionals give a small energy gap that is

usually positive but often somewhat smaller than with the older BPW91 functional: for example, the revPBE functional [96, 130] gives a difference of only 6.3 kJ/mol. Adding SOC gives the same trend as seen in the BPW91 calculation: the $^3\Phi_2$ state becomes the ground state.

Basis sets and frozen cores

Another feature that might change the results is the effect of the basis set and the frozen core on uranium. All previously reported calculations were performed at TZ2P level freezing all orbitals below the uranium 5*d* orbitals. To check basis set truncation and the frozen core error we also performed a calculation with a larger basis set: QZ4P and with no frozen core. This calculation gave ΔE=11.3 kJ/mol in good agreement with the ΔE=10.0 kJ/mol found in the smaller basis so we may conclude that basis set truncation errors are marginal.

CC and MR-CC method

Basis sets

For computational efficiency we have carried out most ab initio calculations using the medium sized basis set of de Jong and coworkers [125] that has no *g*- or *h*-functions. To check the validity of this choice, we also did calculations with the much larger Faegri set [126]that includes three *g* and one *h* functions.

In the computation of ΔE_2, we found that the $^3\Phi_2$ states benefits most from the increased flexibility of the basis set. At DC-HF level, the ΔE_2 is lowered by 5.0 kJ/ to 41.8 kJ/mol. At the correlated CCSD(T) level of theory we find that the energy gap, ΔE_2 , is decreased by 7.5 kJ/mol to 33.1 kJ/mol. Given the relatively small changes due to the basis set we, however, decided to continue to work with the smaller basis set of de Jong.

Active space

Previously we indicated that it is the correlation energy that is responsible for keeping ΔE_2 positive. We now want to investigate which spinors of the uranium atom should be taken active or, in other words, to see what the differential effect of core-valence correlation is. We did so by choosing three different active spaces still using a virtual orbital threshold of 10 au. This is in agreement with our rule of thumb that at least all virtuals that lie below 2 times the energy of the lowest occupied active orbital should be taken into account.

Table 3.4 shows that the CCSD(T) correlation energy brings ΔE_2 from 36.8 kJ/mol at DHF level to 58.2 kJ/mol in the largest active space (34e), a total relative shift of 95.0 kJ/mol. If only the valence shell spinors (12e in the active space)

Table 3.4: The compound energy differences (kJ/mol) relative to the $^1\Sigma_0^+$ energy for various *ab initio* approaches

		CCSD			CCSD(T)			MR-CCSD			CASPT2
	DHF	12e	22e	34e	12e	22e	34e	12e	22e	34e	
SF	2.9		74.1			79.9					10.5
SO $\Omega = 2$	-36.8	2.5	34.3	49.8	3.3	40.6	58.2	23.0	34.3	57.3	-39.7
SO $\Omega = 4$	33.1		121.3			102.9					

of the uranium atom are taken into account a relative shift of only 40.2 kJ/mol (42% of the total shift) is computed. The subvalence U_{6s}, U_{6p} and C_{2s} electrons contribute thus 37.2 kJ/mol (39%) to the relative difference in correlation energies and a non-negligible 19% is provided by the subvalence $5d$ orbitals of the uranium atom. It is well known that the $6p$ orbitals of the uranium are chemically active and the differential effect of this core-valence correlation contribution for two states with a rather large change in C-U bond length may therefore not be so surprising. It is interesting to note, however, that also the correlation of the $5d$ orbitals is important to get quantitatively correct results. Again we also checked the outcome by comparing with MR-CCSD calculations and found that the choice of reference spinors has some effect, but does not change the qualitative picture of the importance of core-valence correlation effects. This does not solve the puzzle posed by Roos and coworkers [117] who called the ground state of CUO a "mystery".

They compared the CASSCF and CASPT2 ΔE values and found a shift of 28 kJ/mol when correlating 34 electrons, with the CASPT2 correction decreasing ΔE_2 instead of increasing it as we find in the CC calculations. This remarkable difference in the effect of dynamic correlation should be due to the difference with our approach. In our calculations all correlation effects are described at the CC level, while the CASSCF calculations already accounts for nondynamic correlation. In our calculation there is no puzzle to be solved: a ΔE_2 of 58.2 kJ/mol fits with the experimental picture in which interaction with a number of Ar atoms is required to change the ground state.

3.5 Conclusions

It is difficult to produce quantitatively the small energy difference and ordering of the two lowest lying state of the CUO molecule. At SFDC-HF level of theory the two states $^1\Sigma^+$ and $^3\Phi$ are almost degenerate and we may distinguish the role of electron correlation and SOC on the relative energies of both states. Our results show that these two effects oppose each other. Correlation tends to stabilize the more compact singlet state by almost 100 kJ/mol more than it does in the triplet state. Core-valence correlation is important and is responsible for almost half of this difference. SOC gives a consistent energy splitting of the triplet state contribution that does not depend much on the method used to compute a splitting. It lowers the lowest component, the $^3\Phi_2$ by about 40 kJ/mol. Nevertheless the effect of correlation is large enough to keep the $^1\Sigma^+$ state as ground state. At the highest level of accuracy the difference is 58.2 kJ/mol. Such an energy difference agrees well with the experimental data in

which interaction with a number of heavier noble gas atoms (Ar or Kr) is required to reverse the order of the $^3\Phi_2$ and $^1\Sigma_0^+$ states.

This clear picture is not supported by other methods. Both ZORA-DFT and DKH-CASPT2 give a very small ΔE_2 that becomes negative upon inclusion of SOC. Whereas the ZORA-DFT results are difficult to analyze further it would be interesting to compare the DKH-CASPT2 approach with a similar approach based on two- or four-component orbitals that would allow for a more detailed characterization of the $^3\Phi_2$ state.

CHAPTER 4

The electronic structure of UO_2 revisited

> Teacher: Talk about your research, Napoleon...
> Napoleon Dynamite: Last week, Japanese scientists placed explosive detonators at the bottom of Lake Loch Ness to blow Nessie out of the water. Sir Godfrey of the Nessie Alliance summoned the help of Scotland's local wizards to cast a protective spell over the lake and its local residents and all those who seek for the peaceful existence of our underwater ally.
>
> *from the movie Napoleon Dynamite (2004)*

4.1 Abstract

The ground and excited states of the UO_2 molecule have been studied using a Dirac-Coulomb intermediate hamiltonian multireference coupled cluster approach [DC- IHF-SCC]. This method is unique in describing dynamical and non-dynamical correlation energies at relatively low computational cost, and allowed us to correlate in the active space 40 electrons, using 37 unoccupied Kramer pairs for the non-dynamical contribution. We included the 6*d* orbitals, that have so far been left out of the active space in theoretical descriptions. Spin-orbit coupling effects have been fully included by utilizing the 4-component Dirac-Coulomb Hamiltonian from the outset. Our calculations confirm the assignment of the ground state of this molecule as a $^3\Phi_{2u}$ state

that arises from the $5f^17s^1$ configuration. The first state from the $5f^2$ configuration is found above 10,000 cm^{-1}, whereas the first state from the $5f^16d^1$ configuration is found at 5,047 cm^{-1}.

4.2 Introduction

The study of small actinide molecules presents a challenge for experimental and theoretical chemists [116]. The nearly degenerate $5f$, $6d$, $7s$ and $7p$ orbitals gives rise to a multitude of possible configuration interactions and a dense manifold of low-lying states, which complicates computations and renders assignment of experimental spectra difficult. A joint effort of experimentalists and theoreticians is therefore needed to resolve the electronic structure of these systems. An example is the ionization potential (IP) of the UO_2 molecule, measured as 5.4 eV by Capone et al. [134] using the electron impact technique. Theoretical calculations [135] consistently gave a higher value. Gagliardi et al. [136], who had done accurate complete active space second order perturbation theory (CASPT2) calculations that gave an IP of 6.27 eV, proposed that the experimental data was in error. A new measurement by Han et al. [137], using enhanced multiphoton ionization (REMPI), gave a value of 6.13 eV, in very good agreement with the theoretical values.

Other aspects of these small actinide molecules are, however, less well understood, as different theoretical and experimental techniques give conflicting information. A particularly interesting aspect is the interaction of small actinide molecules with noble gas matrices. Laser ablation spectroscopy has been used by Andrews and coworkers to trap UO, UO_2 and CUO in noble gas matrices [2, 110, 112–115, 129, 135, 138–140] and measure vibrational frequencies as a function of the matrix composition (Ne, Ar, Kr, Xe or mixtures thereof). An intriguing feature of both CUO and UO_2 is the large red shift (about 130 cm^{-1}) in the antisymmetric stretch found when replacing a neon matrix by an argon matrix. Li, Andrews and coworkers suggested this is due to a change in the electronic ground state, and presented density functional (DFT) calculations indicating that a weak bond arises by donation of electron density of the noble gas into the empty uranium $6d$ orbitals in CUO and UO_2 [113, 140]. In argon and heavier noble gas matrices this bonding interaction is strong enough to change the ordering of the ground and first excited state, leading to the observed strong red shifts. A convincing argument was the very good agreement between the calculated and observed asymmetric stretch frequencies. Since in these initial DFT calculations the effect of spin-orbit coupling (SOC) was neglected, theoreticians

nevertheless questioned the validity of the simple picture presented. This spurred extensive theoretical work, notably by Gagliardi and Roos [117, 136, 141, 142], who applied the more sophisticated CASPT2 method and also studied the effect of SOC.

In CUO the two competing states are the uranyl-like closed shell state, with two formal triple bonds between uranium and carbon and oxygen, and a triplet in which the C-U bonding orbital and the uranium $5f_\phi$ orbital are singly occupied. The latter state has a longer CU bond length, allowing for a more effective interaction with a matrix than the singlet state. In argon this interaction is sufficiently strong to reverse the order of the two states, while in the more weakly interacting neon matrix the the ordering is the same as in the gas phase. This explanation of the large matrix effect is currently generally accepted for CUO, even though the CASPT2 calculations of Roos et al. [117] gave the triplet $^3\Phi$ at slightly lower energy in the gas phase. Our previous work [143] using the Dirac-Coulomb coupled cluster method, DC-CCSD(T), as well as later CASPT2 work by Vallet [144], give the closed shell state as ground state in the gas phase, in agreement with the original picture. More important is that all methods predict small energy differences between the two states in the gas phase, and do not invalidate the explanation given by Andrews et al.

The situation is more complicated for the UO_2 molecule. Likely candidates for the ground state are the $5f^1 7s^1\ ^3\Phi_u$ and $5f^2\ ^3H_g$ states. These states differ in occupation of the $5f_\delta$ orbital (the ^3H_g state) versus the $7s$ orbital (the $^3\Phi_u$ state). Both orbitals are nonbonding but the $7s$ orbital is more diffuse, leading to stronger and shorter bonds in the $^3\Phi_u$ state. Vibrational spectroscopy gives an asymmetric stretch in the Ne matrix of 915 cm^{-1} vs. 776 cm^{-1} in the Ar matrix [2,135,145], which suggests that also the ground states of UO_2 varies with the matrix. Bonding of the noble gas atoms to the ^3H_g state would not only be favored by the longer bond length of that state, but also by the lack of repulsive interaction with the electron in the $7s$ orbital. This picture is corroborated by DFT calculations [140] of vibrational frequencies for gas phase UO_2. The $5f^1 7s^1\ ^3\Phi_u$ and $5f^2\ ^3H_g$ states match the experimental frequencies in the neon and argon matrices, respectively. In this case there is, however, additional experimental data available. Heaven and coworkers carried out electron spectroscopy in gas phase [137, 146, 147] and in Ar matrices [148]. These experiments, using the resonantly enhanced multiphoton ionization (REMPI) technique in the gas phase and electronic emission spectroscopy in the matrix, do not indicate a reordering of the states. Both the gas phase and matrix spectra can only be rationalized by assuming that the first excited state lies slightly above the ground state (360 cm^{-1} in the gas phase, 408 cm^{-1} in the argon matrix) and has the same parity. This fits well with

the assignment of the ground state as the lower components of the spin-orbit split $^3\Phi_u$ state. SOC is rather large, leading to significant admixture of $^3\Delta_u$ character in both the $2u$ ground state and the $3u$ first excited state (better described in a jj-coupling picture as pure $5f^1_{5/2}7s^1_{1/2}$ states). Actual calculations on gas phase UO_2 by Chang [149], Gagliardi [136, 142] and Fleig [150] reproduce this splitting well. The manifold of SOC-split gerade states does not have two so closely spaced states at low energy. If the ^3H_g state would be the lowest state in the argon matrix, the next gerade state would be expected to lie several thousand cm^{-1} higher. Han et al. [137] and later Gagliardi et al. [136] discussed the difficulties in explaining both experimental findings but could not present definite theoretical or experimental data to settle the issue of matrix induced ground state swapping.

A survey of the theoretical and experimental data that is available leads to more questions. For example, the third and fourth excited states in the argon matrix [148] lie, experimentally, at 1094 and 1401 cm^{-1}, whereas the CASPT2 values [142] are, respectively, 2567 and 2908 cm^{-1}, about 1500 cm^{-1} off. Is this large discrepancy caused by the differences induced by the argon matrix, by deficiencies in the calculation, such as limits on the size of the active space used, or by both? The generalized active space configuration interaction (GASCI) results by Fleig et al. [150] agree better with experiment and with older spin orbit configuration interaction (SOCI) calculations of Chang [149], but both calculations were done in rather modest basis sets and could suffer from basis set incompleteness errors. It is therefore clear that more theoretical work is desirable.

Accurate calculations of the quasidegenerate states of UO_2 and similar actinide systems, where d and f orbitals belong to the valence space, are extremely difficult. First principles methods aimed at such systems should not only be based on size-extensive, size-consistent and balanced treatment of the dynamic and nondynamic correlation effects, but also include the relativistic effects on equal footing from the outset. The aim of our paper is to reanalyze the UO_2 molecule using one of the most advanced tools in the arsenal of quantum chemistry, which satisfies all these requirements, the relativistic multereference coupled cluster method. We intend to substantially increase the accuracy of calculations using a more precise relativistic Hamiltonian, larger basis sets, a larger active space, correlating more electrons and more virtual spinors, compared to CASSCF/CASPT2 [142] or GASCI [150] . In this way, we want to attain higher accuracy at all stages of the calculations, adding missing parts of relativistic, correlation and basis set effects via the relativistic Fock-space coupled cluster (FSCC) method [1] and its intermediate Hamiltonian modifications.

This should give us a level of accuracy not reached before, by a method tested already for the computation of the spectrum of some heavy and super-heavy atoms [83, 151]. An advantage of our approach is its relatively low computational cost, allowing for use of active spaces that include all relevant orbitals. The largest calculation performed in the current work had 41 Kramer pairs in the P part of the active space. The method scales, like regular coupled cluster, as N^6 in the number of correlated electrons, N. This scaling is sufficiently low to make calculations on UO_2 surrounded by one or more argon atoms feasible in the near future. Such calculations were, however, not possible with the computers currently available to us.

4.3 Methodology

All-electron single- and multi-reference correlated calculations were done utilizing a locally modified version of the DIRAC04 program [48]. The relativistic 4-component Dirac-Coulomb (DC) Hamiltonian [74,121] includes SOC from the outset, so that mixing of orbitals with different orbital angular momenta occurs already at the Hartree-Fock (HF) level. This makes it possible to use shorter wave function expansions than in methods in which SOC is treated as a perturbation at the configuration interaction stage of the calculation. To facilitate analysis, and for comparison with more conventional approaches, we also used the spin-free modified DC (SFDC) Hamiltonian [152], in which SOC is projected out, leaving only the scalar relativistic effects in a 4-component framework. For the correlated calculations we used two different methods: a single-reference relativistic coupled cluster with explicit inclusion of single and double excitations and perturbative treatment of triples [DC-CCSD(T)] [73, 153], and the multi-reference (Fock-space) [DC-FSCC] approach [1].

All correlated runs were performed in linear symmetry, $D_{\infty h}$. The basis set on the oxygen atoms is the uncontracted cc-pVTZ [122–124] basis. For the uranium atom we used an all-electron dual family $26s21p17d12f$ basis set by de Jong [125], as well as the larger $33s29p21d15f3g1h$ even-tempered basis set provided by Faegri [126], both found to be sufficiently accurate in the study of the CUO molecule. The convergence of the calculated excitation energies with basis set size was checked by adding diffuse functions to the Faegri basis (see below). In most of the calculations we correlated the 24 electrons that occupy the $6p$ orbitals of the uranium atom and the formally fully occupied $2s$ and $2p$ orbitals of the oxygen atoms. The stability of the results with number of electrons correlated was tested by including the U $6s$ and $5d$ shells in some benchmark calculations. The last two electrons in the valence shell were treated

differently in the single reference and multireference approaches. In the former, open shell orbitals were generated by a restricted Hartree-Fock method that averages the energy expression of the lowest $5f7s$ or $5f^2$ open shell singlet and triplet (borrowing the nomenclature from nonrelativistic work; a more accurate description is that we place one electron in each of the two highest occupied Kramers spinor pairs). The CC calculation is then carried out with a $|5f_{5/2}7s_{\pm 1/2}|$ reference determinant corresponding to the lowest state. This method is valid since, in contrast to approaches in which SOC is added a posteriori, the single determinants $|5f_{5/2}7s_{\pm 1/2}|$ and $|5f_{5/2}5f_{3/2}|$ provide good first approximations to the 2_u, 3_u and 4_g states.

This single reference approach is complemented by the genuinely multireference Fock-space approach [1], in which we start from a common closed shell reference determinant of the UO_2^{2+} molecule, then add two electrons successively in sectors (0,1) and (0,2). A full CI (P-space diagonalization) is performed in the selected Fock-space valence sectors, in order to obtain the non-dynamical correlation energy and the multi-reference wave function characteristics of each excited state. The choice of the model space, P, is nontrivial, because one needs to find a balance between accuracy and the ease of convergence of the CC equations. The largest P space for which the traditional FSCC scheme can be converged comprises the $7s$, 2 of the 5 $5d$ and 6 of the 7 $5f$ spinors, excluding the higher lying $5f_{\sigma_{1/2}}$. Further increase of the model space is not possible, because it leads to intruder states, in particular in sector (0,2). A recent improvement of the FSCC method, which alleviates the intruder states problem in many cases, is given by the intermediate Hamiltonian (IH) approach [83–85, 151]. In the IH approaches the P space is partitioned into two subspaces, the main P_m and intermediate P_i, providing an effective separation between the low-lying P_m and the complementary Q space and eliminating intruder states. An intermediate Hamiltonian in P is then constructed, giving exact solutions only for states whose main components are in P_m. The other eigenvalues, dominated by the intermediate (P_i) components, are less accurate. The flexibility resulting from the less stringent requirements on H_{eff} may be used to formulate special conditions on problematic $P_i \rightarrow Q$ transitions (those affected by intruder states), which resemble but are not identical with the Bloch equation. Several such IH schemes, based on different $P_i \rightarrow Q$ conditions, have been implemented in the framework of the relativistic multireference Fock-Space coupled cluster atomic code. The IH approach allows the use of very large model spaces, much larger than in traditional FSCC, yielding converged results for many states not accessible by the latter. Moreover, states calculated by both schemes exhibited much better accuracy in the intermediate Hamiltonian approach [83–85,

151]. Two particular intermediate Hamiltonian schemes, tested in atomic calculations [85,154], have recently been implemented in the framework of the molecular relativistic DIRAC code. The scheme employed here uses a very simple condition on the $P_i \rightarrow Q$ transition amplitudes of the wave function operator, equating them to zero, which makes the scheme easy and efficient to use. More advanced schemes [155] that require a sequence of calculations, like the novel extrapolated intermediate Hamiltonian (XIH) method, are implemented as well but were not used in this work.

Large P_i spaces facilitate the convergence and improve results for P_m states. P_i should include at least all intruders relative to the selected P_m. Here we started from the simplest model spaces, with P_m coinciding with the FSCC P space, and systematically extended this space to check for convergence of the calculated spectrum.

To determine the equilibrium geometry of the ground state we performed IHFSCC calculations using an evenly spaced (0.005 Å) grid of U-O bond distances, spanning the range from 1.680 Å to 1.840 Å. Since IHFSCC provides the energy of all states in one calculation, we thus obtained not only the equilibrium geometry of the ground state but that of many excited states as well. These data are used to compute adiabatic excitation and ionization energies.

4.4 Results and Discussion

4.4.1 Orbital composition and UO_2^+

In Figure 4.1 we sketch orbital energy and electron affinity diagrams of UO_2^{2+} in the spin-free (SFDC) and full (DC) Dirac-Coulomb approximations. We chose the uranyl, UO_2^{2+}, orbital energies, because these present the first step in the Fock-space calculation and give a conceptually simple interpretation of the spectrum of singly ionized UO_2. There is an extensive literature on the uranyl molecule, which is famous for assuming a closed-shell configuration despite the complexity of the heavy element involved. Most of the discussion centers on the nature of the bonding orbitals, in particular on the existence of the so-called $6p$ hole, which arises due to the participation of $6p$ in bonding. In this paper, we are not so much interested in the occupied molecular orbitals, but rather in the the composition of the virtual ones, which become occupied in the excited states.

If we assign a formal oxidation state of +6 to uranium and compute the orbital energies using HF, we find that the lowest unoccupied orbitals appear in the order $5f$, $6d$, $7s$, and $7p$. In uranyl the order is changed due to the splitting induced by the oxo ligands, that makes the $5f$ and $6d$ manifolds overlap and places $7s$ slightly below $5f$

Figure 4.1: The energy affinities of the $5f$, $7s$, $6d$ and $7p$ orbitals have been sketched for the UO_2^{2+} molecule. On the left, the spin-free and spin-orbit coupling contributions calculated at DC-HF level. On the right, the more accurate values from sector (0,1) of the IHFSCC calculations are given. The correlated space for dynamical energy was (24e/6au), while the P model space was (17g,20u) with 7p's orbitals included in the P_m. All these calculations were performed with the Faegri basis set. The bond distance is 1.770 Å.

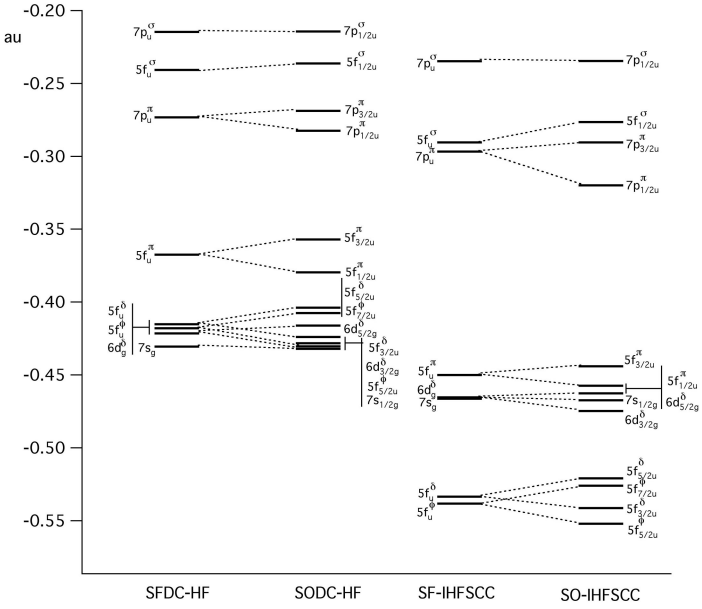

as the LUMO. This crude Koopmans estimate is improved by the IHFSCC method, which gives correlated electron affinities. These are listed in Figure 4.1, where we see a lowering of the $5f$ manifold that fits with experimental evidence that the unpaired electron resides in the $5f_\phi$ orbital. Inclusion of SOC is important, because it produces a splitting of the same order as the crystal field splitting. This strong SOC effect is also reflected in the composition of the $5f$ orbitals. The lower $5f_{5/2}$ orbital can be described as 87% $5f_\phi$ and 13% $5f_\delta$, while the upper $5f_{5/2}$ orbital is 13% $5f_\phi$ and 87% $5f_\delta$. Given these rather large admixtures, it is clear that a jj-coupling picture is appropriate.

One advantage of the Fock-space method is that the calculation of UO_2 energies also gives the energies for the UO_2^+ and UO_2^{2+} ions. We compute the UO_2^+ energies as electron affinities of uranyl, and thus obtain the ionization energy of UO_2 (calculated

in this model as the second electron affinity) by subtracting the energy of the lowest UO_2^+ state from that of the lowest UO_2 state. This procedure gives an adiabatic value of 5.92 eV, taking equilibrium bond distances of 1.770 Å for UO_2 and 1.739 Å for UO_2^+. This value is significantly below the experimental value of 6.13 eV [137]. A possible reason could be the fact that the neutral molecule is decribed using the orbitals from the dication, with orbital relaxation only accounted for in the CC calculation, thus biasing the cation, for which orbital relaxation effects should be smaller. This common orbital effect is small, as can be seen by comparing the vertical ionization energy of 5.97 eV computed with FSCCSD with the values obtained by DC-CCSD and DC-CCSD(T), 6.00 eV and 6.04 eV, respectively. These values agree well with to the CCD result of 6.01 eV reported by Balasubramanian [156] indicating that CC type methods tend to underestimate the ionization energy of UO_2.

The IHFSCC second ionization energy is 14.63 eV, which lies within the interval 12.8 – 18.0 eV that was estimated by Cornehl et al. [157] on basis of thermochemical data. Cornehl et al. also performed pseudopotential coupled cluster calculations that gave an ionization energy of 15.0 eV but argued that this value is probably smaller than the exact value. Our calculations as well as the CASPT2 calculations (14.36 eV, see reference [142]) give a value considerably below 15 eV, however, and do not support that assumption.

4.4.2 Basis-set convergence

Electron correlation calculations require large and flexible basis sets. In relativistic calculations including SOC effects it is convenient to employ uncontracted scalar basis sets to describe the spin-orbit split components of a given shell equally well. We considered the economical de Jong basis set [125] (deJong) and the larger Faegri basis set [126](Faegri). The Faegri set contains $3g$ and $1h$ polarization function; to check the sensitivity of the results to this aspect we also performed calculations with a set, denoted Faegri2, in which we replaced the original set of $3g1h$ polarization functions by the $5g2h$ set developed by the MOLCAS group [142] A shell of diffuse functions (with exponents s: 0.016, p: 0.013, d: 0.0211, f: 0.0726) were furthermore added to each of the s, p, d, f shells in these sets, to obtain our largest bases (Faegri+ and Faegri2+). Figure 4.2 displays the effect that the choice of basis has on the computed spectrum.

The $5f \rightarrow 5f$ transitions in the region 0–9,000 cm^{-1} are not very sensitive to the basis set, with excitation energies differing by at most 300 cm^{-1}. These excitation energies are well described in all sets. The $7s \rightarrow 5f$ transitions span the region from

Figure 4.2: The effect of the the basis-set size has been given. Polarization and diffuse functions have been added to the standard Faegri basis-set to obtain Faegri2 and Faegri+. For sake of comparison we also sketched the excitation energies of the low-level de Jong basis set. In all the runs, the dynamical correlation energy was accounted by a selection of the (24e/6au) correlated space; the static correlation energy was computed by choosing the (17g,20u) P model space with the 7p's included in the P_m. The bond distance is 1.770 Å.

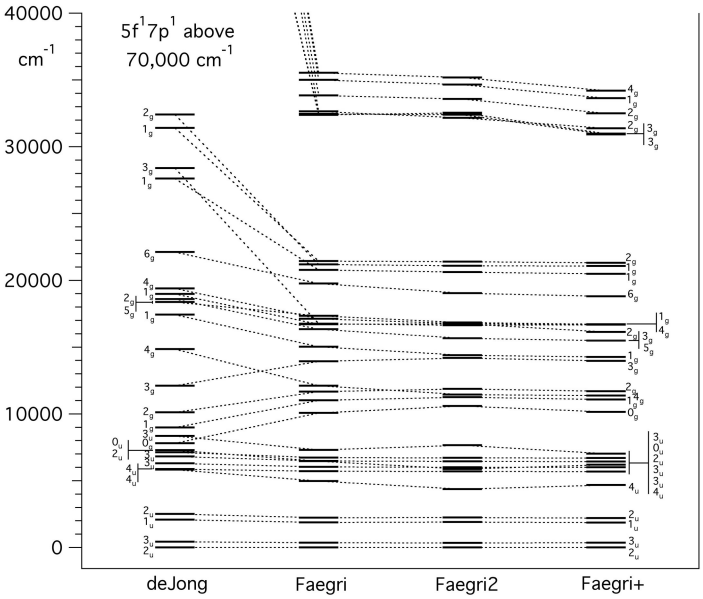

9,000 to about 30,000 cm^{-1} and are well described by the Faegri sets, but not by the unpolarized de Jong basis set. The extension of the original Faegri set does not lead to large changes in this region, with differences of 500 cm^{-1} (0.06 eV) at most. Such extensions are of some importance in the region above 30,000 cm^{-1} where the description of the $7p$ orbital is important. The de Jong basis is again not suitable for this purpose, but also the Faegri set requires additional diffuse functions to reach a converged result. The replacement of the $3g1h$ set of polarization functions by the more extensive $5g2h$ set has little effect on the transition energies.

We conclude that the deJong basis can be used for calculations that do not probe the $7p$ shells, like on uranyl or the isoelectronic CUO molecule, but is inadequate for the higher excited states of neutral UO_2. The $7s$ to $5f$ transitions are well represented

by the standard Faegri set, while the higher $5f^17s^1 \rightarrow 5f^17p^1$ transitions require additional diffuse functions (Faegri+).

4.4.3 Active space convergence

Number of electrons correlated. The importance of core-valence interactions is demonstrated in Fig.4.4.3. that depicts the changes in the spectrum upon increasing the number of electrons that is correlated and/or decreasing number of virtual orbitals that is deleted. Following our usual rule of selecting all virtual orbitals within minus two times the energy of the lowest occupied orbital, we specified a 6 a.u. threshold for inclusion of virtual orbitals for the correlation of 14 or 24 electrons. To estimate the contribution of higher, core-like virtuals, we also did calculations in which we increased this threshold to 10 and 100 au. When the inner $5d$ and $5p$ were also correlated, a large threshold of 200 a.u. was chosen to include all relevant correlating orbitals.

The smallest ansatz, which includes only the 14 electrons in the bonding $\sigma_{1/2_u}$, $\pi_{1/2_u}$, $\pi_{3/2_u}$ and $\sigma_{1/2_g}$ orbitals (mainly localized at the oxygen atoms), gives the lowest excitation energies already in good agreement with larger active spaces (differences are at most 200 cm^{-1}). Larger differences are, however, found in the higher regions, where errors may amount to as much 6,000 cm^{-1}, if we correlate only 14 electrons. This can be rationalized by realizing that core-valence correlation is more important for the compact $5f$ and $6d$ orbitals than for the diffuse $7s$ orbital. The $6p$ orbitals of uranium are important in this respect and give the major differential correlation contribution. Inclusion of the $5d$ orbitals is less important, although correlation of these core orbitals still changes the spectrum by about 1,000 cm^{-1} (0.06 eV) for some transitions.

P_m model space. As anticipated, many of the states of the UO_2 molecule show near degeneracies that are not well described by single-reference approaches. The Fock-space method does describe this kind of nondynamical correlation, but the results depend on the size and partitioning of the P model space chosen. The spectra resulting from four different choices are depicted in Figure 4.4: (a) a (3g, 29u) P space, in which P_m contains all important ungerade orbitals at the expense of leaving out most of the $6d$ orbitals; (b) a more balanced (17g, 20u) P space, in which P_m consists of the $7s$, $6d_\delta$ and all of the $5f$, with the exception of the high lying $5f_\sigma$; (c) the same P space, but including the $5f_\sigma$, the $6d_\pi$ and $7p$ orbitals in P_m instead of P_i; (d) an enlarged P space, with P_m including also the $8s$, $8p$ orbitals.

The first feature that we notice is that all four P spaces give qualitatively the same

Figure 4.3: Different correlated space have been chosen to compute the dynamical correlation energy. The effect of the cutoff of the virtual space has been tested by correlating 24 electrons. A bigger calculation with 40e/200au has been used as reference. All these runs were performed with the Faegri basis set and the P model space for computing the static correlation energy equals was the (17g,20u) with 7p's included in the P_m. The bond distance is 1.770 Å.

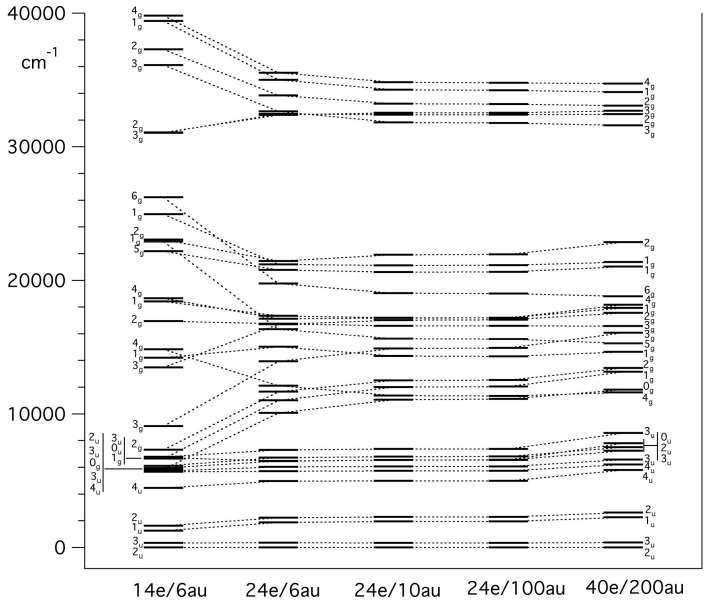

ordering. The manifolds of states that arise from the different configurations do not shift much in energy relative to each other, although inclusion of the $7p$ orbitals in P_m has of course a large effect on the $5f^17p^1$ states that can only be reliably calculated in the last two model spaces. The inclusion of the $7p$ in the P_m space does also leads to some reordering of states within the $5f^2$ manifold, that mix with the $5f^17p^1$ states. In the most accurate model (d) the excitations to the $7p$ are found starting from 30,000 cm^{-1} and seem reasonably well converged with respect to extension of the model space, given the differences of at most 800 cm^{-1} between model spaces (c) and (d).

Model space (c), correlating 24 electrons with a virtual orbitals cutoff value of 6 a.u., and including (51g,43u) inactive virtual orbitals was chosen to compute excitation energies as functions of U-O bond distance and determine equilibrium bond

Figure 4.4: The static correlation energy has been computed by choosing different partitioning of the P model space. The effect on the excitation energies has been plotted. All the calculations were performed with Faegri basis-set quality and a correlated space of (24e/6au). The bond distance is 1.770 Å.

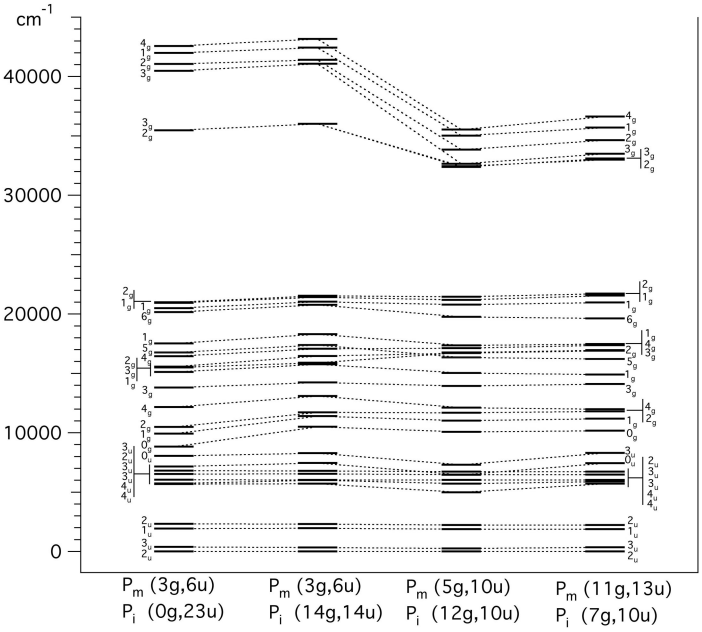

distances, vibrational frequencies, and adiabatic excitation energies.

4.4.4 Analysis of the excited states: scalar relativistic results

The spin-free Dirac-Coulomb (SFDC) approach facilitates comparison of 4-component calculations with scalar relativistic results obtained by the Douglas-Kroll-Hess and Effective Core Potental approaches, as the method eliminates all SOC effects in the calculation. In Table 4.1 we show the values of the excitation energies up to 35,000 cm^{-1} in the SFDC-FSCC model. To guide the eye we have grouped states that arise from primarily the same configuration together. Configurations of interest, for the interpretation of the experimental spectroscopic data, are $5f^1 7s^1$, $5f^2$, $5f^1 6d^1$, and $5f^1 7p^1$. The $7s^2\ ^1\Sigma_g^+$ state appears also at low energy, but cannot be easily reached from the ground state and should have a strongly repulsive interaction with noble gas atoms in a matrix. From the composition of the excited states, obtained by analyzing

Table 4.1: The excitation energies at IHFSCC level are given at our best level of approximation for the Spin Free case with 24 electrons correlated and 6 au as the threshold for the virtual space. The bond distance for our calculation is 1.770 Å using the Faegri basis set. The P model space is (17g, 20u) with the 7p orbitals included in the P_m. The composition of each state is based on the type of orbitals that occupy the open and closed shell configurations, and are not referred to determinants. CASPT2 values [142] are also given at 1.827 Å. The full manifold of excited states up to 32,000 cm^{-1} is shown.

Sym	Excited States		
	CASPT2 [142]	IHFSCC 24e Fægri	Composition
$^3\Phi_u$	0	0	97% $(5f_\phi 7s)$
$^3\Delta_u$	1,990	575	97% $(5f_\delta 7s)$
$^1\Phi_u$	991	826	100% $(5f_\phi 7s)$
$^1\Delta_u$	2,852	1,300	100% $(5\bar{f}_\delta 7s)$
$^1\Sigma_u^+$		5,544	100% $(5f_\delta 6d_\delta)$
^3H_u		6,038	100% $(5f_\phi 6d_\delta)$
$^3\Gamma_u$		7,250	100% $(5f_\delta 6d_\delta)$
$^3\Sigma_u^-$		7,508	100% $(5f_\delta 6d_\delta)$
$^1\Sigma_g^+$	22,119	7,549	83 $(7s7s)$, 14% $(6d_\delta 6d_\delta)$
$^3\Pi_u$		9,193	97% $(5f_\phi 6d_\delta)$
$^3\Delta_g$		9,760	91% $(7s6d_\delta)$
^1H_u		9,910	94% $(5f_\phi 6d_\delta)$
$^3\Sigma_u^+$		10,244	97% $(5f_\delta 6d_\delta)$
$^1\Gamma_u$		11,101	100% $(5f_\delta 6d_\delta)$
^3H_g	5,954	12,863	97% $(5f_\phi 5f_\delta)$
$^1\Sigma_u^-$		13,815	100% $(5f_\delta 6d_\delta)$
$^1\Gamma_g$	11,921	13,865	32% $(5f_\delta 5f_\delta)$ + 30% $(5f_\phi 5f_\pi)$ + 28% $(6d_\delta 6d_\delta)$
$^3\Sigma_g^-$	7,271	13,926	50% $(5f_\phi 5f_\phi)$ + 30% $(5f_\delta 5f_\delta)$ + 18% $(6d_\delta 6d_\delta)$
$^3\Pi_u$	12,645	14,789	97% $(7s5f_\pi)$
$^1\Delta_g$		14,865	52% $(7s6d_\delta)$ + 20% $(5f_\phi 5f_\pi)$ + 20% $(5f_\phi 7p_\pi)$
$^1\Pi_u$		15,459	100% $(5f_\phi 6d_\delta)$
$^3\Sigma_g^-$	15,549	15,526	55% $(5f_\delta 5f_\delta)$ + 42% $(6d_\delta 6d_\delta)$
$^3\Pi_g$	9,076	15,574	88% $(5f_\phi 5f_\delta)$ + 8% $(5f_\pi 5f_\delta)$
$^1\Sigma_g^+$	12,164	16,331	58% $(5f_\phi 5f_\phi)$ + 20% $(5f_\delta 5f_\delta)$ + 11% $(6d_\delta 6d_\delta)$
$^1\Pi_u$	14,320	16,824	87% $(7s5f_\pi)$ + 8% $(5f_\pi 6d_\delta)$
$^1\Pi_g$	13,106	17,410	80% $(5f_\phi 5f_\delta)$ + 8% $(5f_\delta 5f_\pi)$ + 8% $(5f_\delta 7p_\pi)$
$^3\Gamma_g$	14,262	18,529	54% $(5f_\phi 5f_\pi)$ + 44% $(5f_\phi 7p_\pi)$

Table 4.2: Continuation of Table 4.1

Sym	Excited States		
	CASPT2 [142]	IHFSCC 24e Fægri	Composition
$^3\Phi_g$	17,625	19,373	52% $(5f_\delta 5f_\pi)$ + 44% $(5f_\delta 7p_\pi)$
$^3\Delta_g$	14,472	19,418	49% $(5f_\phi 5f_\pi)$ + 43% $(5f_\phi 7p_\pi)$
$^1\Sigma_g^+$		20,237	66% $(5f_\delta 5f_\delta)$ + 24% $(6d_\delta 6d_\delta)$
$^3\Pi_g$	20,676	20,518	52% $(5f_\delta 7p_\pi)$ + 37% $(5f_\delta 5f_\pi)$
$^3\Phi_u$		21,486	100% $(5f_\pi 6d_\delta)$
$^1\Phi_g$	23,117	21,551	65% $(5f_\delta 7p_\pi)$ + 30% $(5f_\delta 5f_\pi)$
$^1\Pi_g$	22,081	21,709	52% $(5f_\delta 7p_\pi)$ + 24% $(5f_\delta 5f_\pi)$ + 16% $(5f_\phi 5f_\delta)$
$^1\Delta_g$	17,816	22,015	34% $(5f_\delta 7p_\pi)$ + 30% $(6d_\delta 7s)$ + 28% $(5f_\phi 5f_\pi)$
$^1\Gamma_g$		22,440	44% $(5f_\phi 5f_\pi)$ + 44% $(5f_\delta 5f_\delta)$
$^3\Pi_u$		22,598	100% $(5f_\pi 6d_\delta)$
^1I_g	22,337	23,931	97% $(5f_\phi 5f_\phi)$
^1H_g	20,949	24,396	50% $(5f_\phi 5f_\delta)$
$^1\Phi_u$		24,564	83% $(5f_\pi 6d_\delta)$
$^1\Pi_u$		24,587	92% $(5f_\pi 6d_\delta)$
$^1\Gamma_g$		25,109	56% $(6d_\delta 6d_\delta)$ +34% $(5f_\delta 5f_\delta)$
$^3\Sigma_g^+$		26,246	52% $(5f_\phi 5f_\phi)$ + 25% $(6d_\delta 6d_\delta)$ +17% $(5f_\delta 5f_\delta)$
$^1\Sigma_g^+$	30,157	31,858	40% $(5f_\phi 5f_\phi)$ + 18% $(5f_\pi 5f_\pi)$ +16% $(6d_\delta 6d_\delta)$
$^3\Phi_g$	36,917	32,089	90% $(5f_\phi 7p_\sigma)$
$^1\Phi_g$	37,518	32,277	90% $(5f_\phi 7p_\sigma)$

the eigenvectors of the effective Hamiltonian, we see that many states show significant configurational mixing. Comparison with the CASPT2 relative energies given by Gagliardi et al. [136] shows close agreement between the two methods with respect to singlet-triplet splittings and, in general, all differences between states that arise from the same configuration. The striking difference in the $^3\Phi_u$-$^3\Delta_u$ vertical excitation energy can be explained by considering the large difference in bond distances used in the two calculations. The CASPT2 calculations were done at 1.827 Å, while the Fock space calculations were done at 1.770 Å. Recalculating the vertical excitation energy at 1.827 Å gives 1219 cm^{-1}, in much better agreement with the CASPT2 value.

From Table 4.1 it is, however, also clear that there are large discrepancies between the methods for energy differences between states that come from different configurations. The FSCC energy of the $5f^2\ ^3H_g$ state relative to the $5f^1 7s^1\ ^3\Phi_u$ ground state

is again smaller (11,989 cm^{-1}) at the longer CASPT2 bond length, but remains much higher than the CASPT2 excitation energy of 5,954 cm^{-1}. In general we find states with primarily $5f^2$ character at rather high energies, sometimes heavily mixed with low-lying $5f^17p^1$ and $6d^2$ states. The first state with significant $5f^17p^1$ character, the $^1\Delta_g$, appears at 14,865 cm^{-1} above the ground state.

The ^3H_g excitation was considered important for the reasons we have outlined in the introduction. Li et al. [140] have shown that at the ECP-CCSD(T) level of theory on UO_2(Ar), the ^3H_g is sufficiently low in energy that the effect of spin-orbit coupling could be strong enough to change the ground-state. Gagliardi et al. [142] also do not disregard this possibility, but point out that this would make it very difficult to interpret the fluorescence and REMPI data of Heaven and coworkers [137, 148]. The relative energy of the $5f^2$ ^3H_g state, as calculated by the SFDC-IHFSCC is in qualitative disagreement with these results, as the energy gap with the ground state is too large to make matrix-induced ground state switching probable.

Our calculations include, however, the $5f^16d^1$ states that have not been studied so far, and which could also be of importance to explain the experimental findings. We find the lowest state from that manifold, the ^3H_u state, just 6,000 cm^{-1} above the ground state. This small energy difference makes it likely that the ^3H_u state plays a role in the chemistry of UO_2. Important is furthermore that transition to the ground state is parity forbidden so that the state might have a sufficiently long lifetime to present an alternative for the suggestion of Gagliardi [142] that the older experimental value of the ionization potential (5.4 eV) could be due to ionization from a metastable excited state. She proposed that this would be the ^3H_g state, which would be thermally populated in the production of UO_2 in a laser ablation process. Our results indicate a similar possibility, but now based on thermal population of the ^3H_u state, followed by ionization from the $6d_\delta$ orbital.

A more detailed analysis of all aspects of the available spectroscopic data requires of course the introduction of SOC, which will perturb the relatively simple scalar relativistic picture sketched above. We will discuss this aspect in the next section.

4.4.5 Analysis of the excited states: the spin orbit (SODC) case

Adding SOC, or rather, not switching it off in our calculations, leads to a much more crowded manifold of states below 35,000 cm^{-1} (see Table 4.3). To reduce the number of entries in the table we use the dipole selection rules and consider only the allowed u $\rightarrow$ g and $\Delta\Omega$=0,$\pm$1 excitations, with the exception of the higher components of the

Table 4.3: The excitation energies at IHFSCC level are given at our best level of approximation with 40 electrons correlated and 45 au as the threshold for the virtual space. The P model space is (17g, 20u) with the 7p orbitals included in the P_m. The basis set used was a Faegri2+ at a bond distance of 1.770 Å . The composition of each state is given in percentage. Single reference CCSD and CCSD(T) transition energies are computed with 24 electrons in the active space and a threshold of 6 au. Only the excited states that satisfy the selection rule $\Delta\Omega = 0, \pm 1$ have been selected, with the exception of the first 5_g, 6_g, 5_u and 6_u states. All states composed by double excitations have been also removed. Only the experimental values that can be unambiguously determined are shown in the Table.

Sym	Excited States							
	Exp. [137, 148]	GASCI [150]	CASPT2 [142]	CCSD 24e Fægri	CCSD(T) 24e Fægri	IHFSCC 24e Fægri	IHFSCC 40e Fægri2+ +spdf	Composition
2_u	0	0	0	0	0	0	0	97% $\|5f_{\phi,5/2u}7s_{\sigma,1/2g}\|$
3_u	360	427	378	417	384	348	368	96% $\|5f_{\phi,5/2u}7s_{\sigma,-1/2g}\|$
1_u	1,094[a]	1,089	2,567	1,841	2,052	1,877	2,231	98% $\|5f_{\delta,3/2u}7s_{\sigma,1/2g}\|$
2_u	1,401[a]	1,542	2,908	2,224	2,421	2,224	2588	96% $\|5f_{\delta,3/2u}7s_{\sigma,1/2g}\|$
4_u				3,079	3,521	4,975	5,047	98% $\|5f_{\phi,5/2u}6d_{\delta,3/2g}\|$
4_u						5,706	6,148	97% $\|5f_{\phi,7/2u}7s_{\sigma,1/2g}\|$
3_u						6,028	6,501	85% $\|5f_{\phi,7/2u}7s_{\sigma,-1/2g}\|$, 10% $\|5f_{\delta,5/2u}7s_{\sigma,1/2g}\|$
0_u						6,470	7,081	48% $\|5f_{\delta,3/2u}6d_{\delta,3/2g}\|$, 48% $\|5f_{\delta,3/2u}6d_{\delta,3/2g}\|$
3_u						6,725	7,152	86% $\|5f_{\delta,5/2u}7s_{\sigma,1/2g}\|$, 9% $\|5f_{\phi,7/2u}7s_{\sigma,-1/2g}\|$
2_u						6,460	7,431	97% $\|5f_{\delta,5/2u}7s_{\sigma,1/2g}\|$
3_u						7,291	7,867	95% $\|5f_{\delta,3/2u}6d_{\delta,3/2g}\|$
5_u						8,532	8,746	70% $\|5f_{\phi,5/2u}6d_{\delta,5/2g}\|$, 14% $\|5f_{\phi,7/2u}6d_{\delta,3/2g}\|$
6_u						12,970	13,458	98% $\|5f_{\phi,7/2u}6d_{\delta,5/2g}\|$
4_g				5,545	6,991	12,103	10,914	95% $\|5f_{\phi,5/2u}5f_{\delta,3/2u}\|$
0_g				12,012	8,970	10,065	11,436	73% $\|7s_{\sigma,1/2g}7s_{\sigma,-1/2g}\|$, 15% $\|6d_{\delta,3/2g}6d_{\delta,-3/2g}\|$

[a] in Ar matrix

Table 4.4: Continuation of Table 4.3

Sym	Excited States							
	Exp. [137, 148]	GASCI [150]	CASPT2 [142]	CCSD 24e Fægri	CCSD(T) 24e Fægri	IHFSCC 24e Fægri	IHFSCC 40e Fægri2+ +spdf	Composition
1_g						11,017	12,564	92% $\|7s_{\sigma,-1/2g}6d_{\delta,3/2g}\|$
2_g						11,667	12,958	62% $\|7s_{\sigma,1/2g}6d_{\delta,3/2g}\|$, 17% $\|7s_{\sigma,-1/2g}6d_{\delta,5/2g}\|$
1_g						15,024	13,919	79% $\|5f_{\phi,5/2u}5f_{\delta,-3/2u}\|$
5_g						16,335	15,408	54% $\|5f_{\phi,5/2u}5f_{\delta,5/2u}\|$, 46% $\|5f_{\phi,7/2u}5f_{\delta,3/2u}\|$
3_g						13,926	15,502	88% $\|7s_{\sigma,1/2g}6d_{\delta,5/2g}\|$
3_g						16,753	16,625	63% $\|5f_{\phi,5/2u}5f_{\pi,-1/2u}\|$, 29% $\|5f_{\phi,5/2u}7p_{\pi,1/2u}\|$
1_g						17,345	16,949	48% $\|5f_{\phi,-5/2u}5f_{\phi,7/2u}\|$, 36% $\|6d_{\delta,5/2g}6d_{\delta,-3/2g}\|$
2_g						16,703	17,340	38% $\|5f_{\phi,5/2u}5f_{\pi,-1/2u}\|$, 20% $\|5f_{\phi,5/2u}7p_{\pi,1/2u}\|$
4_g						17,120	17,516	32% $\|5f_{\delta,5/2u}5f_{\delta,3/2u}\|$, 27% $\|6d_{\delta,5/2g}6d_{\delta,3/2g}\|$
6_g						19,756	18,913	69% $\|5f_{\phi,5/2u}5f_{\phi,7/2u}\|$, 31% $\|5f_{\delta,5/2u}5f_{\phi,7/2u}\|$
1_g						20,778	20,801	40% $\|5f_{\delta,3/2u}5f_{\pi,-1/2u}\|$, 34% $\|5f_{\delta,3/2u}7p_{\pi,-1/2u}\|$
1_g						21,180	21,247	51% $\|5f_{\phi,5/2u}7p_{\pi,-3/2u}\|$, 40% $\|5f_{\phi,5/2u}5f_{\pi,-3/2u}\|$
2_g						21,443	22,307	22% $\|7s_{\sigma,1/2g}6d_{\delta,3/2g}\|$, 22% $\|7s_{\sigma,-1/2g}6d_{\delta,5/2g}\|$
3_g						32,644	30,853	34% $\|5f_{\phi,5/2u}7p_{\pi,1/2u}\|$, 27% $\|5f_{\phi,5/2u}5f_{\pi,1/2u}\|$
2_g						32,378	31,125	81% $\|5f_{\phi,5/2u}7p_{\sigma,-1/2u}\|$, 15% $\|5f_{\phi,5/2u}5f_{\sigma,-1/2u}\|$
3_g						32,444	31,203	80% $\|5f_{\phi,5/2u}7p_{\sigma,1/2u}\|$, 15% $\|5f_{\phi,5/2u}5f_{\sigma,1/2u}\|$
2_g						33,841	32,071	31% $\|5f_{\phi,5/2u}7p_{\pi,-1/2u}\|$, 27% $\|5f_{\phi,5/2u}5f_{\pi,-1/2u}\|$
1_g						35,007	33,189	47% $\|5f_{\phi,5/2u}5f_{\pi,-3/2u}\|$, 28% $\|5f_{\phi,5/2u}7p_{\pi,-3/2u}\|$
4_g						35,530	33,832	39% $\|5f_{\phi,5/2u}5f_{\pi,3/2u}\|$, 20% $\|5f_{\phi,5/2u}7p_{\pi,3/2u}\|$

SO-split ^3H_g and ^3H_u states that are relevant in the discussion of spectroscopic data. A full list of computed excitation energies is given in the supplementary material to this paper. From the analysis of the eigenvectors of the effective Hamiltonian we may distinguish between single, double and mixed single-double excitations relative to the ground state. In our method it is not yet possible to compute the oscillator strengths, but we assumed that double excitations have a very small intensity and can be safely discarded in the comparison with experimental data.

For convenience we again divided Table 4.3 in different sections to illustrate the main parentage of the states.

Region 0 to 3,000 cm^{-1} : $5f^1 7s^1$ states

As discussed in the introduction, the first two states are best described in a jj-coupling picture as pure $5f^1_{\phi,5/2u}7s^1_{\sigma,1/2g}$ states. The small energy difference between the 2_u and 3_u state is a signature of the diffuse character of the $7s$, as the energy difference between these states is in first approximation equal to the exchange integral $(7s_{\sigma,1/2g}5f_{\phi,5/2u}|7s_{\sigma,1/2g}5f_{\phi,5/2u})$. Likewise we have a 357 cm^{-1} difference between the next two states (with $5f^1_{\delta,3/2u}7s^1_{\sigma,1/2g}$ configuration), that should be approximately equal to the exchange integral $(7s_{\sigma,1/2g}5f_{\delta,3/2u}|7s_{\sigma 1/2g}5f_{\delta,3/2u})$. These energy differences are consistent with earlier calculations, although the GASCI calculation of Fleig et al. [150] gives a significantly smaller value for the excitation from $5f_{\phi,5/2u}$ to $5f_{\delta,3/2u}$. This is probably due to the fact that fewer electrons were correlated in the GASCI calculation; if we also correlate only 14 electrons we obtain energies of 1621 and 1911 cm^{-1}. The experimental data for the transition to the $5f^1_{3/2}7s^1_{1/2}$ states is based on the measurements in the argon matrix [148]. Also with SOC the discrepancy between these data and the theoretical values (that were all done in the gas phase) [135,136,142,149,150] remains much larger than would be expected from a matrix effect on the energy differences between four rather similar states. It is curious that almost the same vibrational frequency (776 cm^{-1}) in the argon matrix that was assigned by Andrews and coworkers [2,135] to the asymmetric stretch of the ^3H_g (4_g) is also seen as a vibrational band (771 cm^{-1}) in the fluorescence spectra. Lue et al. [148] assign this band to a symmetric stretch of 776 cm^{-1} that they deduce from the observation of a 728 cm^{-1} band of ^{18}OU^{16}O by Gabelnick et al. [158]. This value is, however, much lower than the $^3\Phi_u$ symmetric stretch frequency computed by DFT [140] (856 cm^{-1}), large basis set CASPT2 [142] (948 cm^{-1}), and DC-FSCC (961 cm^{-1}). In the paper of Li [140], the symmetric stretch of the 4_g state is reported at 779 cm^{-1}, which does fit the experimental band found in the fluorescence experiment.

This interpretation is, however, not corroborated by our calculations, as we compute a symmetric stretch vibration of 911 cm^{-1} for this state.

Region 3,000 to 9,000 cm^{-1}: $5f^17s^1$ and $5f^16d^1$ ungerade states

These states have the same parity as the ground state and are difficult to observe directly. The fluorescence data, that were already discussed above, give some bands in the range of 470-600 nm. From these experiments of Lue et al. [148] it could not be deduced whether these peaks were caused by direct or indirect emission. If the emission occurs from the state excited by the 380.5 nm (26,281 cm^{-1}) laser, there should be accessible states that have energies in the range 5,000 to 9,600 cm^{-1}. Our calculations give both $5f^17s^1$ states and $5f^16d^1$ states in this range, but the composition of these states does not make it probable that they obtain much intensity.

Region 10,000-22,000 cm^{-1} : $5f^2$ gerade states

The second interpretation of the fluorescence bands that was given is that they are caused by an indirect process, in which an upper level is populated by nonradiative transfer before exhibiting radiative decay to the ground state. This should correspond to a strong emission from a state at 21,280 cm^{-1} to the ground state. In our calculations we find a $1g$ state at 21,247 cm^{-1} that has a large contribution of the $5f^17p^1$ configuration and should indeed have a good oscillator strength. Other states that could contribute to this fluorescence band are the 3g at 16,625 cm^{-1} and the 2g at 17,340 cm^{-1}. Since these fluorescence measurements were done in the argon matrix it is hard to compare directly, but the predicted bands at 470, 577 and 602 nm are not incompatible with the observed fluorescence.

For this region of the spectrum one may, however, also consider the much more precise gas phase REMPI data of Han et al. [137]. On the basis of theoretical data available at that time [149] they assigned a state at 17,859 cm^{-1} to a $4g$ state and two states at 18,159 and 18,423 cm^{-1} to $1g$ states. The CASPT2-SO calculations of Gagliardi et al. [142] lead to a reassignment of the first state to $2g$. Our calculations give both a $4g$ state at 17,516 cm^{-1} and a $2g$ state at 17,340 cm^{-1}, and can not distinguish between the two possibilities. Accessible $1g$ states lie above 20,000 cm^{-1} in our calculations, and do not readily explain the absorptions that were attributed to the $1g$ states.

Like in the spin-free case, we find significant differences with the CASPT2 results. We find the lowest $5f^2$ state at 10,914 cm^{-1}, whereas with CASPT2 this state is only 3,330 cm^{-1} above the ground state. Also the $5f^17p^1$ states come out somewhat higher

than with CASPT2-SO. As discussed in the previous section, part of the cause for the discrepancy is the difference in bond length used to compute these vertical excitation energies, but this is only a relatively small effect. The same holds for the way in which relativity is treated, such differences usually gives rather small deviations for valence properties. This leads us to conclude that differences should be primarily due to the completely different approach to electron correlation that is chosen in both methods. As the Fock space approach is not yet tested much in molecular applications yet, we decided to perform also some calculations with the more established DC-CCSD(T) method. The two states of interest, the $5f^17s^1$ $2u$ and the $5f^2$ $4g$ state, are both well described by a single determinant reference, which makes it possible to compute the $2u \rightarrow 4g$ excitation energy with such a single reference approach. The DC-CCSD calculation gives a rather small excitation energy of 5,545 cm^{-1} that increases to 6,991 cm^{-1} if triple excitations are included with the DC-CCSD(T) approach. This is significantly higher than the CASPT2 value, but also significantly lower than the DC-FSCC value. The discrepancy between the two CC approaches can be due to two factors: the CCSD(T) approach has a large T_1 diagnostic value of 0.040 in the $4g$ calculation which, together with the large effect of the (T) correction, could be indicative of a breakdown in the single reference approach. On the other hand, we base the Fock space approach on orbitals that are obtained in a HF calculation of the dication, and the DC-CCSD(T) calculation on orbitals optimized for the neutral molecule. This could also lead explain discrepancy as it will make the orbitals used in the Fock space calculation tighter, possibly favoring the $5f^17s^1$ configuration above the $5f^2$. To assess this effect we repeated the CCSD calculation using the same orbitals (from the dication, uranyl) as employed in the IHFSCCSD calculation. This resulted in a CCSD excitation energy of 5,247 cm^{-1}, indicating that difference in orbitals is only marginally important. An additional CCSD calculation, this time on the ^3H_u state, reinforces the conclusion, that the lower $5f^16d^1$ states lie below the lower $5f^2$ states and can not be neglected in the analysis of experimental observations.

Region 30,000 - 50,000 cm^{-1} : $5f^17p^1$ gerade states

This region includes mainly $5f^17p^1$ states. Experimentally, both the absorption REMPI spectrum [137] and the fluorescence spectrum in Ar matrix [148] give an intense band at about 27,000 cm^{-1}. This is regarded as evidence for the suggestion that the ground state does not change in an argon matrix. In both cases the transitions should then be due to an intense $7s \rightarrow 7p$ transition. Our calculations are in qualitative agreement with this assignment, but give transitions to the $5f^17p^1$ states

starting around 30,000 cm^{-1} with all excitations in the region between 22,000 to 30,000 corresponding to double excitations, which should have too weak intensities. The difference of 3,000 cm^{-1} could, however, be due to a flaw in the calculations, possibly a remaining basis-set deficiency. The $7p$ orbitals are very diffuse and may require more diffuse functions than the single shell that we added. Still, even though a quantitative agreement of the REMPI data is not yet reached, we think that the assignment of this series of peaks to $7s \rightarrow 7p$ transitions is correct.

4.5 Conclusions

We applied the relativistic Fock-space coupled cluster method and its intermediate Hamiltonian modifications to analyze the electronic spectrum of the UO_2 molecule. The method is size-extensive and combines highly accurate treatment of dynamic and non-dynamic correlation effects, which is crucial for correct calculation and interpretation of the complicated UO_2 spectrum. The ease with which a full manifold of excited states is computed in a single run is an important asset of the method. The IH-FSCC approach scales as N^6, but this can be ameliorated by applying linear scaling techniques, because all computationally intensive terms are similar to those that occur in regular CC algorithms.

For the first time, the $6d$ shell has been included explicitly in the correlated calculation. A 4_u state arising from the $5f^16d^1$ configuration is found at about 5,000 cm^{-1}, which makes it an interesting alternative for explaining the low values found in older IP measurements [134]. The first gerade state, 4_g, is found at more than 10,000 cm^{-1}, which is much higher than predicted by previous theoretical calculations. This value could be slightly overestimated, but it appears unlikely that this state is the lowest when the UO_2 molecule is trapped in an Ar matrix. We propose that it is more likely that the $5f^16d^1$ $4u$ state is of importance in the heavier noble gas matrices. Also our calculations can not fully explain all experimental observations, but they add more pieces to the complex puzzle that nature has posed.

4.6 Supplementary Materials

ALL excitation energies up to 34,000 cm^{-1} are given at our best level of approximation (IHFSCC) with the Faegri2+ basis, 40 electrons correlated and 45 au as the threshold for the virtual space. The P model space is (17g, 20u) with the 7p orbitals included in the P_m. The bond distance is 1.770 Å .

Sym	Excited States	
	IHFSCC 40e Faegri2+ +spdf	Composition
2_u	0	97% $\|5f_{\phi,5/2u}7s_{\sigma,1/2g}\|$
3_u	368	96% $\|5f_{\phi,5/2u}7s_{\sigma,-1/2g}\|$
1_u	2,231	98% $\|5f_{\delta,3/2u}7s_{\sigma,1/2g}\|$
2_u	2,588	96% $\|5f_{\delta,3/2u}7s_{\sigma,1/2g}\|$
4_u	5,047	98% $\|5f_{\phi,5/2u}6d_{\delta,3/2g}\|$
4_u	6,148	97% $\|5f_{\phi,7/2u}7s_{\sigma,1/2g}\|$
3_u	6,501	85% $\|5f_{\phi,7/2u}7s_{\sigma,-1/2g}\|$, 10% $\|5f_{\delta,5/2u}7s_{\sigma,1/2g}\|$
0_u	7,081	48% $\|5f_{\delta,3/2u}6d_{\delta,3/2g}\|$, 48% $\|5f_{\delta,3/2u}6d_{\delta,3/2g}\|$
3_u	7,152	86% $\|5f_{\delta,5/2u}7s_{\sigma,1/2g}\|$, 9% $\|5f_{\phi,7/2u}7s_{\sigma,-1/2g}\|$
2_u	7,431	97% $\|5f_{\delta,5/2u}7s_{\sigma,1/2g}\|$
3_u	7,867	95% $\|5f_{\delta,3/2u}6d_{\delta,3/2g}\|$
1_u	8,268	92% $\|5f_{\delta,5/2u}6d_{\delta,-3/2g}\|$
5_u	8,746	70% $\|5f_{\phi,5/2u}6d_{\delta,5/2g}\|$, 14% $\|5f_{\phi,7/2u}6d_{\delta,3/2g}\|$
0_u	10,089	92% $\|5f_{\phi,5/2u}6d_{\delta,-5/2g}\|$
4_g	10,914	95% $\|5f_{\phi,5/2u}5f_{\delta,3/2u}\|$
4_u	11,221	73% $\|5f_{\delta,3/2u}6d_{\delta,5/2g}\|$, 25% $\|5f_{\delta,5/2u}6d_{\delta,3/2g}\|$
0_g	11,436	73% $\|7s_{\sigma,1/2g}7s_{\sigma,-1/2g}\|$, 15% $\|6d_{\delta,3/2g}6d_{\delta,-3/2g}\|$
1_u	11,510	73% $\|5f_{\delta,3/2u}6d_{\delta,-5/2g}\|$, 15% $\|5f_{\delta,5/2u}6d_{\delta,-3/2g}\|$
0_u	12,310	90% $\|5f_{\delta,3/2u}6d_{\delta,-3/2g}\|$
1_g	12,564	92% $\|7s_{\sigma,-1/2g}6d_{\delta,3/2g}\|$
0_g	12,700	51% $\|5f_{\phi,5/2u}5f_{\phi,-5/2u}\|$, 23% $\|5f_{\delta,3/2u}5f_{\delta,-3/2u}\|$
2_g	12,958	62% $\|7s_{\sigma,1/2g}6d_{\delta,3/2g}\|$, 17% $\|7s_{\sigma,-1/2g}6d_{\delta,5/2g}\|$
6_u	13,458	98% $\|5f_{\phi,7/2u}6d_{\delta,5/2g}\|$
1_g	13,919	79% $\|5f_{\phi,5/2u}5f_{\delta,-3/2u}\|$
2_u	14,104	94% $\|5f_{\phi,7/2u}6d_{\delta,-3/2g}\|$
5_u	14,654	77% $\|5f_{\phi,5/2u}6d_{\delta,5/2g}\|$, 14% $\|5f_{\phi,7/2u}6d_{\delta,3/2g}\|$
1_u	14,995	81% $\|5f_{\delta,5/2u}6d_{\delta,-3/2g}\|$, 15% $\|5f_{\delta,-3/2u}6d_{\delta,5/2g}\|$
0_u	15,196	90% $\|5f_{\delta,5/2u}6d_{\delta,-5/2g}\|$
5_g	15,408	54% $\|5f_{\phi,5/2u}5f_{\delta,5/2u}\|$, 46% $\|5f_{\phi,7/2u}5f_{\delta,3/2u}\|$
4_u	15,455	72% $\|5f_{\delta,3/2u}6d_{\delta,3/2g}\|$, 23% $\|5f_{\delta,3/2u}6d_{\delta,5/2g}\|$
3_g	15,502	88% $\|7s_{\sigma,1/2g}6d_{\delta,5/2g}\|$
0_u	15,860	90% $\|7s_{\sigma,1/2g}5f_{\pi,-1/2u}\|$
0_u	15,945	96% $\|7s_{\sigma,1/2g}5f_{\pi,-1/2u}\|$

Sym	Excited States	
	IHFSCC 40e Faegri2+ +spdf	Composition
3_g	16,625	63% $\|5f_{\phi,5/2u}5f_{\pi,-1/2u}\|$, 29% $\|5f_{\phi,5/2u}7p_{\pi,1/2u}\|$
1_u	16,786	81% $\|7s_{\sigma,1/2g}5f_{\pi,1/2u}\|$, 11% $\|5f_{\phi,7/2u}6d_{\delta,-5/2g}\|$
1_g	16,949	48% $\|5f_{\phi,-5/2u}5f_{\phi,7/2u}\|$, 36% $\|6d_{\delta,5/2g}6d_{\delta,-3/2g}\|$
1_u	17,058	85% $\|5f_{\phi,7/2u}6d_{\delta,-5/2g}\|$
0_g	17,127	33% $\|5f_{\delta,3/2u}5f_{\delta,-3/2u}\|$, 27% $\|5f_{\delta,5/2u}5f_{\delta,-5/2u}\|$
2_g	17,340	38% $\|5f_{\phi,5/2u}5f_{\pi,-1/2u}\|$, 20% $\|5f_{\phi,5/2u}7p_{\pi,1/2u}\|$
4_g	17,516	32% $\|5f_{\delta,5/2u}5f_{\delta,3/2u}\|$, 27% $\|6d_{\delta,5/2g}6d_{\delta,3/2g}\|$
0_g	17,606	93% $\|5f_{\phi,5/2u}5f_{\delta,-5/2u}\|$
0_g	18,355	52% $\|5f_{\phi,5/2u}5f_{\delta,-5/2u}\|$, 29% $\|5f_{\delta,3/2u}5f_{\delta,-3/2u}\|$
2_g	18,596	84% $\|5f_{\phi,7/2u}5f_{\delta,-3/2u}\|$
6_g	18,913	69% $\|5f_{\phi,5/2u}5f_{\phi,7/2u}\|$, 31% $\|5f_{\delta,5/2u}5f_{\phi,7/2u}\|$
2_g	19,105	64% $\|5f_{\delta,3/2u}5f_{\pi,-1/2u}\|$, 26% $\|5f_{\delta,3/2u}7p_{\pi,-1/2u}\|$
1_g	19,317	64% $\|5f_{\delta,5/2u}5f_{\delta,-3/2u}\|$, 26% $\|6d_{\delta,5/2g}6d_{\delta,-3/2g}\|$
5_u	19,491	53% $\|5f_{\phi,7/2u}6d_{\delta,3/2g}\|$, 21% $\|5f_{\delta,5/2u}6d_{\delta,5/2g}\|$
0_u	20,123	91% $\|5f_{\delta,5/2u}6d_{\delta,5/2g}\|$
2_u	20,746	97% $\|7s_{\sigma,1/2g}5f_{\delta,3/2u}\|$
1_g	20,801	40% $\|5f_{\delta,3/2u}5f_{\pi,-1/2u}\|$, 34% $\|5f_{\delta,3/2u}7p_{\pi,-1/2u}\|$
4_g	21,129	32% $\|5f_{\delta,5/2u}5f_{\delta,3/2u}\|$, 28% $\|5f_{\delta,5/2u}5f_{\pi,3/2u}\|$
1_g	21,247	51% $\|5f_{\phi,5/2u}7p_{\pi,-3/2u}\|$, 40% $\|5f_{\phi,5/2u}5f_{\pi,-3/2u}\|$
2_u	21,412	97% $\|6d_{\delta,3/2g}5f_{\pi,1/2u}\|$
1_u	21,442	76% $\|7s_{\sigma,1/2g}5f_{\pi,3/2u}\|$, 19% $\|6d_{\delta,3/2g}5f_{\pi,-1/2u}\|$
0_g	22,142	56% $\|5f_{\phi,7/2u}5f_{\phi,-7/2u}\|$, 21% $\|5f_{\delta,5/2u}5f_{\delta,-5/2u}\|$
2_g	22,307	22% $\|7s_{\sigma,1/2g}6d_{\delta,3/2g}\|$, 22% $\|7s_{\sigma,-1/2g}6d_{\delta,5/2g}\|$
3_g	23,198	36% $\|5f_{\delta,3/2u}5f_{\phi,3/2u}\|$, 31% $\|5f_{\delta,3/2u}5f_{\pi,3/2u}\|$
1_g	23,479	78% $\|5f_{\phi,7/2u}5f_{\delta,-5/2u}\|$
0_g	23,484	52% $\|5f_{\delta,3/2u}7p_{\pi,-3/2u}\|$, 35% $\|5f_{\delta,3/2u}5f_{\pi,-3/2u}\|$
0_g	23,721	56% $\|5f_{\delta,3/2u}7p_{\pi,-3/2u}\|$, 35% $\|5f_{\delta,3/2u}5f_{\pi,-3/2u}\|$
1_u	24,433	70% $\|6d_{\delta,3/2g}5f_{\pi,-1/2u}\|$, 11%$\|7s_{\sigma,1/2g}5f_{\pi,1/2u}\|$
2_g	24,955	56% $\|5f_{\delta,5/2u}5f_{\pi,-1/2u}\|$, 30% $\|5f_{\delta,5/2u}7p_{\pi,-1/2u}\|$
5_g	25,096	39% $\|5f_{\phi,7/2u}5f_{\delta,3/2u}\|$, 32% $\|5f_{\phi,5/2u}5f_{\delta,5/2u}\|$
4_g	25,180	51% $\|5f_{\delta,5/2u}5f_{\delta,3/2u}\|$, 13% $\|5f_{\phi,5/2u}7p_{\pi,3/2u}\|$
3_u	25,215	68% $\|6d_{\delta,5/2g}5f_{\pi,1/2u}\|$, 29%$\|6d_{\delta,3/2g}5f_{\pi,3/2u}\|$

Sym	Excited States	
	IHFSCC 40e Faegri2+ +spdf	Composition
3_g	25,471	37% $\|5f_{\delta,3/2u}5f_{\pi,1/2u}\|$, 24%$\|5f_{\delta,5/2u}7p_{\pi,1/2u}\|$
6_g	25,657	62% $\|5f_{\phi,7/2u}5f_{\phi,5/2u}\|$, 38% $\|5f_{\phi,7/2u}5f_{\delta,5/2u}\|$
2_u	25,730	94% $\|6d_{\delta,5/2g}5f_{\pi,-1/2u}\|$
0_g	25,745	62% $\|5f_{\delta,5/2u}7p_{\delta,-5/2u}\|$, 18% $\|6d_{\delta,5/2g}6d_{\delta,-5/2g}\|$
5_g	26,957	37% $\|5f_{\phi,7/2u}5f_{\pi,3/2u}\|$, 35% $\|5f_{\phi,7/2u}7p_{\pi,3/2u}\|$
4_g	27,096	39% $\|5f_{\delta,5/2u}5f_{\pi,3/2u}\|$, 37% $\|5f_{\delta,5/2u}7p_{\pi,3/2u}\|$
0_u	27,304	96% $\|5f_{\pi,3/2u}6d_{\delta,5/2g}\|$
0_g	27,412	19% $\|6d_{\delta,3/2g}6d_{\delta,-3/2g}\|$, 18% $\|5f_{\phi,5/2u}5f_{\phi,-5/2u}\|$
2_g	28,172	41% $\|5f_{\phi,7/2u}7p_{\pi,-3/2u}\|$, 30% $\|5f_{\phi,7/2u}5f_{\pi,-3/2u}\|$
3_u	28,462	65% $\|6d_{\delta,3/2g}5f_{\pi,3/2u}\|$, 26%$\|6d_{\delta,5/2g}5f_{\pi,1/2u}\|$
1_u	28,516	40% $\|5f_{\delta,5/2u}7p_{\pi,-3/2u}\|$, 26%$\|5f_{\delta,5/2u}5f_{\pi,-3/2u}\|$
4_u	29,210	97% $\|6d_{\delta,5/2g}5f_{\pi,3/2u}\|$
4_g	29,539	45% $\|6d_{\delta,5/2g}6d_{\delta,3/2g}\|$, 14% $\|5f_{\delta,5/2u}7p_{\pi,3/2u}\|$
1_g	29,656	19% $\|5f_{\delta,5/2u}7p_{\pi,-3/2u}\|$, 18% $\|5f_{\delta,7/2u}5f_{\phi,5/2u}\|$
1_u	30,819	88% $\|6d_{\delta,5/2g}5f_{\pi,-3/2u}\|$
3_g	30,853	34% $\|5f_{\phi,5/2u}7p_{\pi,1/2u}\|$, 27% $\|5f_{\phi,5/2u}5f_{\pi,1/2u}\|$
2_g	31,125	81% $\|5f_{\phi,5/2u}7p_{\sigma,-1/2u}\|$, 15% $\|5f_{\phi,5/2u}5f_{\sigma,-1/2u}\|$
3_g	31,203	80% $\|5f_{\phi,5/2u}7p_{\sigma,1/2u}\|$, 15% $\|5f_{\phi,5/2u}5f_{\sigma,1/2u}\|$
2_u	31,235	92% $\|5f_{\phi,5/2u}6d_{\pi,-1/2g}\|$
3_u	31,380	92% $\|5f_{\phi,5/2u}6d_{\pi,1/2g}\|$
2_g	32,071	31% $\|5f_{\phi,5/2u}7p_{\pi,-1/2u}\|$, 27% $\|5f_{\phi,5/2u}5f_{\pi,-1/2u}\|$
1_g	33,189	47% $\|5f_{\phi,5/2u}5f_{\pi,-3/2u}\|$, 28% $\|5f_{\phi,5/2u}7p_{\pi,-3/2u}\|$
2_g	33,741	40% $\|5f_{\delta,3/2u}7p_{\pi,-1/2u}\|$, 23% $\|5f_{\delta,3/2u}5f_{\pi,-1/2u}\|$
4_g	33,832	39% $\|5f_{\phi,5/2u}5f_{\pi,3/2u}\|$, 20% $\|5f_{\phi,5/2u}7p_{\pi,3/2u}\|$

CHAPTER 5

On the Performance of the Intermediate Hamiltonian Fock-Space Coupled–Cluster Method on Linear Triatomic Molecules: the Electronic Spectra of NpO_2^+, NpO_2^{2+} and PuO_2^{2+}

Maya: What's the title of your book ?
Miles Raymond: The Day After Yesterday.
Maya: Oh... You mean today?
from the movie Sideways (2004)

5.1 Abstract

In this paper we explore the use of the novel Relativistic Intermediate Hamiltonian Fock–Space Coupled–Cluster method (IHFSCC) in the calculation of the electronic spectrum for small Actinyl ions (NpO_2^+, NpO_2^{2+} and PuO_2^{2+}). It is established that the method, in combination with uncontracted double–zeta quality basis sets, yields excitation energies in good agreement with experimental values, and better than those obtained previously with other theoretical methods. We propose the reassignment of some of the peaks that were observed experimentally, and confirm other assignments.

5.2 Introduction

Considerable attention has been paid to actinide chemistry in recent years, due to the need to find new techniques for storage and reprocessing of spent nuclear fuel [6, 159, 160]. One of the most important steps of the PUREX (Plutonium URanium EXtraction) process remains the separation of uranium(VI), plutonium(IV) and neptunium(VI) from fission products with aid of the tributylphosphate (TBP) extractant. In this process Pu^{4+} is complexed with two nitrate ions and two TBP ligands, while the other two elements are extracted in the form of the triatomic actinyls UO_2^{2+} and NpO_2^{2+} [161].

The small size of these actinyls makes calculations feasible, and their energetical and structural parameters are reasonably well characterized [9,162]. Studies regarding the spectroscopic properties of actinyls focused mainly on the uranyl ion, but some studies have also been performed on neptunyl and plutonyl [163–165]. All three actinyl molecules have rather dense spectra due to the low–lying $5f$ and $6d$ orbitals localized on the metal. This characteristic poses a challenge to the currently available theoretical models, as they should describe the manifestation of relativistic effects as well as the multireference character of many of the states that significantly mix under the influence of spin–orbit coupling (SOC).

Among the theoretical methods that have already been used to investigate the spectra of small actinide compounds, single–reference Coupled–Cluster (CC) theory, both in its non–relativistic and relativistic formulations, is arguably the most accurate method to calculate dynamical correlation energy. Its applicability is, however, severely limited due to its inability to handle states which have a considerable multireference character [143]. This has up to now left the Spin–Orbit Complete–Active–Space Second–Order Perturbation Theory (SO–CASPT2) or Spin–Orbit Configuration– Interaction (SO–CI) methods as the only choices for qualitative or quantitative determination of spectra of neptunyl and plutonyl.

These methods, however, are not without important drawbacks, namely: (a) SO–CI methods are reasonably good for qualitative studies, but have difficulties in attaining quantitative agreement with experiment due to the lack of size-extensivity in the electron correlation treatment and to restrictions on the number of configurations that can be included; and (b) SO–CASPT2, at present found to be the most accurate method employed for these systems, due to its ability to handle the use large basis sets, has a steep computational scaling with active space size. This limits the flexibility in choosing a suitable reference space, and negatively affects the quality of the calculated spectra.

It is therefore of interest to assess new methods which could describe the electronic spectra of small actinyl ions accurately while still possessing a reasonably low scaling behavior. In this paper we explore the use of the Intermediate Hamiltonian Fock-Space Coupled–Cluster (IHFSCC) method [82–85] as an alternative to SO–CASPT2 and SO–CI. This method, while well-established and routinely applied in high accuracy calculations of atomic transition energies, has scarcely been applied to molecular systems [166].

The outline of the paper is as follows: in the Methodology section we outline the characteristics of the IHFSCC method and the computational procedure followed; in Results and Discussion, we first present a short analysis of the f^1 configurations, before continuing with our primary interest, the study of the electronic spectrum of the f^2 systems. The last section concerns the bond lengths and symmetric stretch frequencies that were computed for these gas phase model systems, while we conclude by comparing the results of the IHFSCC method to other type of theoretical methods and experiments and discuss the merits and drawbacks of this method.

5.3 Methodology

Fock–Space Coupled–Cluster (FSCC) methods [1] have been very successful in computing the excitation energies of atoms and molecules with very high accuracy [79]. The methods scale like standard CC calculation (e.g., $O(N^6)$ for CCSD), but produce an effective Hamiltonian that, upon diagonalization, yields the energy of several states at once. In this family of methods, the IHFSCC approach [81] represents a breakthrough, as it greatly reduces the likelyhood of intruder states and associated convergence problems in the solution of the CC equations.

The IHFSCC implementation used is that of the molecular 4–component code DIRAC [48, 118], in which the T_1 and T_2 excitation operators are included, giving a IHFSCCSD approach that allows for creation of at most two holes and/or electrons outside the reference closed shell system. While DIRAC can work with various relativistic Hamiltonians, in this application we have used the standard Dirac–Coulomb Hamiltonian, which is capable of describing the strong relativistic and SOC effects in actinyls. As has become common practice in the usage of DIRAC, we neglect contributions from the $(SS|SS)$–type integrals, replacing them by a simple correction [44], and employ a Gaussian finite nucleus model [167,168] with this Hamiltonian. As with all FSCC methods, for the IHFSCC approach the reference state must be a single determinant. This means, in the case of PuO_2^{2+} and NpO_2^{+}, that we start respectively

from the PuO_2^{4+} and NpO_2^{3+} species and add the missing two open shell electrons in the IHFSCC step. This amounts to the addition of two particles in the P space, following the sequence

$$\left.\begin{matrix} NpO_2^{3+} \\ PuO_2^{4+} \end{matrix}\right\}(0h,0p) \rightarrow \left.\begin{matrix} NpO_2^{2+} \\ PuO_2^{3+} \end{matrix}\right\}(0h,1p) \rightarrow \left.\begin{matrix} NpO_2^{+} \\ PuO_2^{2+} \end{matrix}\right\}(0h,2p), \qquad (5.1)$$

which is equivalent to calculating the first and second electron affinities for these highly charged systems. The restriction to two creation operators means that quintet states, important at higher energies, are not included. Such states belong to the (1h,3p) sector of Fock space not yet available in the currenty CCSD-based implementation.

The equilibrium geometries and harmonic frequencies for the ground and some of the excited states were determined by fitting 10th–order polynomials on discrete representations of the potential energy surfaces. As these molecules are known to be linear in their ground state, we have only considered the displacements along the symmetric stretch of the An–O bonds (An=Pu,Np). Under these circumstances, it is possible to exploit linear symmetry ($D_{\infty h}$) with the DIRAC program. Due to limitations in the computational resources, we did not explore displacements along the other vibrational modes, as the lowering of symmetry brought about by displacements along the asymmetric ($C_{\infty v}$) and bending modes (C_{2v}) would have increased the computational costs significantly.

Since the starting point in the SCF calculations were ions with a +2 charge higher than the actual species, it was necessary to ensure that the ordering of the spinors, particularly in the HOMO–LUMO region, was consistent and adequate for the subsequent correlation treatment. This made us reorder the spinors in some cases, particularly for bond lengths larger than the equilibrium distance, in such a manner that the $5f$ shells in the starting species were always left empty.

The number of electrons correlated, apart from the two electrons that are included during the IHFSCC treatment, is 24; 10 in spinors of g symmetry and 14 electron in spinors of u symmetry. The virtual space was truncated by excluding spinors with energies larger than 6 au. This cutoff is consistent with our more extensive work on UO_2 that will be reported separately [169].

For the IHFSCC calculations, a partitioning of the P,Q spaces, hereby named "IH-u" was employed for all systems considered. In this partitioning 25 spinors of u symmetry were included in the P space. The P space was further partitioned as follows: the six lowest–lying unoccupied $5f$ spinors from the Pu and Np atoms were included in the P_m space, and the remaining $7p$ and $5f^\sigma$ spinors placed in the P_i space. In the orthogonal Q space all virtual spinors of g symmetry, and the spinors of

u symmetry not included in the $P = P_m + P_i$, were included. To check convergence with active space size, for PuO_2^{2+} and NpO_2^{+} a second partitioning, hereby named "IH-u+g", was also explored. This consisted of the same P_m space as in "IH-u", but with 20 spinors of g symmetry added to the P_i space, in order to have a more balanced description of the P space. The calculations with the latter are substantially more demanding and turned out to give negligible differences in excitation energies for states up to 30,000 cm^{-1} relative to the "IH-u" space.

The basis set employed for the actinides was that of double–zeta quality developed by Dyall [170]. These sets were used in their uncontracted form, and are of size 26s23p17d10f1g1h. For oxygen the valence correlation–consistent triple–zeta (cc-pVTZ) set of Dunning [122] was used, also in uncontracted form. It should be noted that the TZ set was used here instead of the DZ set due to the need to add additional tight functions in a relativistic calculation that uses a non–relativistic basis set. We also performed exploratory runs using a TZ quality basis set on the actinide element (33s29p20d12f3g2h) on the equilibrium bond distances. As there was little variation upon enlargement (the excited states are shifted at most by about 200 cm^{-1} for each of the excited states) and the computational cost for each point on the potential energy surface scan was greatly increased, we have opted to employ the uncontracted DZ set on the heavy element.

5.4 Results and Discussion

5.4.1 Electronic structure of the ground state of NpO_2^{3+} and PuO_2^{4+}

As previously noted, to study the electronic spectrum of NpO_2^{+} and PuO_2^{2+} using the IHFSCC approach one has to start from a closed-shell model molecule, and then proceed by computing the first and second electron affinities successively. Before discussing the results for NpO_2^{+} and PuO_2^{2+}, we first analyze the composition of the virtual orbitals of NpO_2^{3+} and PuO_2^{4+}, as these give a first indication of the expected low–lying states of the f^2 ions. The ordering of the $5f$ orbitals is presented in Table 5.1. It should be noted that the energies, given in relative energies for ease of comparison with experimental results, are obtained not from the energies of the virtual Hartree-Fock orbitals of the closed-shell systems, but rather from the excitation energies, calculated with the IHFSCC method for the f^1 molecules. These energies are thus relative to the $^2\Phi_u$ ground state that results from occupying the

Figure 5.1: Orbital energy diagrams including the $5f$, $7s$, $6d$ and $7p$ orbitals for the UO_2^{2+}, NpO_2^{3+} and PuO_2^{4+} molecules. The correlated values from sector (0,1) of the IHFSCC calculations using the "IH-u" model space are shown. The bond distances are 1.770 Å, 1.701 Å and 1.645 Å , respectively

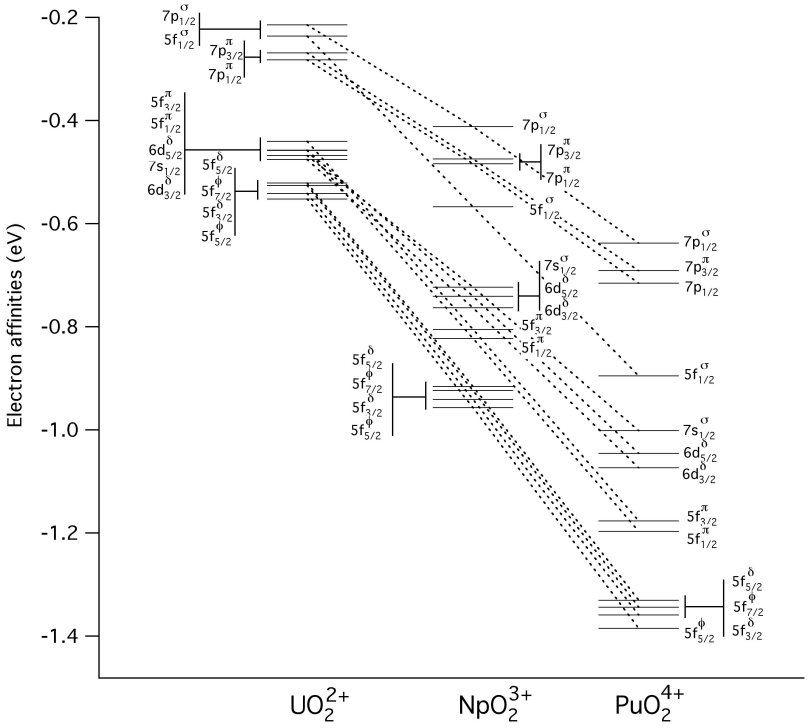

$5f^{\phi}_{5/2}$ orbital. For comparison we also show the first electron affinities for the UO_2^{2+} molecule, which is isoelectronic with NpO_2^{3+} and PuO_2^{4+}.

A qualitative model for the electronic structure of actinyl ions has been given by Matsika et al [163, 171]. The lowest two unoccupied orbitals are the nonbonding $5f^{\phi}$ and $5f^{\delta}$ orbitals, which are fully localized on the metal ion. The higher unoccupied orbitals are the antibonding combinations of the oxygen $2p$ and metal $5f^{\pi}$ and $5f^{\sigma}$ orbitals that are also mainly localized on the metal. The nonbonding $6d^{\delta}$ orbital lies relatively high in neptunyl and plutonyl, and only plays a role in explaining the observed spectral intensities [171]. In Figure 1 we show the f^1 affinities (in absolute values) computed with the IHFSCC method. The increasing nuclear charge, going

from U to Pu, leads to a stronger binding of the electrons in these isoelectronic systems.The lowering of the $5f$ level is the most pronounced and results in bringing the less shifted $6d$ and, in particular, the $7s$ and $7p$ levels, at too high energies to be of relevance in Np(V) and Pu(VI). All low-lying excited states are thus well described in terms of the $5f^2$ configuration only. In UO_2 the situation is different, since for U(IV) the $6d$, $7s$ and $7p$ orbitals all lie at similar energies as the $5f$'s, yielding a denser and more complicated spectrum more easily perturbed by intermolecular interactions. The UO_2 molecule has attracted much attention lately since matrix spectroscopy studies indicate that the ground state in a neon matrix could differ from that in an argon matrix [135, 136, 142, 150, 169]. An investigation of UO_2 employing the IHFSCC method and including all relevant configurations ($5f^1 7s^1$, $5f^2$, $5f^1 6d^1$) will be reported separately [169].

In Table 5.1, the available experimental values for f^1 NpO_2^{2+} are also included. It should be noted that these absorption spectra were measured in water [172], but studies in other polar solvents and crystals indicate that the transition energies are not much affected by the environment [173–175]. This suggests that the gas-phase excitation energies should be a good approximation for the excited states occurring in solution. From our calculations, the energies of the third and fourth levels are in very good agreement with the excitation energies measured in water.

The first excited state lies too low to be seen experimentally. The maximum error for these first two transition energies is 749 cm^{-1}. Comparing these values to those of Matsika and coworkers [163], obtained from SOCI calculations, our results appear to be more accurate, as Matsika's show larger (about 1,200-1,500 cm^{-1}) discrepancies with respect to the experimental values.

Eisenstein and Pryce [176–178] interpreted the transitions at 17,990 and 21,010 cm^{-1} as belonging to f-f type excitations, occupying the $5f^\pi$ orbital. As our computed $5f^\pi$ energy is much higher, we believe that these transitions are more likely to be due to charge transfer states in which one of the σ_u electrons in NpO_2^{2+} is excited to a higher level. These transitions were not accessible in our calculations, as the current implementation of the method only considers Fock space sectors that differ by two creation or annihilation operations from the reference space. Matsika and coworkers [163] have computed energies of such charge transfer states and found them to lie within this experimental range.

Table 5.1: Correlated electron affinities of the $5f$, $7s$, $6d$ orbitals for the UO_2^{2+}, NpO_2^{3+} and PuO_2^{4+} molecules computed from sector (0,1) of the IHFSCC calculations. The correlation space was (24e/6au), with a (17g,20u) P model space. All calculations were performed at the equilibrium bond distance of 1.770 Å for UO_2^+, 1.701Å for NpO_2^{2+} and 1.645Å for PuO_2^{3+}. The assignment of the experimental transitions [176] in parentheses is uncertain. The excitation energies are given in cm^{-1}.

spin	UO_2^+	NpO_2^{2+}	PuO_2^{3+}	NpO_2^{2+}	Experiment on NpO_2^{2+}		
				SOCI [163]	H_2O [176]	$Cs_2UO_2Cl_4$ [175]	$CsUO_2(NO_3)_3$ [174]
$5f^{\phi}_{5/2u}$	0	0	0	0	0	0	0
$5f^{\delta}_{3/2u}$	2376	3544	5746	447	–	1000	–
$5f^{\phi}_{7/2u}$	5736	7227	8990	5515	6760	6880	6459
$5f^{\delta}_{5/2u}$	6843	8929	11907	6565	8180	7990	9420
$6d^{\delta}_{3/2g}$	16820	42524	68400	–	–	–	–
$7s^{\sigma}_{1/2g}$	18479	51276	84178	–	–	–	–
$6d^{\delta}_{5/2g}$	20642	47443	74493	–	–	–	–
$5f^{\pi}_{1/2u}$	20764	29441	41312	–	(17990)	–	–
$5f^{\pi}_{3/2u}$	24535	33356	45747	–	(21010)	–	–
$7p^{\pi}_{1/2u}$	59179	103844	146927	–	–	–	–
$7p^{\pi}_{3/2u}$	62170	107330	152277	–	–	–	–
$5f^{\sigma}_{1/2u}$	69317	85553	107476	–	–	–	–
$7p^{\sigma}_{1/2u}$	74148	119663	164003	–	–	–	–

5.4.2 Electronic spectrum of NpO_2^+ and PuO_2^{2+}

In NpO_2^+ and PuO_2^{2+} both open shell electrons occupy the $5f^{\delta}_{3/2u}$ and the $5f^{\phi}_{5/2u}$ orbitals, resulting in a 4_g ground state. Since all lower excited states also belong to the $5f^2$ configuration, transitions between the ground and these excited states are electric dipole forbidden. The experimental spectra [176,179] are consistent with this picture, since most of the measured peaks have low intensity [171,176,178,180–183]. There is one intense peak at 10,204 cm^{-1} for NpO_2^+ and at 12,037 cm^{-1} for PuO_2^{2+}. The assignment of the spectrum is relatively easier for PuO_2^{2+} than for NpO_2^+, due to the larger splitting of the $5f$ orbitals in the former. Above 20,000 cm^{-1} the assignment becomes less certain for both NpO_2^+ and PuO_2^{2+}, as quintet charge transfer states also appear in this regio [163].

In Table 5.2 we present all the excitations up to 26,000 cm^{-1} for NpO_2^+ and, in Table 5.3, the excitations up to 34,000 cm^{-1} for PuO_2^{2+}. The experimental spectra were originally interpreted by Eisenstein and Pryce [176]on the basis of semiempirical ligand field calculations. These assignments were later reconsidered on the basis of more accurate calculations [163,165]. However, even in these recent results, there were typical errors of a few thousand wave numbers, making some of the assignments still uncertain. Our new calculations improve upon the excitation energies computed previously since we include all relativistic effects from the start and could also correlate more electrons, but a shortcoming is that we are not yet able to calculate oscillator strenghts with the current IHFSCC implementation. We therefore resorted to estimating the shape and intensities of the expected peaks on basis of the composition of the excited states, shown in Table 5.4. Eisenstein and Pryce [178] have previously argued that transitions between states that differ only on the sign of the z-component of the angular momentum, L_z, of one of the two unpaired electrons have to be narrow. This occurs because the charge distribution remains basically unchanged when going from the ground to the excited state. For excitations that involve a change of the absolute value of L_z, the peaks are broader due to vibrational excitations. This type of reasoning, combined with the fact transitions to doubly excited states should have a low intensity, gives sufficient information to assign the spectra of NpO_2^+ and PuO_2^{2+} on basis of our data.

From Table 5.4 one can furthermore see the high degree of similarity of the two isoelectronic actinyl ions. There are in general only slight differences in the values of the contributions from different configurations (for instance, the ground state of PuO_2^{2+} is more mixed than the NpO_2^+ ion, with more contribution of the higher-lying $5f^{\pi}_{3/2u}$ orbital), so the two spectra can be discussed together. To better structure

Table 5.2: Vertical excitation energies (E, in cm^{-1}) for NpO_2^+, calculated with the IHF-SCC method using the "IH-u" model space. The computed energies are evaluated at 1.701Å(equilibrium bond length). Previous assignment based on SOCI results from Matsika [163] and the experimental data are also given [164, 176]. The assignment of the experimental transitions in parenthesis is uncertain.

SOCI Matsika [163] $r_e = 1.720$Å		IHFSCC This work $r_e = 1.701$Å		Experimental Ref. [176]		Experimental Ref. [164]	
State	E (cm-1)	state	E (cm-1)	state	E (cm-1)	state	E (cm-1)
4_g	0	4_g	0	$^3H_4$	0	0	
0_g	3366	0_g	2527	Σ_0	–	Σ_{0g}	
5_g	4721	1_g	4102	Π_1	–	Π_{1g}	–
1_g	4938	5_g	5379	$^3H_5$	6173	$^3H_{5g}$	–
6_g	8867	0_g	8628	$^3\Pi_0$	8953	$^3\Pi_{0g}$	8953
1_g	9076	1_g	8929	$^3\Sigma_1$	9146	$^3\Sigma_{1g}$	9116
0_g	9537	0_g	9378	$^3\Pi_0$	9780	$^3\Pi_{0g}$	9777
0_g	9708	6_g	9690	$^3H_6$	–	$^3H_{6g}$	–
2_g	11187	2_g	10056	$^3\Pi_2$	10208	$^3\Pi_{2g}$	10202
				vib.	11160	vib.	10952
0_g	14415	0_g	14105	$^3\Gamma_3$	13020	$^3\Phi_{2g}$	12995
4_g	15249	4_g	14422	Σ_0	13824	–	–
1_g	16156	1_g	15031	$^1\Gamma_4$	14577	$^1\Pi_{1g}$	14558
0_g	19647	0_g	16551	$^3\Sigma_1$	16220	$^3\Delta_{2g}$	16221
1_g	21672	1_g	18992	$^3\Phi_2$	16100	–	–
5_g	22031	3_g	19735	Δ_2	16906	–	–
1_g	23079	5_g	19761	Σ_0	–	–	–
6_g	23327	6_g	20035	$^3\Delta_1$	18116	–	–
2_g	23649	2_g	21877	Π_1	(19360)	–	–
3_g	24834	2_g	23322	$^1I_6$	21008	–	21004
4_g	26592	4_g	25119	$^3\Delta_3$	(21700)	–	–
–	–	1_g	25436	$^3\Pi_0$	22600	–	–

the discussion about the assignments, we have divided the spectra into three regions, each possessing some features that are used for the interpretation of the experiment.

Region I: from 0 to 7,000 cm^{-1}

These three excited states differ by a single excitation from the ground state. In all cases there is a dominant determinant in which one electron belongs to either $5f^{\delta}$ or $5f^{\phi}$, both of which are occupied in the ground state. This region is not well sampled experimentally and therefore a clear comparison with our calculated data cannot be given. We confirm the original assignment of the peak at 6,173 cm^{-1} for the NpO_2^+ ion as a 5_g state [176] with a slightly lower computed energy of 5,379 cm^{-1} for this $4_g \rightarrow 5_g$ transition.

Region II: from 7,000 to 13,000 cm^{-1}

In this region we find excellent agreement with the experimental transition energies for both the neptunyl and plutonyl ions, with errors of about few hundred wavenumbers. The characteristic feature in both spectra is the intense peak that appears 10,204 cm^{-1} for NpO_2^+ and at 12,037 cm^{-1} for PuO_2^{2+}. A mechanism that can explain the intensity of this dipole-forbidden transition is described in detail by Matsika and coworkers [171], who considered systems with one, three and five chloride ions in the equatorial plane. Their calculations show that the ligand field from the latter arrangement gives sufficient mixing of the $5f^{\phi}$ and $6d^{\delta}$ to cause an intense $^3H_{4g} \rightarrow ^3\Pi_{2g}$ transition.

From the decomposition given in Table 5.4 it is clear that this 2_g state for NpO_2^+ is dominated by a single determinant, accounting for 93% of the total wave function. With respect to the ground state configuration, this state corresponds to the excitation of an electron from the $5f^{\phi}_{5/2u}$ to the $5f^{\phi}_{-7/2u}$ orbital. This is also the case for PuO_2^{2+}, for which the weight of the relevant determinant in the 2_g state is slightly smaller (at 83% of the total wave function), corroborating Matsika's [171] assignment.

The 6_g state is found close to the 2_g state, but it is unclear whether transitions to this state have enough intensity to be detected. Eisenstein and Pryce [176] suggested that the peak at 11,160 cm^{-1} is either due to this state or to vibrational progression of the 2_g transition. Our analysis shows a 6_g wave function dominated by two determinants, where one with the highest weight corresponds to a double excitation from the ground state. Combined with the fact that a transition energy below 10,000 cm^{-1} was obtained, we conclude that the assignment of the 11,160 cm^{-1} peak to 6_g is unlikely, and that the interpretation as a vibrational band is probably correct.

Regarding the assignment of the remaining peaks in region II, there are three other excited states, namely 0_g, 1_g and 0_g, that could be contributing. They all arise from orbitals that have the same δ and ϕ character as the ground state, but with different

Table 5.3: Vertical excitation energies (E, in cm^{-1}) for PuO_2^{2+}, calculated with IHF-SCC method using the "IH-u" model space. The computed energies are evaluated at 1.645Å(equilibrium bond length). For comparison the results of Maron [184] and Clavaguéra–Sarrio [165] are shown, along with the experimental data [179].

SDCI+Q+SO Maron [184] $r_e = 1.699$Å		CASPT2+SO Clavaguéra–Sarrio [165] $r_e = 1.677$Å		IHFSCC This work $r_e = 1.645$Å		Experimental Ref. [179]	
state	E (cm-1)	state	E (cm-1)	state	E (cm-1)	state	E (cm-1)
4_g	0	4_g	0	4_g	0	$^3H_4$	0
0_g	4295	0_g	4190	0_g	2530	Σ_0	–
5_g	6593	1_g	6065	1_g	4870	Π_1	–
1_g	7044	5_g	8034	5_g	6700	$^3H_5$	–
0_g	7393	0_g	12874	0_g	10334	$^3\Pi_0'$	10185
6_g	7848	1_g	12906	1_g	10983	Σ_1	10500
0_g	9415	6_g	14326	0_g	11225	$^3\Pi_0$	10700
1_g	12874	0_g	14606	6_g	11651	$^3H_6$	–
2_g	14169	2_g	14910	2_g	12326	$^3\Pi_2$	12037
						vib.	12660
5_g	16984	–	–	0_g	16713	$^1\Gamma_4$	15420
4_g	23091	–	–	1_g	17737	Σ_0	16075
1_g	27005	–	–	4_g	18565	Σ_1	17800
6_g	30254	–	–	0_g	20029	$^3\Gamma_3$	19100
3_g	33164	–	–	1_g	22703	Σ_0	19810
0_g	33314	–	–	6_g	22889	$^3\Phi_2$	21200
4_g	33318	–	–	5_g	23022	$^1H_5$	21840
3_g	33366	–	–	3_g	29710	Π_1	–
2_g	33388	–	–	2_g	32198	Δ_2	–
1_g	34520	–	–	0_g	32759	$^3\Gamma_4$	–
0_g	35210	–	–	1_g	34080	$^1I_6$	–
2_g	35670	–	–	4_g	34702	$^1I_5$	–
1_g	36703	–	–	2_g	34982	$^3\Delta_1$	–

signs of the L_z component (see Table 5.2 and 5.3). All the peaks should be narrow but differ in intensities. The calculations by Matsika [171] show that the transition to the 1_g state is more intense than the ones to the 0_g states. This leads to the conclusion that the peaks (at 9,146 cm^{-1} for NpO_2^+ and at 10,500 cm^{-1} for PuO_2^{2+}) should be

assigned to the 1_g state. While this interpretation had already been put forward with a good deal of certainty in previous works [171, 176], the IHFSCC results serve as a litmus test for this assignment as we can compare the spacing of the computed and observed peaks.

In the experimental spectrum of NpO_2^+ (Figure 1 of reference [171]) three narrow peaks are visible to the right (higher wave length) of the strong 2_g transition. The lowest energy transitions are separated by only 163 cm^{-1}, while the higher energy transitions appear as a well resolved shoulder on the 2_g transition at 9,780 cm^{-1}. Of the three peaks, the middle one is clearly the most intense. The relative energies of the 0_g, 1_g and 0_g states are indeed consistent with this spectrum, with the 1_g appearing in the middle separated by 301 cm^{-1} from the lower 0_g state and by 449 cm^{-1} from the higher 0_g state. The deviations from the experimental peak positions are thus maximally 400 cm^{-1}, which should be considered very good agreement for a gas phase model. In the less resolved PuO_2^{2+} spectrum [176], the 0_g, 1_g and 0_g states lie practically in the same band, with the 1_g peak at 10,500 cm^{-1}. This peak has one left shoulder, almost completely resolved at 10,185 cm^{-1}, and one right shoulder, hidden in the 1_g at 10,700 cm^{-1}. In our calculations a similar trend is found, with the lower 0_g and 1_g states again separated by a somewhat larger value (649 cm^{-1}) than the spacing that is experimentally observed (315 cm^{-1}). The calculated upper 0_g state is only 240 cm^{-1} higher than the 1_g, which is in very good agreement with the fit of the experimental data (where a distance of about 200 cm^{-1} is given).

Region III: above 13,000 cm^{-1}

For the higher excited states agreement with experiment cannot be expected to be as good, as there are larger effects due to the surroundings, and the possible presence of charge transfer states. Looking at the experimental spectra [176, 179], in the region we find for both neptunyl and plutonyl peaks with qualitatively similar shapes, with the most intense transition at about 16,000 cm^{-1} surrounded by satellite shoulders. For NpO_2^+ these shoulders are resolved and narrow, while for PuO_2^{2+} they are quite broad.

In our calculations we find five excited states (0_g, 4_g, 1_g, 0_g and 1_g) in this region, mainly made up by determinants containing δ and ϕ electrons in open shells. Based on the arguments put forth at the beginning of this section, this means that the associated peaks should be narrow. The oscillator strengths calculated by Matsika [171] indicate that the most intense of these peaks should be the 1_g state. Our calculations place this state at 15,031 cm^{-1} for NpO_2^+ and at 17,737 cm^{-1} for PuO_2^{2+}, whereas the

Table 5.4: Composition (in %) of the ground and some of the lowest excited states for NpO_2^+ and PuO_2^{2+}, together with the spinors occupied in the different IHFSCC sectors with respect to the closed shell species NpO_2^{3+} and PuO_2^{4+}. All values are obtained at the calculated equilibrium geometries (r_e = 1.701 Å and 1.645 Å, respectively) for the "IH-u" model space.

	IHFSCC configuration		weight (%)	
State	(0h,2p)	(0h,1p)	NpO_2^+	PuO_2^{+2}
4_g	$5f^{\delta}_{3/2u}$	$5f^{\phi}_{5/2u}$	94	81
	$5f^{\pi}_{3/2u}$	$5f^{\phi}_{5/2u}$	4	16
0_g	$5f^{\phi}_{5/2u}$	$5f^{\phi}_{-5/2u}$	59	70
	$5f^{\delta}_{3/2u}$	$5f^{\delta}_{-3/2u}$	32	18
1_g	$5f^{\delta}_{-3/2u}$	$5f^{\phi}_{5/2u}$	80	71
	$5f^{\phi}_{-5/2u}$	$5f^{\phi}_{7/2u}$	11	12
	$5f^{\delta}_{-3/2u}$	$5f^{\delta}_{5/2u}$	4	13
5_g	$5f^{\phi}_{5/2u}$	$5f^{\delta}_{5/2u}$	55	56
	$5f^{\delta}_{3/2u}$	$5f^{\phi}_{7/2u}$	43	36
0_g	$5f^{\phi}_{5/2u}$	$5f^{\delta}_{-5/2u}$	49	49
	$5f^{\delta}_{5/2u}$	$5f^{\phi}_{-5/2u}$	49	49
1_g	$5f^{\delta}_{-3/2u}$	$5f^{\delta}_{5/2u}$	55	41
	$5f^{\phi}_{-5/2u}$	$5f^{\phi}_{7/2u}$	28	37
	$5f^{\delta}_{-3/2u}$	$5f^{\phi}_{5/2u}$	12	10
0_g	$5f^{\phi}_{5/2u}$	$5f^{\delta}_{-5/2u}$	29	27
	$5f^{\delta}_{5/2u}$	$5f^{\phi}_{-5/2u}$	29	27
	$5f^{\delta}_{3/2u}$	$5f^{\delta}_{-3/2u}$	24	18
	$5f^{\delta}_{5/2u}$	$5f^{\delta}_{-5/2u}$	6	6
6_g	$5f^{\delta}_{5/2u}$	$5f^{\phi}_{7/2u}$	67	57
	$5f^{\phi}_{5/2u}$	$5f^{\phi}_{7/2u}$	33	43
2_g	$5f^{\delta}_{-3/2u}$	$5f^{\phi}_{7/2u}$	93	82
	$5f^{\pi}_{-3/2u}$	$5f^{\phi}_{7/2u}$	4	16
0_g	$5f^{\delta}_{5/2u}$	$5f^{\delta}_{-5/2u}$	31	20
	$5f^{\phi}_{5/2u}$	$5f^{\phi}_{-5/2u}$	25	23
	$5f^{\phi}_{5/2u}$	$5f^{\delta}_{-5/2u}$	14	16
	$5f^{\delta}_{5/2u}$	$5f^{\phi}_{-5/2u}$	14	16
	$5f^{\delta}_{3/2u}$	$5f^{\delta}_{-3/2u}$	11	15
4_g	$5f^{\delta}_{3/2u}$	$5f^{\delta}_{5/2u}$	83	72
	$5f^{\pi}_{3/2u}$	$5f^{\delta}_{5/2u}$	5	18
1_g	$5f^{\phi}_{5/2u}$	$5f^{\phi}_{-7/2u}$	43	43
	$5f^{\delta}_{5/2u}$	$5f^{\phi}_{-7/2u}$	38	26
	$5f^{\delta}_{3/2u}$	$5f^{\delta}_{-5/2u}$	11	19

	IHFSCC configuration		weight (%)	
0_g	$5f^{\phi}_{7/2u}$	$5f^{\phi}_{-7/2u}$	35	47
	$5f^{\delta}_{5/2u}$	$5f^{\delta}_{-5/2u}$	27	33
	$5f^{\delta}_{3/2u}$	$5f^{\delta}_{-3/2u}$	21	12
1_g	$5f^{\delta}_{5/2u}$	$5f^{\phi}_{-7/2u}$	56	65
	$5f^{\phi}_{5/2u}$	$5f^{\phi}_{-7/2u}$	23	14
	$5f^{\delta}_{3/2u}$	$5f^{\delta}_{-5/2u}$	20	19
3_g	$5f^{\phi}_{5/2u}$	$5f^{\pi}_{1/2u}$	96	97
5_g	$5f^{\delta}_{3/2u}$	$5f^{\phi}_{7/2u}$	55	50
	$5f^{\phi}_{5/2u}$	$5f^{\delta}_{5/2u}$	44	43
6_g	$5f^{\phi}_{5/2u}$	$5f^{\phi}_{7/2u}$	67	56
	$5f^{\delta}_{5/2u}$	$5f^{\phi}_{7/2u}$	33	43
2_g	$5f^{\phi}_{5/2u}$	$5f^{\pi}_{-1/2u}$	91	96
2_g	$5f^{\delta}_{3/2u}$	$5f^{\pi}_{1/2u}$	93	80
	$5f^{\pi}_{3/2u}$	$5f^{\pi}_{1/2u}$	2	19
4_g	$5f^{\phi}_{5/2u}$	$5f^{\pi}_{3/2u}$	58	62
	$5f^{\phi}_{7/2u}$	$5f^{\pi}_{1/2u}$	37	20
1_g	$5f^{\phi}_{5/2u}$	$5f^{\pi}_{-3/2u}$	89	73
	$5f^{\phi}_{5/2u}$	$5f^{\delta}_{-3/2u}$	2	21

experimental positions are almost the same for both ions (16,220 cm^{-1} and 16,075 cm^{-1}, respectively).

Matsika, however, suggested that this peak results from a transition to a $^3\Delta_{2g}$ state arising from occupation of the $5f^{\pi}$ orbital. As already discussed in the previous section on NpO_2^{2+}, the $5f^{\pi}$ orbital is at a rather high energy relative to the $5f^{\phi}$ and $5f^{\delta}$. Consequently, all states with significant $5f^{\pi}$ character are found too high in energy (around 20,000 cm^{-1} for NpO_2^{+} and 30,000 cm^{-1} for PuO_2^{2+}) to be associated with transitions at 16,000 cm^{-1}. While this may be an artifact of our gas phase model, it could also be that the the observed transition is to the 1_g state, rather than the 2_g state. This is particularly the case for PuO_2^{2+}, where it does not seem probable that the the surrounding water molecules lower this metal-to-metal transition to half the gas phase value. We therefore propose to reassign this transition to the 1_g state.

Another reassignment may be necessary for the experimental peak at 13,020 cm^{-1} for NpO_2^{+}. This peak was previously assigned to a 3_g state by Eisenstein and Pryce [176], and later to a 2_g state by Matsika [171]. In both cases, the composition of this excited state included a $5f^{\pi}$ orbital that we anticipate to get occupied only at much higher energies. It is difficult to assign these peaks with certainty, because

the differences in energies involved are rather small. We notice, however, that the calculated 4_g state lies at lower energies than the more intense 1_g for NpO_2^+, while appearing at higher energies for PuO_2^{2+}. This agrees with the experimental spectra, where one small peak at lower energies than the state we assigned as the 1_g is found in the plutonyl spectrum, whereas two peaks are found for neptunyl.

Given the uncertainties related to the position of charge transfer peaks (found slightly above 20,000 cm^{-1} in the calculations of Matsika and Pitzer [163]), we do not attempt to compare our computed excitation energies at higher energies to the experimental data.

Comparison with previous calculations

Comparing our computed excitation energies for NpO_2^+ with those of Matsika and Pitzer [163], we see that a more rigorous treatment of electron correlation and relativistic effects indeed results in smaller deviations from experiment. This is so for the lower excited states (below 10,000 cm^{-1}), but also for most of the higher states, especially the important 2_g state, which differs from experiment by less than 200 cm^{-1}, compared to over 1,500cm^{-1} for previous calculations.

More theoretical calculations are available for the plutonyl ion, so the relative accuracy of our results and the strenghts and weaknesses of the IHFSCC method can better be assessed. The calculations of Maron and coworkers [184], and of Clavaguéra–Sarrio and coworkers [165], give rise to a rather similar assignment of the lower excited states, but report excitation energies quite different from ours and from experiment. For instance, the results of Maron [184] underestimate the low–lying transitions (region I) and strongly overestimate the upper states (region III), with discrepancies with respect to the experimental transitions of more than 10,000 cm^{-1}. Our calculations show errors on the 1,000-2,000 cm^{-1} range for these states. The later calculations of Clavaguéra–Sarrio are better than those of Maron [184] for region II states, but their errors are still quite large (more than 2,000 cm^{-1}) when compared to what can be achieved with the IHFSCC method, that shows deviations of about 500 cm^{-1}.

5.4.3 Potential Energy Curves

As the IHFSCC method allows the determination of multiple states available in a single calculation, it was quite easy to determine the equilibrium bond distances and vibrational symmetric stretch frequencies for a number of different states. These quantities are shown in Table 5.5. An important difference between these results and

Table 5.5: Bond Lenghts (in Å) and Harmonic frequencies (in cm^{-1}) for the first 14 states of NpO_2^+ and PuO_2^{2+}, derived from potential energy surfaces for the symmetric stretch. These surfaces were obtained with IHFSCC method using the "IH-u" model space.

	NpO_2^+			PuO_2^{2+}	
State	r_e (Å)	ω_e (cm^{-1})	State	r_e (Å)	ω_e (cm^{-1})
4_g	1.700	1073	4_g	1.643	1144
0_g	1.701	1061	0_g	1.654	1048
1_g	1.699	1069	1_g	1.643	1162
5_g	1.699	1080	5_g	1.637	1334
0_g	1.699	1081	0_g	1.637	1361
1_g	1.698	1072	1_g	1.637	1351
0_g	1.695	1082	0_g	1.634	1324
6_g	1.701	1075	6_g	1.642	1087
2_g	1.697	1063	2_g	1.636	1281
0_g	1.691	1093	0_g	1.637	1332
4_g	1.698	1086	1_g	1.630	1284
1_g	1.701	1083	4_g	1.636	1400
0_g	1.701	1179	0_g	1.637	1439
1_g	1.724	1564	1_g	1.640	1377

those of previous calculations is the difference of the bond lenghts for the ground state of both molecules. For neptunyl, the bond length is about 0.02 Å shorter that the value given by Matsika [163], whereas for plutonyl the bond length is about 0.05 Å shorter than reported by Clavaguéra–Sarrio [165] and 0.03 Å shorter than given by Maron [184]. These differences could be due to the inclusion of $6p$ orbitals in the correlated active space in our calculations, allowing the oxo ligands to move closer to the actinide, but we have not investigated this in detail.

The differences in the calculated excited energies shown here and those of previous works decrease to some extent if IHFSCC calculations are performed at the corresponding equilibrium geometries, thus indicating that part of these discrepancies are due to geometrical effects. We observed, however, that also in these situations the IHFSCC calculations generally show better agreement with experiment.

The harmonic frequencies of the ground state of neptunyl and plutonyl differ by about 69 cm^{-1} (1,073 cm^{-1} and 1,144 cm^{-1}), which is of course mainly due to the difference in charge. It is interesting that the frequencies for the low-lying excited states of neptunyl are very similar to that of the ground state whereas for plutonyl variations of up to 200-300 cm^{-1} are seen. Comparison to experimental data is

difficult as it is well-known that solvation and complexation lowers the vibrational frequencies of actinyls considerably [185]. Madic et al. [186] give Raman data for these ions in aqueous solution. The difference in values for the symmetric stretch of NpO_2^+ and PuO_2^{2+} (767 and 833 cm^{-1}, respectively) of 66 cm^{-1} is remarkably similar to our computed gas phase difference of 71 cm^{-1}

5.5 Conclusions

In this work we have investigated the ground and excited states of the actinyl ions NpO_2^+ and PuO_2^{2+}. While the spectra of these ions had been studied before, there was still a good deal of uncertainty with respect to the ordering and spacing of different electronic states. In this work we were able to improve upon previous calculations on both aspects. First, we have established with great certainty that the experimentally most intense peak found for both the actinyl ions has a 2_g symmetry. Second, the average errors we obtain compared to previous calculations are much smaller so that more definite assignments of these spectra could be made. This is particularly important for the higher excited states, where results from previous calculations varied considerably.

The use of the IHFSCC method allowed for the economical determination of several electronic states at once, while accurately describing both static and dynamic correlation energies. The IHFSCC method in its current form, however, is not without drawbacks. Important is the limitation on the Fock space sectors that are implemented. For instance, by using only sector (0h,2p) only triplet f^2 states can be described, making charge transfer states of the neptunyl ion unaccessible. For quintet states, a mixed sector (1h,3p) must be employed, but it is yet to be implemented in the DIRAC code. Another drawback is related to issues of convergence, which still demand experimentation with the P, Q partitioning, and prevent the method to be used in a "black–box" manner that is desired when using the method for larger and more complex systems.

5.6 Acknowledgements

The authors wish to thank the Netherlands Organization for Scientific Research for financial support via the "Jonge Chemici" programme and like to acknowledge stimulating discussions with Dr. Ephraim Eliav and prof. Uzi Kaldor on the application of their IHFSCC methods.

Part II

Part II : DFT calculations on aqueous systems

CHAPTER 6

A QM/MM study on the aqueous solvation of the tetrahydroxouranylate $[UO_2F_4]^{2-}$ complex ion

The Big Lebowski: Are you employed, sir?
The Dude: Employed?
The Big Lebowski: You don't go out looking for a job dressed like that? On a weekday?
The Dude: Is this a... what day is this?

form the movie The Big Lebowski (1998)

6.1 Abstract

The aqueous solvation of the uranylfluoride $[UO_2F_4]^{2-}$ complex was studied using full quantum mechanical and hybrid quantum mechanical / molecular mechanics methods. Inclusion of a complete first solvation shell was found necessary to reproduce the experimentally observed hepta-coordination of uranium. An efficient and accurate computational model is proposed that consists of structure optimization of the coordinated uranium complex as quantum mechanical region, followed by a single point full QM calculations to compute relative energies. This method is proven feasible for studies of large solvated actinide complexes.

6.2 Introduction

Trying to achieve quantitative understanding of the rich chemistry of the actinides is challenging for both experimental and theoretical chemists. Experimental work is difficult due to the precautions that need to be taken due to the radioactivity and high toxicity of the materials. The interpretation of experiments in terms of a simple model is furthermore far from trivial because many orbitals may contribute to chemical bonding [187]. This situation calls for invocation of theoretical methods both as an aid in the interpretation of the experiment and as an independent tool to study details of reaction mechanisms. The most accurate of the theoretical methods is in principle the fully relativistic four-component wave function approach combined with a coupled cluster expansion to describe the correlations in the electronic motion [188,189]. One can, however, only apply this method for rather small molecules. The description of the larger actinide complexes requires the introduction of approximations in both the relativistic and the electron correlation treatment. Here we will focus on one of the most popular methods, the zero-order regular approximation (ZORA) [54] of the Dirac equation, combined with gradient corrected Density Functional Theory. This computational model has been proven to be applicable to rather large molecules with an accuracy of a few kJ/mol in the energy and a few pm in typical bond lengths.

The migration and complexation of actinides in aqueous solution is of central importance in many situations of practical interest [190–192]. To describe such solvated complexes that are often in strongly acidic or alkaline solution [193], we want to augment the ZORA model with a reliable description of solvation effects. Purpose of the present work is to assess the reliability of a ZORA-DFT QM/MM approach in studies of solvated actinides.We chose to concentrate on the modelling of the uranyl ion that forms the basis for several stable complexes. This molecule has been extensively studied in the gas-phase using a variety of computational models [194–198]. Coordination in a solvent was studied by Schreckenbach et al. [199] who considered four hydroxy ions. We will focus on the $[UO_2F_4]^{2-}$ complex [200], in which the uranyl ion is equatorially coordinated by four fluorine atoms, since the recent EXAFS experiment Vallet et al. [201] provides experimental information to compare our computed structures to. Because Vallet et al. [201] also did a theoretical investigation to determine the effect of a first shell of three water molecules on the structure of the $[UO_2F_4]^{2-}$ their work serves as a good starting point for our investigation on the inclusion of explicit solvent layers. We expect that this detailed description of hydrogen bonding and other microscopic interactions will improve upon the description of solvated uranyl complexes by continuum models. As a secondary objective we can also gauge the

reliability of the QM/MM scheme itself by comparison with full QM calculations of the solvent shells.

Experimentally the $[UO_2F_4(H_2O)]^{2-}$ complex is known to be hepta-coordinated in solution, i.e. with one water molecule being coordinated to the uranium atom. Since theoretically the hypothetical gas-phase (isolated) complex is a logical reference point, we started by analyzing the conformations of the $[UO_2F_4(H_2O)]^{2-}$ complex in both gas and liquid phases. This offers a conceptual framework that makes it possible to understand how the solvent affects the structure and reactivity of these compounds in the condensed phase. This is detailed by surrounding this central complex by an increasing amount of water molecules that will represent the first and second solvation layer.

The outline of the paper is as follows: section 2 describes the computational method that we will use while we discuss the results of this approach in section 3. This section is subdivided according to the different results obtained as: geometry (6.4.1), bonding in the gas-phase (6.4.2) and bonding in the solvent (6.4.3). In section 6 we conclude by giving recommendations for further work.

6.3 Methodology

As discussed above, a relativistic treatment of the uranyl is mandatory as electrons reach relativistic velocities close to the highly charged nucleus of uranium. We employ the scalar relativistic ZORA-DFT method [54–57, 202] as implemented in the ADF2002 code developed by Baerends et al. [119,120]. The spin restricted Kohn-Sham method is used to compute ground state properties applying the BPW91 gradient-corrected functional which involves the exchange functional by Becke88 [92] and the Perdew-Wang correction for the correlation part [203].

The $[Xe]4f^{14}5d^{10}$ core of the uranium atom and the $1s^2$ core of the oxygen and fluorine atoms are kept frozen. The basis set is an uncontracted triple-ζ Slater Type Orbital (STO) augmented by two polarization functions (TZ2P). In order to take account of the relativistic effects in the core regions, an auxiliary program is applied to compute the relativistic core densities and core potentials using the X-alpha local density approximation [204]. The hybrid QM/MM method developed by Woo, Cavallo and Ziegler [106] serves to introduce water molecules to the basic $[UO_2F_4(H_2O)]^{2-}$ complex. For the molecular mechanics region, the AMBER95 program [107]is utilized as implemented in the ADF2002 version. The potential energy is computed in the

following way:

$$E_{MM}^{II} = \sum_{r}^{bonds} K_b(r-r_0)^2 + \sum_{\theta}^{angles} K_\theta(\theta-\theta_0)^2 + \sum_{n}^{dihedrals} V_n(1+\cos(n\phi-\gamma)) + \\ + \sum_{i<j}^{atoms} \epsilon\left[\left(\frac{R^*}{R_{ij}}\right)^{12} - 2\left(\frac{R^*}{R_{ij}}\right)^{6}\right] + \sum_{i<j}^{atoms} \frac{q_i q_j}{R_{ij}} \quad (6.1)$$

with K_b representing the bond stretching force constants and K_θ the bending constants; V_n is the rotational potential; ϵ is the well-depth, with R^* as the van der Waals bond length; q_i is the charge on atom i. Most parameters could be taken from the default AMBER95 parameterization but force field parameters that involve the uranium atom had to be added explicitly. For the van der Waals interaction part we treated the oxygen atoms linked to the uranium as carbonyl oxygen atoms and took $R^* = 1.400$ Å and $\epsilon = 0.12$ kJ/mol, as was recommended by Guilbaud and Wipff [205]. The stretching and bending parameters for the atoms bonded to uranium were obtained from a reference full quantum mechanical (BPW91/TZ2P) calculation on the $UO_2F_4(H_2O)^{2-}$ complex surrounded by eleven water molecules using Badgers rules [108]. All torsional contributions involving uranium were set to zero. The fit of the reference DFT data is not very critical in this case because all parameters that describe the bonding to uranium are only used in MM-only computations. In the QM/MM calculations all bonds to uranium belong to the QM region and are computed explicitly. The most relevant MM parameters are the charges (q) used in the evaluation of the electrostatic interaction. We thereby chose multipole derived charges [109], that were initialized to the values obtained from the reference calculation on $[UO_2F_4(H_2O)]^{2-}$, and were updated in a self-consistent manner during the geometry optimizations of the complex under study. Since the QM/MM scheme does not allow for polarization of the QM part, exerting only a mechanical coupling between the two regions, this relaxation should not be interpreted as measuring the direct influence from the surrounding but rather as correcting for the changes induced by the change of geometry in the QM part.

All structure optimizations were performed using tight convergence criteria on the gradient (10^{-4}) for both the QM and the MM region. The same accuracy (10^{-4}) was also used in the determination of the grid for numerical integration.

6.4 Results and Discussion

6.4.1 Structure of the $[UO_2F_4(H_2O)]^{2-}$ in the gas and solvent phases. MM modeling.

The uranium ion can assume two possible configurations: a square bipyramidal (hexa) geometry or a pentagonal bipyramid (hepta). For the uranium fluoride compound, the axial ligands are the oxygen atoms, forming the uranyl UO_2^{2+} ion while the four fluorine ions (hexa coordination) or four fluorine ions plus one-water molecule (hepta coordination) lie in the equatorial plane. In aqueous solution the latter coordination presents the most stable configuration.

We start by investigating the hypothetical $[UO_2F_4(H_2O)]^{2-}$ gas-phase complex. This complex was also studied by Vallet et al. [201] using both an ab initio (MP2) and a hybrid DFT (B3LYP) approach. We repeated their gas calculation using the non-hybrid DFT BPW91 approach to assess the difference that the choice of functional makes. The resulting geometrical parameters are given in Table 6.1 and 6.2. The C_{2v} symmetric hepta-coordinated $[UO_2F_4(H_2O)]^{2-}$ complex has a H_2O molecule with the hydrogen atoms directed externally. The BPW91 functional gives elongated U-O and U-O_{H_2O} bond distances (differences of 0.028 Å and 0.104 Å respectively compared to the B3LYP description) while the axial U-F_a and U-F_b bonds differ only by 0.004 Å and 0.008 Å, respectively. Analysis of the frequencies shows, however, that the optimized geometry is a saddle point with two imaginary frequencies: 496i cm^{-1} (b_1) and 322i cm^{-1} (b_2). The hexa-coordinated compound (C_{2v}), for which the H_2O molecule is bound by two hydrogen bonds, is a (local) minimum as could be verified by explicit optimization and frequency analysis.

From these results it is clear that the presence of other water molecules is required to obtain the hepta-coordination that is found experimentally. The question is then how many of such water molecules need to be added and how many of these molecules need to be described as quantum mechanical objects. To answer both questions we added an increasing number of water molecules and studied the convergence of the hepta-hexa coordination energy difference. In doing so we also looked at the division of the entire complex (solute + solvent) in the QM and MM regions. Since we are interested in an accurate, but also computationally efficient scheme, we want to keep the amount of QM water as low as possible. Using a full QM approach we first investigated three kinds of solvent models: a minimal approach, computing only the $[UO_2F_4(H_2O)]^{2-}$(1) complex; Vallets ansatz [201], in which the complex and a first shell of three equatorial water molecules $[UO_2F_4(H_2O)]^{2-}\cdot 3H_2O$ (2) are included;

Table 6.1: Geometrical parameters (bonds in Å and angles in degrees) of the hexa-coordinated tetrafluorouranylate ion with different QM/MM partionings of the system.

	No. of	QM	MM				
Complex	waters	region	region	U-O_{ax}	U-F_a	U-F_b	U-O_{H_2O}
0	0	$[UO_2F_4]^{2-}$	None	1.86	2.23	2.23	–
Hexacoordinated							
1a	1	$[UO_2F_4H_2O]^{2-}$	None	1.84	2.27	2.21	3.96
2a	4	$[UO_2F_4H_2O]^{2-}\cdot 3H_2O$	None	1.82	2.26	2.26	3.94
2b	4	$[UO_2F_4H_2O]^{2-}$	$3H_2O$	1.83	2.26	2.23	3.72
3a	12	$[UO_2F_4H_2O]^{2-}\cdot 11H_2O$	None				
3b	12	$[UO_2F_4H_2O]^{2-}$	$11H_2O$	1.84	2.25	2.21	3.77
3c	12	$[UO_2F_4H_2O]^{2-}\cdot 3H_2O$	$8H_2O$	1.83	2.27	2.23	3.58
4	17	$[UO_2F_4H_2O]^{2-}$	$16H_2O$	1.84	2.24	2.21	3.83
5	30	$[UO_2F_4H_2O]^{2-}$	$29H_2O$	1.84	2.24	2.20	3.77
Exp.				1.80	2.26	2.26	2.48

Table 6.2: Geometrical parameters (bonds in Å and angles in degrees) of the hepta-coordinated tetrafluorouranylate ion with different QM/MM partionings of the system.

Complex	No. of waters	QM region	MM region	U-O_{ax}	U-F_a	U-F_b	U-O_{H_2O}
0	0	$[UO_2F_4]^{2-}$	None	1.86	2.23	2.23	–
Heptacoordinated							
1a	1	$[UO_2F_4H_2O]^{2-}$	None	1.85	2.22	2.30	2.85
2a	4	$[UO_2F_4H_2O]^{2-}\cdot 3H_2O$	None	1.83	2.27	2.31	2.70
2b	4	$[UO_2F_4H_2O]^{2-}$	$3H_2O$	1.84	2.24	2.30	2.72
3a	12	$[UO_2F_4H_2O]^{2-}\cdot 11H_2O$	None	1.85	2.27	2.28	2.65
3b	12	$[UO_2F_4H_2O]^{2-}$	$11H_2O$	1.85	2.22	2.29	2.68
3c	12	$[UO_2F_4H_2O]^{2-}\cdot 3H_2O$	$8H_2O$	1.83	2.27	2.30	2.62
4	17	$[UO_2F_4H_2O]^{2-}$	$16H_2O$	1.85	2.21	2.29	2.70
5	30	$[UO_2F_4H_2O]^{2-}$	$29H_2O$	1.84	2.21	2.28	2.65
6	30	$[UO_2F_4H_2O]^{2-}$	$71H_2O$	1.84	2.21	2.28	2.65
Exp.				1.80	2.26	2.26	2.48

and a more elaborate approach where the first solvation shell consists of eleven water molecules, $[UO_2F_4(H_2O)]^{2-}\cdot 11H_2O$ (3). Model (2) allows for the quantum mechanical description of the six hydrogen bonds with the fluorine atoms while in the full model (3) the water molecules also provide for hydrogen bonds with the F_a, F_b atoms and with the O_{yl}. To study the effect of the partitioning we then also constructed the larger models from the smaller models by adding MM waters instead of QM waters. To distinguish between the different QM/MM partitionings we append the label (a) to full QM models, (b) to QM/MM models that have only the smallest possible QM region and (c) to mixed models where one part of the solvation shell is modeled by QM waters and another part by MM. In all QM/MM cases we performed full structure optimizations in C_1 symmetry, using explicit constraints to keep the hepta coordinated complex from relaxing to the hexa coordinated form. In principle this goal should also be attainable by imposing C_s (or C_{2v}) symmetry in the geometry optimization but for technical reasons this was not possible in the ADF-2002 QM/MM implementation. The full QM computation of the (3a) complex takes about six times longer than that of the (2a) and about twenty times longer than that of the (1a) while the molecular mechanics computations takes a negligible amount of time, also for large numbers of water molecules.

In Table 6.1 and 6.2 we see the effect on the geometry of the primary complex that is induced by the solvent molecules as a function of system size and partitioning. Adding three water molecules shortens the uranyl bond, elongates the U-F distances, and makes the coordinated water approach the uranium more closely. Replacing the three QM water molecules in (2a) by their MM counterparts (2b) does not alter this qualitative picture but makes the effects less pronounced. When we pass on to the complete first shell model (3) the uranyl bond becomes longer again in all QM/MM partitionings. For the U-F bond distance, where experiment can not distinguish between U-F_a and U-F_b and provides the single value 2.26 Å , we see that the partitionings (3a) and (3b) give an average value that is in good agreement with each other and the experimental value, while model (3c) deviates by about 0.02 Å . The most significant changes are seen in the uranium-water bond distance. In all approaches we find a shortening of this bond that amounts to 0.2 Å in the full QM approach (3a). One could describe this as the surrounding water molecules pushing one water molecule towards the uranium atom.

We thus see that the solvent indeed modifies the structure of the complex significantly and that the choice of the method to describe the solvent is to some extent secondary since both the full QM and the QM/MM models give the same trend. Three

equatorial water molecules are not enough to describe the first shell solvation shell but eleven water molecules are sufficient to provide a realistic model. Throughout the rest of the paper, we will focus on the (1a) partitioning because this provides the most economical treatment. The (2a) model where we have three additional water molecules does not improve the situation, possibly because it introduces an artificial distinction between molecules from the first shell. This makes the (1a) model give results closer to the most complete model (3a). We have not tried to test with full QM models beyond 11 water molecules since we encountered problems in the structure optimization. Already with 3 water molecules the procedure needs a large number of optimization cycles to converge the structure and beyond 11 QM water molecules we expect difficulties in reaching a stationary point at all. This gives another incentive to keep the number of explicitly treated water molecules in the QM region as small as possible and favors the minimal choice (3b) where model (1a) is augmented by 11 MM water molecules.

We now extend the layer of MM water molecules further to consider also the second shell, the ensemble of water molecules that embeds the (1a)+11H_2O complex. Table 6.3 shows that the effect on the bond distances induced by the aqueous solution beyond the first shell is rather small. For example, the U-O_{yl} bond distance achieves a minimum value of 1.844 Å for 60 water molecules in the second shell and a maximum of 1.846 Å (4 H_2O in the second shell) an oscillation of only 0.002 Å. The behavior of the other bonds is similar, with the exception of the U-O_{H_2O}, which is also sensitive to the second shell: the contraction of this bond length (0.050 Å) is smaller than the first-shell contribution (0.204 Å), but the outer water molecules can not entirely be neglected. We will see in the next section that even though the second solvation shell does not have a large influence on the geometrical parameters it is important for the difference in solvation energy of hexa and hepta conformations.

6.4.2 Electronic structure of the $[UO_2F_4(H_2O)]^{2-}$ complex in the gas-phase. The difference between hexa and hepta coordination.

Given the optimized structures we may now explain the behavior of the hexa and hepta compounds in both the gas and solvent phases. We thereby employ the fragment decomposition scheme by Ziegler and Rauk [206, 207] to analyze the interaction between the $[UO_2F_4]^{2-}$ fragment and the H_2O molecule. In the gas-phase the hexa form is more stable by 146.1 kJ/mol. This energy difference comes mainly (121.4

Figure 6.1: The (1a) complex represents the hexa and hepta structures in the gas phase. For the larger complexes we display only the hepta conformation. The (2a) complex represents (1a) surrounded by an incomplete first shell of three water molecules; the (3a) complex represents the (1a) complex embedded by a full first shell of eleven H_2O. The (6) complex represents the largest cluster used and contains 72 water molecules.

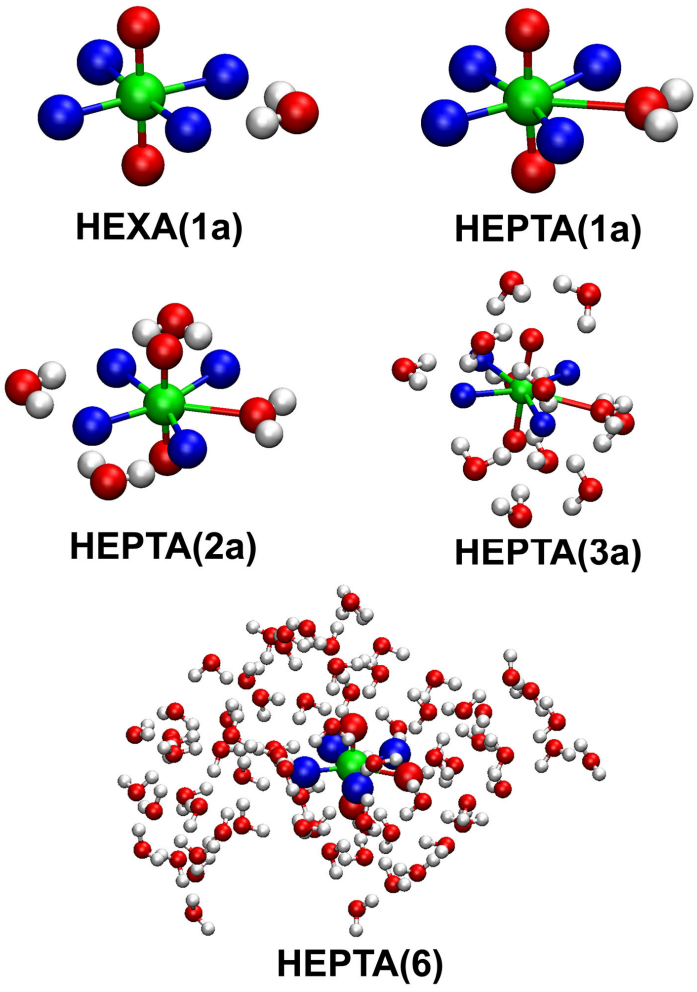

Table 6.3: Bonding Energies (kJ/mol) between the $UO_2F_4^{2-}$ and H_2O fragments in the Gas-phase. The interaction energy is further decomposed into electrostatic, Pauli repulsion, and orbital interaction terms. All values are computed using the BPW91/TZ2P functional.

	hexa	hepta	Δ(hexa-hepta)
$[UO_2F_4]^{2-}$ fragment	-4752.0	-4728.2	-23.9
H_2O fragment	-1377.9	-1377.0	0.8
Interaction Energy	-104.7	16.7	-121.4
Total Energy	-6234.6	-6088.4	-146.1
Interaction Energy			
Electrostatic Interaction	-127.3	-50.2	-77.0
Pauli Repulsion	78.3	96.3	-18.0
Orbital Interactions	-55.3	-29.3	-26.0
Pauli+Orbital	23.0	67.0	-44.0

kJ/mol) from the difference in interaction between the two fragments $[UO_2F_4]^{2-}$ and H_2O, that is strongly negative in the hexa structure (-104.7 kJ/mol) and slightly positive in (+16.7 kJ/mol) in the hepta structure. There are different ways to partition this interaction energy further. One may either sum the steric interactions (Pauli repulsion plus electrostatic term) and leave the orbital interaction term alone, or add the short-range quantum-mechanical interactions (Pauli repulsion and orbital interaction) and consider the long-range classical electro-static part separately. Since we are interested in comparing clusters of various sizes as well as classical QM/MM and full QM calculations we chose the latter decomposition.

Table 6.3 shows that the main difference (77.0 kJ/mol) between the hexa and hepta molecules is caused by the difference in electrostatic interaction that is much more negative for the hexa structure (-127.3 kJ/mol) than for the hepta structure (-50.2 kJ/mol). This large difference illustrates the difficulty in describing the negative central complex in a gas phase model. In hepta-coordination the negative oxygen atom needs to penetrate between the negative fluorine atoms. The larger Pauli repulsion and the less favorable orbital interactions work in the same direction. In the hexa coordination we find the oxygen atom at the outside with the hydrogen atoms pointing towards the fluorine ions and forming hydrogen bonds. Apart from being obviously more favorable for the electrostatic interaction this also leads to a more favorable Pauli repulsion term and orbital interactions. For the latter term the difference comes mainly from the interaction in the B_2 irrep where a small charge transfer (0.03e) interaction between the $7b_2$ orbital from the $[UO_2F_4]^{2-}$ fragment (localized on the

p orbitals of the fluorines) towards the unoccupied $2b_2$ (predominantly hydrogen s) orbital of the water is possible. This charge transfer is only 0.01e in the case of the hepta complex, illustrating the less effective hydrogen bonds in that structure.

6.4.3 Electronic structure of the HEXA and HEPTA complexes in the solvent phase.

As anticipated we found by explicit computation that the gas phase calculations cannot explain the hepta-coordination that is found experimentally. The solvent must thus induce the change of the structure from hexa to the hepta form and the question is how many water molecules need to be taken into account to reproduce this effect. To make this analysis possible we computed energies for the different models fully quantum mechanically in single-point SCF calculations at geometries obtained with the QM/MM method. Having the total QM energies at hand we can then also compare the hexa-hepta energy differences with those found at the QM/MM level of theory.

The computed energy gap (E_{HEXA}-E_{HEPTA}) as a function of the number of water molecules (Figure 6.2) does indeed decrease with an increasing number of solvent molecules and confirms the hypothesis that the solvent stabilizes the hepta structure more than the hexa structure. Important is also that this decrease is independent of the method chosen (QM/MM or full QM) to compute the energy. In both cases one finds that the energy of the hepta-coordinated complex is lower than that of the hexa-coordinated complex as soon as the first solvation shell is completed.

We can look into more detail how this mechanism works by employing once more the fragment decomposition scheme. This time we will focus on the charge transfer between the uranyl fluoride $[UO_2F_4(H_2O)^{2-}]$ fragment and the water surrounding it because it serves to reduce the unfavorable electrostatic interaction in the hepta structure. In Table 6.4, we summarize the contributions of 3, 11, 16 and 29 water molecules taking the entire complex (1) as one fragment and the solvation shell as the other. The energy difference between the hexa and hepta structures can be attributed to three factors: the energy of the solute, the energy of the solvation shell and their interaction energy. The first term concerns the different energies of the hexa and hepta coordinated complexes themselves. This energy difference remains rather stable around at the gas phase value of 146.1 kJ/mol reported in the previous section. The energy difference between interactions in the solvent layers of the hexa and hepta structures depends mainly on the structure optimization that tries to maximize the number of hydrogen bonds that are formed between the water molecules. Here we

Table 6.4: Decomposition of the $\Delta(E_{HEXA} - E_{HEPTA}$ Energy Difference (kJ/mol) taking the $[UO_2F_4(H_2O)]^{2-}$ and the surrounding water shell as Fragments.The interaction energy is further decomposed into electrostatic, Pauli repulsion, and orbital interaction terms (for a full QM system) and into electrostatic and van der Waals terms (for QM/MM). All QM terms are computed using the BPW91/TZ2P functional at the geometries optimized with the QM/MM scheme.

		3	11	16	29
$[UO_2F_4(H_2O)]^{2-}$ (I)	QM	-146.1	-144.9	-147.0	-147.4
	MM	15.1	-16.3	-33.5	-25.1
Water cluster (II)	QM	-7.1	-79.1	-92.5	-55.7
	MM	-8.8	-78.7	-102.6	-92.9
Interaction (I-II)	QM	55.7	179.6	189.7	206.8
	MM	56.9	198.5	220.2	240.7
Total (I + Interaction I-II)	QM	-90.4	34.3	42.3	59.5
	MM	72.0	182.1	186.7	215.6
	QM/MM	-89.2	53.6	73.3	93.4
Interaction Energy (QM)					
Electrostatic		67.0	247.9	273.3	305.2
Pauli		-52.3	-168.7	-222.3	-288.9
Orbital interaction		41.0	100.5	138.6	190.5
Pauli + Orbital		-11.3	-68.2	-83.7	-56.5
Interaction Energy (QM/MM)					
Electrostatic		70.8	216.0	253.3	279.7
van der Waals		-13.8	-17.6	-32.7	-38.5

encounter the limitations of the cluster-embedding model because, upon going to large numbers of water molecules, this energy becomes dominated by the peripheral water molecules. The truncation of the water droplet and accompanying loss of hydrogen bonding possibilities makes the model sensitive to the different constraints that hexa and hepta coordination impose. This adds an unpredictable artifact that makes the difference in total energies unreliable. To avoid this cluster dependent contribution we decided to use as reference energy the sum of the contributions of the QM region $[UO_2F_4(H_2O)^{2-}]$ plus the interaction energy, instead of the total relative energy of the hexa and the hepta coordinated clusters. A reference energy that is defined in this manner will only depend on the position of the first shell of water molecules and not on the uncontrollable cluster truncation effects caused by the peripheral H_2O

molecules.

Given this definition of the energy difference between the hexa and hepta structure we may analyze the variation in interaction energy caused by the enlargement of the solvation model. The sum of the short range Pauli repulsion and orbital interactions terms favors the hexa coordination in the three water model and increases until the first solvation shell is completed. This trend is, however, compensated by the difference in electrostatic interaction that favors the hepta coordination and also increases in absolute magnitude when the cluster is enlarged.

To see what is causing these changes we divided the system with 29 water molecules into four fragments: the $[UO_2F_4]^{2-}$ complex, the water molecule connected (hepta structure) or not (hexa structure) to it, the first solvation shell of the 11 waters and the truncated second shell consisting of $18H_2O$. We then computed, via the Hirsfeld charge analysis provided by the ADF program, the charge transfer from the negative main fragment to the surrounding solvent molecules and the distribution of this charge over the different solvent fragments. We found that the total transfer of electrons from the $[UO_2F_4(H_2O)]^{2-}$ complex is significant and higher for the water-coordinated compound: 0.48e for the hepta structure and 0.42e for the hexa structure. In both cases we find that almost half an electron (0.47e hepta and 0.46e hexa) moves to the second shell. Most of this charge is provided by the $[UO_2F_4]^{2-}$ fragment, that looses 0.4e in both the hepta (0.40e) and the hexa (0.39e) structures. The higher flux of charge for the total $[UO_2F_4(H_2O)]^{2-}$ complex in the hepta structure is caused by an additional charge transfer from the coordinated water molecule to the first solvation shell of 0.08e. The two charge transfers from the water and the negative central complex make it possible for the water molecule to move inbetween the fluorine ions and become coordinated. In the hexa case the water molecule belongs to the first-shell, which is slightly oxidized (0.02e for the water plus 0.05e for the rest of the shell) and acts as an electronic bridge between the complex and the outside water molecules. Due to the reduced distance to the uranium in the larger clusters we see a relative increase in Pauli repulsion for the hepta-coordinated water but this effect is small enough to be compensated by the electrostatic interaction.

In order to compare the full QM and the QM/MM approaches we go back to the original partitioning into two fragments and give the MM energies for each fragment in Table 6.4. We recall that in the QM/MM method, the total energy is decomposed as $E_{TOT}=E^{I}_{QM}+E^{II}_{MM}+E^{I-II}_{MM}$, where I indicates the first fragment, i.e. $[UO_2F_4(H_2O)]^{2-}$ in our calculations; II is the surrounding water layer and I-II indicates the interaction energy between the two subsystems, that it is now solely com-

Figure 6.2: Variation of the energy difference between the hexa and hepta structures upon addition of water molecules to the system. The full QM energies are determined by single-point calculations on the geometries optimized with the hybrid QM/MM method.

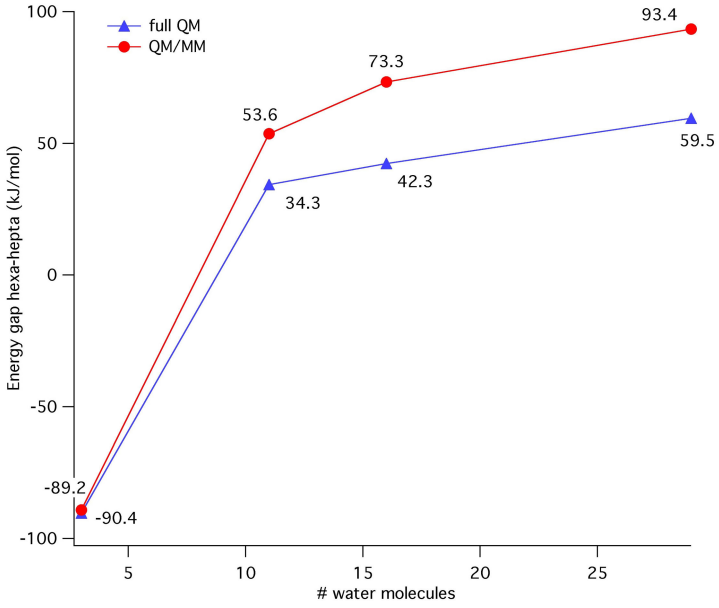

puted with molecular mechanics. A full MM approach, in which E^I_{QM} is changed with E^I_{MM}, would favor the hepta over the hexa structure for all layers, which is due to the poor description of region I. To make the MM energy reliable one should devise a MM parameter set that can correctly account for the subtle differences in coordination of the uranium atom. This is obviously not possible in the simple parameterization that we made according to Badgers rules. A completely different behavior is found for the region II, where both the QM and MM methods are in good agreement with a maximum discrepancy on the order of 21 kJ/mol. This is due to the well-calibrated AMBER95 force field parameterization that was available for water-water interactions. The MM interaction energy between the two regions, finally, can also be decomposed into its contributions: bond, angle, electrostatic and van der Waals. The first two are zero since there are no parameterized bonds between the two regions (hydrogen bonds are not included in the force field). The only two terms contributing are the electrostatic and the van der Waals interactions. The former is by far the largest and follows the same trend as seen in the QM calculation, as

might expected. Here one can easily compare the two approaches since the QM/MM interaction model is simply a point charge fit of the distributed charge interaction of the QM scheme. The good agreement shows the quality of the multipole-derived charge analysis [208] that is used to obtain these charges. The remaining van der Waals term could tentatively be compared to the orbital contribution term of a full QM calculation although this is stretching the validity of the decomposition schemes using approximate density functionals. If we compare this term, we do indeed obtain a trend similar to the van der Waals term.

6.5 Conclusions

The aim of this work was to find a suitable scheme to model the effect of a solvent on the structure of uranyl compounds. By performing a detailed study of the complexation of uranyl fluoride in water we have demonstrated that this is possible with a QM/MM method. We find that the optimal choice of QM and MM regions consists of the uranyl fluoride and a first solvation shells of eleven water molecules in the QM region, while a second solvation shell can be added by MM. Geometry optimization is, however, better done by keeping all solvating water molecules in the MM region since it makes the optimizations faster and numerically more stable.

A detailed study of the energy difference between hexa and hepta coordinated uranyl fluoride revealed that the unfavorable electrostatic interaction, that prevents formation of the hepta-coordinated complex in the gas phase, is reduced due to charge transfer in the solvated complex. This favors the hepta coordination and confirms the experimental EXAFS data.

The hybrid QM/MM approach thus provides a good compromise between accuracy and computational efficiency, also for aqueous actinide complexes. The trends found in geometrical and electronic properties are quite well represented even though a full QM calculation at the optimized geometry significantly improves the quantitative accuracy in the energy differences. The central complex of interest should preferably be represented in a QM approach anyway because the interaction with the uranium atom is hard to parameterize in a classical scheme. It would be interesting to try to incorporate such QM corrections also in large-scale Molecular Dynamics and Monte Carlo simulations that are usually done in an MM-only scheme for these kinds of systems.

CHAPTER 7

A QM/MM study on the aqueous solvation of the tetrahydroxouranylate $[UO_2(OH)_4]^{2-}$ complex ion

Randal Graves: Which did you like better? "Jedi" or "The Empire Strikes Back"?
Dante Hicks: "Empire".
Randal Graves: Blasphemy!
Dante Hicks: "Empire" had the better ending. I mean, Luke gets his hand cut off, finds out Vader's his father, Han gets frozen and taken away by Boba Fett. It ends on such a down note. I mean, that's what life is, a series of down endings. All "Jedi" had was a bunch of Muppets.

from the movie Clerks (1994)

7.1 Abstract

We report a QM augmented QM/MM study on the coordination of the tetrahydroxouranylate ion in aqueous solution. QM/MM geometry optimizations followed by full QM single-point calculations on the optimized structures show that a hexa-coordinates structure is more stable than the hepta-coordinated structure by 43 kJ/mol. Charge transfer of the tetrahydroxouranylate to the solvating water molecules is relatively modest and can be modelled by including a solvation layer consisting of 12 explicit water molecules.

7.2 Introduction

Optimization of existing and development of new actinide separation procedures is important to improve the storage and reprocessing of spent nuclear fuel [6, 159, 160]. Most of the current technology concerns liquid-liquid extraction, using the PUREX (Plutonium Uranium Extraction) process, that is based on oil-water extraction using the tributylphosphate extractant as a first step. Even though this process is now in use for over half a century the detailed mechanism of extraction is not yet fully understood, and continues to be subject of analysis. Theoretically this process may be studied by means of molecular dynamics simulations that model the interface region between the solution phases where the interaction of the actinyls with the tributylphosphate takes place [209]. Ideal methods would combine time-dependent simulation of a sufficiently large region of the liquid-liquid interface with a reliable description of the actinide-ligand and actinide-solvent interactions. With the present day methods there are two ways to achieve this goal. One may employ molecular mechanics and parameterize all relevant interactions on basis of a training set of experimental or computational data. If this can be done reliably it is possible to treat realistic model systems. The analysis done by Clavagura-Sarrio et al. [210] shows, however, that a physically transparent parameterization of interactions is difficult to achieve, even in the case of the closed shell uranyl ion UO_2^{2+} in which the electronic state of the actinide complex is well-characterized. An alternative is not to search for parameterizations and apply ab initio molecular dynamics methods that treat the electronic structure parameters explicitly. The problem is then transferred to the generation of a pseudopotential that is able to describe the actinide atoms and to the algorithm optimization that should deal with the much larger computational demands of these ab initio type methods. Simulation boxes of the size that are required to describe an actinide interacting with a realistic extraction agent at the interface between the two solvents are not currently feasible with these type of methods, although progress in this area was reported recently [211]. Nevertheless it is interesting to consider also hybrid QM/MM type of methods in which only a small "difficult and interesting" part of the system is treated quantum mechanically and the MM parameterization is used to compute the interactions between the solvent and the ligand atoms of the actinyl complex. Since most of these complexes are charged, it is of interest to determine how many explicit QM solvent molecules are needed to obtain a correct description of charge transfer effects.

In the current paper we present a follow-up of our earlier paper [212] in which we presented a QM-augmented QM/MM scheme that gave a reliable description of

the coordination of the tetrafluorouranylate complex. We now consider the more challenging tetrahydroxouranylate complex that has been studied extensively, both experimentally and theoretically [193, 199, 201, 213–218]. By including explicit water molecules in the QM region, QM/MM methods can describe the microscopic hydrogen bonding interactions that are absent in polarizable continuum models and serve as a test for full MM parameterizations. This type of partitioning could in the future also be used in a QM/MM based MD procedure.

Evidence for the occurence of a tetrahydroxouranylate complex ion [199] in strongly basic solvents comes from the EXAFS experiments of Clark [193] who proposes, however, that pentahydroxouranylate should be the dominant species. Since the EXAFS technique is known to yield accurate bond lengths but coordination numbers that have a typical uncertainty of $\pm$ 1 [213] it is hard to draw definite conclusions based on EXAFS data alone. Clark's interpretation is refuted by Wahgren, Grenthe, Vallet and coworkers [218] who argue that it is more likely that the four hydroxo complex that is observed in crystal structures, also prevails in solution. This interpretation is supported by recent theoretical work of Sonnenberg et al. [217] who use a continuum model to include solvent effects and find that coordination of a fifth hydroxo ligand is endothermic by 107 kJ/mol. In our earlier work we showed that in case of complexation with fluoride anions reduction of the electrostatic repulsion of the fluoride ligands by charge transfer to the surrounding water molecules is important. In that case the charge reduction of the complex ion was sufficient to allow a water molecule to penetrate in the equatorial plane and coordinate to uranium. This effect is only captured in a computational model that includes an explicit first solvation shell of water molecules, gasphase calculations predict the $[UO_2F_4]^{2-}$ to be more more stable by over a 100 kJ/mol than $[UO_2F_4{\cdot}H_2O]^{2-}$. We wondered whether charge transfer could substantially decrease the energy of the $[UO_2(OH)_5]^{3-}$ as well. To get a lower limit to this effect we study the coordination of water to $[UO_2(OH)_4]^{2-}$. Modeling the coordination of water is easier than the study of the equilibrium between coordination with different numbers of hydroxide ions, since it does not change the charge of the model cluster. The computed energy difference should give a good indication whether $[UO_2(OH)_5]^{3-}$ could be favoured over $[UO_2(OH)_4]^{2-}$ in a more complete cluster model since deprotonation of the coordinated water should be possible without changing the structure much. The model does not describe the effect that the counter ions and solvated hydroxide ions might have since this would require a much larger quantum mechanical model system than is currently feasible.

7.3 Methodology

For the Quantum Mechanical (QM) part of the caclulations we employed Density Functional Theory (DFT) with the gradient-corrected BPW91 exchange correlation functional, developed by Becke [219] and Perdew and Wang [203], and incorporating relativistic effects by means of the ZORA method [54–57]. Other xc functionals than BPW91 were considered in our previous paper [212] in which we concluded that the differences between BPW91 and B3LYP are minor for the kind of properties studied here. We used an uncontracted triple-ζ basis set enlarged by adding two polarization functions (TZ2P) and keeping the cores of the oxygen atoms ($1s^2$) and uranium atom ($[Xe]4f^{14}5d^{10}$) frozen. This basis set is large enough to render BSSE effects in the computed energy differences negligible. The Molecular Mechanics part of the calculation was done using the parameters described previously [212], taking the van der Waals bond length and well-depth for the equatorial hydroxo groups from the AMBER95 force field [107]. Note that we did not need to parameterize bond distances and bond angles for uraniumoxygen interaction because bonds involving uranium are always evaluated in the QM region. Charges needed to represent the interaction between the solute and the solvent molecules in the QM/MM optimization were obtained using multipole-derived charge analysis [109] of the QM density. This method ensures that in every cycle of a QM/MM geometry optimization the charges are updated in response to structural changes.

The solvent cluster models were constructed with 3, 7, 11 and 32 water molecules surrounding the $[UO_2(OH)_4{\cdot}H_2O]^{2-}$ complex in which the water is placed in either a coordinating or a noncoordinating position. The choice of the number of water molecules in the first solvation shell was somewhat arbitrary, by inspection and limited energy minimization, we found that 11 water molecules give a reasonable description of the first solvation shell whereas 32 molecules consitute a first plus second shell environment. The 3 water model served to give an indication of the effect of the most important waters, the ones interacting most strongly with the coordinating hydroxo groups. These models were refined by means of unconstrained geometry optimizations in full QM for the two smallest systems and by QM/MM optimization for the largest model. All structure optimizations were performed using tight convergence criteria (10^{-4}) with the accuracy of the integration grid one order of magnitude higher (10^{-5}). Charge transfer was characterized using the Voronoi Deformation Density (VDD) [220] and Hirshfeld charge analysis [221] methods. The energy analysis was done with the Ziegler and Rauk fragment decomposition scheme [206, 207] in which we identified three molecular fragments: the $[UO_2(OH)_4]^{2-}$ ion, the coordinating water

molecule, and the solvation shell(s). All calculations were done using the ADF2004.01 package [119, 120, 222].

7.4 Results and Discussion

7.4.1 The isolated $[UO_2(OH)_4]^{2-}$ complex

The structure of the bare $UO_2(OH)_4^{2-}$ ion is characterized by the orientation of the hydroxo groups, that can either point towards the adjacent hydroxo group or towards the axial oxygen atoms O_{ax}. We tested the strength of each hydrogen bond by performing a scan along the dihedral angle O_{ax}-U-O_{eq}-H of the molecule depicted in Figure 7.1 (1a). The most stable structure is the D_{2d} trans conformation in which the four hydrogen atoms are alternating above and below to the equatorial plane. This is the same geometry as found by Schreckenbach et al. [199] on basis of ECP-B3LYP type calculations. Rotation of the hydrogen atom along the U-O_{eq} axis gives rise to a transition state at about 90° (i.e. with the hydrogen atom in the equatorial plane) that is only 5.6 kJ/mol higher than the trans conformation. This difference is still sufficiently high to assume that these hydrogen atoms prefer to stick to the axial oxygen atoms, hindering the rotation around the U-O_{eq} bond. The 180° position is a local minimum (i.e. with three hydrogen atoms on one side of the equatorial plane) that is higher in energy by 2.4 kJ/mol. All vibrational analyses on structures with the hydrogen atoms in the equatorial plane give negative eigenvalues with eigenvectors that move these hydrogens out of the equatorial plane.

An interesting feature is the substantial lengthening of the axial U=O bond distance (1.88 Å compared to the 1.72 Å computed for the bare uranyl ion at this level of theory) [214–216]. This lengthening can be attributed to the strong charge transfer from the four hydroxo groups to the uranyl moiety. The Voronoi defomation density (VDD) analysis and Hirshfeld charge analysis indicate a ligand to uranyl transfer of 0.8 and 0.9 electron, respectively. This charge is partly donated to the nonbonding empty uranium $5f_\phi$, $5f_\delta$, and $6d_\delta$ orbitals and partly to antibonding $5f_\sigma$ and $5f_\pi$ orbitals. The first charge transfer weakens the uranyl bonds, as was already noted by McGlynn [223], by decreasing the ionic bond strength between the positive uranium and the negative oxygen. The effect of the charge transfer to the antibonding orbitals is more difficult to quantify because it reduces the covalent bond strength but also puts additional charge on the axial oxygens, thus reinforcing the ionic bond strength. The net result is a strong reduction of bond strength that is reflected in a large IR frequency shift. Calculation of the vibrational frequency using LDA, that is known

Figure 7.1: Three local minima of tetrahydroxouranylate: the trans (top-left), cis (top-right) and 3up-1down conformations. The trans conformer is the most stable.

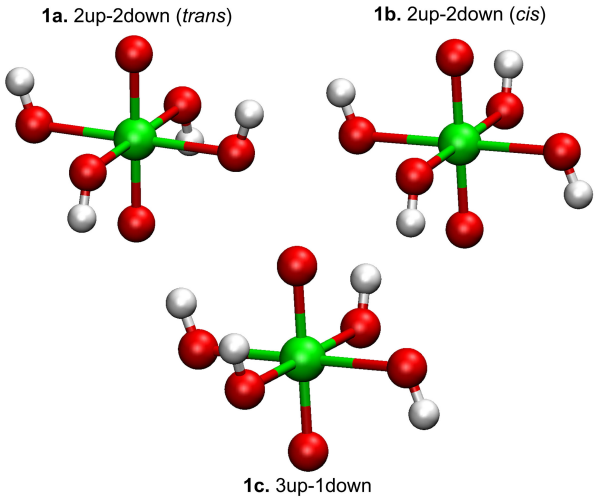

to give consistently better frequencies than BPW91 for uranyl complexes [224], gives a value of 746 cm^{-1} for the symmetric stretch, 50 cm^{-1} lower than Clark et al. [193] measured in $[Co(NH_3)_6]_2[UO_2(OH)_4]_3{\cdot}2H_2O$ crystals, and in reasonabe agreement with the ECP-B3LYP value of 762 cm^{-1} reported by Sonnenberg et al. [217]. The overestimation of the shift in the theoretical work is probably due to the lack of counterions that will reduce the charge transfer.

7.4.2 The isolated $[UO_2(OH)_4]^{2-}$ + H_2O complex

By adding only a single water molecule, that is either coordinated to the uranium atom or positioned as a solvent shell molecule, we studied the relative stability of the six or sevenfold coordination (counting also the axial oxo-ligands) in the absence of charge transfer to the solvent. The hexacoordinated complex does not change its structure much relative to the complex without the added water [Figure 7.2 (2c)] and is a minimum on the potential energy surface. This is not the case for the heptacoordinated complex for which we, similar to the situation in tetrafluorouranyl [212], find a saddle point with two imaginary frequencies that have eigenvectors directed towards the structure of the hexa coordinated complex. If we delete these coordinates from the structure optimization we find that the insertion of the water opens

Table 7.1: Geometrical parameters (bonds in Å and angles in degrees) of the hexa-tetrahydroxouranylate ion with different QM/MM partionings of the system.

	# H_2O	# QM H_2O	# MM H_2O	U-O_{ax}	U-O_a	U-O_b	U-O_{H_2O}	O_{ax}-U-O_{ax}	O_a-U-O_a	O_b-U-O_b	H-O_a-U-O_{ax}
0	0	0	0	1.88	2.31	2.31	–	180.0	90.0	90.0	0.0
hexa-coordinated $UO_2(OH)_4^{2-}\cdot H_2O$											
1a	1	1	0	1.87	2.34	2.29	4.02	179.4	86.5	90.7	7.9
	4	4	0	1.84	2.33	2.33	4.00	179.9	90.7	89.6	-0.3
	4	1	3	1.84	2.34	2.33	4.01	178.1	94.2	89.3	-1.0
	8	8	0	1.83	2.30	2.29	3.91	178.7	86.9	98.8	5.7
	8	4	4	1.85	2.33	2.32	3.96	179.8	89.8	91.0	1.8
	8	1	7	1.86	2.31	2.31	3.89	177.6	88.8	87.9	1.8
	12	12	0	1.85	2.29	2.33	3.91	179.0	92.6	88.1	8.1
	12	8	4	1.85	2.32	2.32	3.97	179.5	93.8	89.2	3.9
	12	1	11	1.85	2.32	2.30	3.87	179.6	91.6	89.7	2.2
	20	8	12	1.86	2.32	2.28	3.91	179.6	88.3	89.6	10.1
	32	8	24	1.85	2.33	2.28	3.98	176.8	92.0	89.7	12.4
Exp				1.83	2.26	2.26					

Table 7.2: Geometrical parameters (bonds in Å and angles in degrees) of the hepta-tetrahydroxouranylate ion with different QM/MM partionings of the system.

	# H_2O	# QM H_2O	# MM H_2O	U-O_{ax}	U-O_a	U-O_b	U-O_{H_2O}	O_{ax}-U-O_{ax}	O_a-U-O_a	O_b-U-O_b	H-O_a-U-O_{ax}
0	0	0	0	1.88	2.31	2.31	–	180.0	90.0	90.0	0.0
hepta-coordinated $[UO_2(OH)_4 \cdot H_2O]^{2-}$											
2a	1	1	0	1.86	2.43	2.32	2.62	173.9	116.5	91.4	90.0
	4	4	0	1.84	2.44	2.35	2.63	179.9	119.2	81.4	-7.8
	4	1	3	1.86	2.42	2.32	2.60	173.4	119.8	82.3	1.8
	8	8	0	1.83	2.51	2.33	2.54	179.8	131.1	81.0	-18.9
	8	4	4	1.85	2.43	2.33	2.59	179.3	119.6	81.7	-7.4
	8	1	7	1.86	2.44	2.29	2.60	179.9	120.4	81.2	0.8
	12	12	0	1.84	2.42	2.35	2.59	179.4	131.2	78.3	-14.7
	12	8	4	1.83	2.50	2.34	2.53	177.7	131.3	83.2	-15.4
	12	1	11	1.85	2.45	2.30	2.59	178.4	120.3	82.2	-0.9
	20	8	12	1.85	2.43	2.29	2.56	176.3	123.7	79.1	-3.9
	32	8	24	1.85	2.46	2.30	2.54	179.5	122.4	80.9	-13.4
Exp				1.83	2.26	2.26					

Table 7.3: Bond energy analysis of the isolated $[UO_2(OH)_4 \cdot H_2O]^{2-}$ complex taking as fragments the tetrahydroxouranylate and the water molecule. All the values are expressed in kJ/mol. The corresponding values [212] for the $[UO_2F_4 \cdot H_2O]^{2-}$ complex are given in parenthesis.

	hexa	hepta	Δ(hexa-hepta)
$[UO_2(OH)_4]^{2-}$ fragment	-6857.6	-6818.8	-38.8 (-23.9)
H_2O fragment	-1373.9	-1369.3	-4.6 (0.8)
Interaction Energy	-122,5	-11.7	-110.9 (-121.4)
Total Energy	-8354.0	-8199.7	-154.3 (-146.1)
Interaction Energy			
Electrostatic Interaction	-151.2	-121.8	-29.5 (-77.0)
Pauli Repulsion	101.1	167.0	-65.9 (-18.0)
Orbital Interactions	-72.4	-56.9	-15.5 (-26.0)
Pauli+Orbital	28.7	110.1	-81.4 (-44.0)

the angle between two hydroxo units and causes the two hydrogen atoms to rotate making equatorial hydrogen bonds with the remaining two OH units [Figure 7.2 (2a)). Another possibility would be to force the water to be tilted or perpendicular relative to the equatorial plane to mimimize steric repulsions but we found that this leads to structures with higher energies. We further notice that the introduction water does only weakly affect the distances to the other ligands. The U-O_{ax} bond contracts by 2 pm while the equatorial U-O_a bonds distances, to the atoms next to the incoming water, are elongated by 12 pm.

These results demonstrate that charge transfer to the solvent is needed to increase the coordination around the uranium. In $[UO_2F_4]^{2-}$ we found that poor stabilization of the hepta conformation in the gas-phase is related to the unfavorable insertion of the negatively charged oxygen into the negative cloud of two adjacent fluoride units, which is furthermore hindered by a larger Pauli repulsion. We list both these earlier results and the new results for $[UO_2(OH)_4]^{2-}$ in Table 7.3. Hexa-coordination $[UO_2(OH)_4 \cdot H_2O]^{2-}$ is more stable than hepta coordination by 110.9 kJ/mol, which is slightly smaller than the difference found for the fluoro complex (-121.4 kJ/mol). Looking at the decomposition of this energy we observe that the electrostatic interaction is more favorable in the hexa conformation (a difference of -29.5 kJ/mol) but that this difference is much smaller than in $[UO_2F_4]^{2-}$ (-77.0 kJ/mol), reflecting the higher electronegativity of fluorine compared to oxygen. The Pauli repulsion and orbital interaction terms show a larger differential effect and favor the hexa conformation as

Table 7.4: Decomposition of the Δ(hexa-hepta) energy difference (kJ/mol) choosing $[UO_2(OH)_4H_2O]^{2-}$ and the surrounding water shell(s) as fragments.

		3	7	11	19	31
$[UO_2(OH)_4H_2O]^{2-}$ (I)	QM	-168.5	-168.8	-161.3	-178.4	-163.2
Water Cluster (II)	QM	-7.6	-8.8	-47.6	-11.0	-51.7
Interaction Energy (I-II)	QM	51.7	88.0	118.8	131.9	120.1
Total (I + Interaction I-II)	QM	-116.8	-80.8	-42.5	-46.5	-43.1
Interaction Energy (I-II)						
Electrostatic Interaction	QM	68.7	109.7	242.8	93.0	236.3
Pauli Repulsion	QM	-62.4	-98.0	-298.0	-92.1	-278.7
Orbital Interactions	QM	-45.5	76.3	174.0	131.0	162.6
Pauli+Orbital	QM	-17.0	-21.7	-214.1	38.9	-116.1

well. These terms amount to -81.4 kJ/mol in $[UO_2(OH)_4]^{2-}$ and to only -44.0 kJ/mol in $[UO_2F_4]^{2-}$. In particular the difference in Pauli repulsion is substantially larger than in $[UO_2F_4]^{2-}$, indicating that it is more difficult for water to move inbetween the larger hydroxo units than inbetween the fluoride ligands. This analysis does reveal a qualitative difference between the two compounds; in spite of an overall hexa-hepta energy difference that is quite similar for the two uranyl compounds, the individual contributions vary substantially. One may thus anticipate a different behavior when solvent molecules are added.

7.4.3 The embedded $[UO_2(OH)_4]^{2-}$ + H_2O complex

The QM/MM structure optimization of the large clusters of water is nontrivial and care needs to be taken to prevent the introduction of artefacts when comparing the coordination energies. We describe the procedure that we followed in more detail in the appendix. It results in comparable structures for the hexa and heptacoordinated complexes that make it possible to study differences in coordination energy as a function of cluster size. In Figure 7.2 we plot this energy difference as a function of the explicit solvent molecules for the QM/MM model and the full QM model. Note that we chose to compare the internal energy of the coordination complex and its interaction with the solvent instead of the total energy of the cluster. This quantity was found to be more reliable because it does not suffer from truncation effects at the periphery of the solvent cluster. As smallest model we used a QM4 partioning of a cluster with 8 water molecules. For the larger clusters ranging from 12 till 30 H_2O,

Figure 7.2: Hepta (on the top-left and top-right) and hexa (bottom) coordinated ions. Note that in the gas-phase the hepta coordinated structure does not represent a minimum. The hexa coordinated complex with the water molecule in the first shell is a minimum.

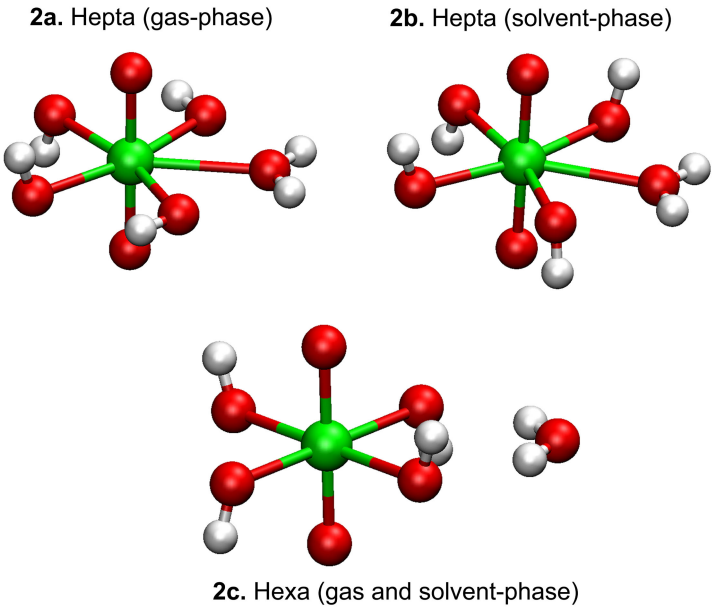

we took the QM8 partitioning for the reasons explained in the appendix. With a few QM molecules in the optimization we find a relatively large Pauli repulsion energy in the single point QM calculations, which is due to the underestimated bond distances that result from the MM force field. This effect is significant in the small models and more important in the hepta structure than in the hexa structure. This problem becomes less severe when we go to more complete second shell models.

We plot in Figure 7.3 the structures found in solution(2b) and in the gas phase (2a). Already in the 3 water model, the hepta complex changes its structure relative to the gas-phase structure, with the equatorial hydrogen atoms of two of the hydroxo groups rotating to a position perpendicular to the plane. This structure allows better hydrogen bonding with the first water shell and does not hinder the solvent molecules that enter the equatorial plane. The bond distance in uranyl remains rather long varying between 1.85-1.88 Å for both the hepta and the hexacoordinated structures in all cluster models that we employed. On average, the equatorial U-OH bonds of the hepta conformation stay longer by about 0.1 Å than those in the hexa ccoordination,

but the U-O_{water} bond distance is steadily decreasing as the cluster is enlarged. In the largest cluster (32 water molecules) the oxygen atom of the water molecule is found at a distance of 2.54 Å from the central uranium, which is only slightly longer than the 2.46 Å of the adjacent U-OH. This similar bond distance suggests that proton exchange behavior between the equatorial water and hydroxo units should be feasible without major structural changes.

Upon increasing the number of water molecules the hepta structure becomes more and more stabilized relative to the hexa structure. This is the same trend as observed in the tetrafluorouranylate ion but the effect is smaller, keeping the hexa conformation the most stable. In an extensive QM/MM MD study, with all first shell water molecules in the QM region, Kritayakornupong et al. [225] have shown that the error in a QM/MM calculation of hydration enthalpies for the Cr(III) ion is of the order of 30 kJ/mol. Assuming that a similar error bar is applicable in our calculations, we conclude that the energy difference between the hexa and hepta coordination (72.4 kJ/mol in the QM/MM model and 43.1 kJ/mol in the full QM model) is large enough to support the interpretation that hexa coordination dominates in aqueous solution.

The interaction energy analysis indicates that addition of the first water molecules in the equatorial plane gives a relative increase of stabilization of the hepta conformation that is of the same order as found in tetrafluorouranylate. Completing the first shell by adding more molecules at axial positions has, however, a smaller effect than in tetrafluorouranylate. The same is true for the subsequent extension of the cluster to a complete second shell. This can be rationalized by considering the Hirshfeld charges [221] in the complex with 30 water molecules. We see two important effects; the first is that the flux of charge from the doubly negative fragment ion to the water cluster is practically the same for hepta and hexa coordination (0.34e), whereas it differed in by 0.06e in tetrafluorouranylate; the second effect is that the absolute value of the charge transferred is consistently lower for the hydroxide complex (0.34e for both hexa and hepta) than in uranyl tetrafluoride (hepta: 0.48e vs. hexa: 0.42e). In uranyl tetrafluoride we have a primarily electrostatic difference between the two compounds that is reduced greatly by charge transfer to the solvent. This allows then a coordinating water to move in between the fluorides. In tetrahydroxouranylate the difference is primarily due to Pauli repulsion and orbital interaction terms that do not change much upon embedding the bare ion in water.

The detailed analysis of the energy as a function of cluster size shows also that, unlike the tetrafluorouranylate ion, the difference in internal energy [defined as Δ(hexa-hepta)] for the $[UO_2(OH)_4{\cdot}H_2O]^{2-}$ ion itself is not constant but varies in a range of 10

Figure 7.3: The change in relative energies of the hexa and hepta coordinated complexes upon adding water molecules in the first and second shell. Both the QM (triangles) and QM/MM (squares) relative energies are plotted. The labels indicate the partitioning that is used in the QM/MM energy evaluation and the geometry optimizations.

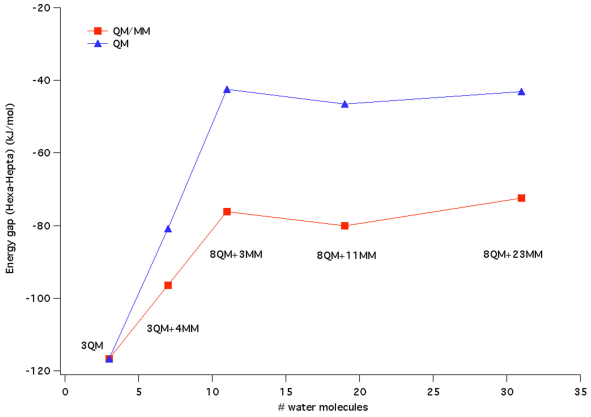

kJ/mol. This is due to the fact that the surrounding water drags the hydrogen atoms around which gives energy effects of the order of the rotational barrier (5.6 kJ/mol) for OH rotation. This effect is compensated by changes in interaction energy that make such reorientations favourable. Internal energy changes in the of the surrounding water are not taken into account in our defintion of the coordination energy. We can include this term to gauge the similarity of the water clusters around the hexa and the hepta conformations and check for differential effects due to cluster truncation. We see such differential effects especially in the 20-water cluster that breaks the trend in the decomposition of the various terms. In the 20-water cluster the energy difference in the water cluster counterbalances the difference in interaction energy. Of course, this effect demonstrates the limitations of our finite cluster approach, but it does not affect the conclusions. A more rigorous solution to solve the problem of dangling bonds is to employ periodic boundary conditions but this is not supported by the computational tools that we used.

7.5 Conclusions

We performed QM/MM calculations on the $[UO_2(OH)_4{\cdot}H_2O]^{2-}$ ion and could attribute the relative stability of the hexacoordinated structure to unfavorable short

range effects in the hepta coordinated complex. Including the first solvation shell lowers the energy difference between the two conformations due to a reduction of the electrostatic interaction but does not lead to an inversion in the stability. It seems unlikely that further sophistication of the model by including additional (solvated) counterions to mimic the experimental conditions better would be sufficient to overcome the large energy difference between the seven and sixfold coordinated species. On these grounds we conclude that coordination of an additional hydroxide to form $[UO_2(OH)_5{\cdot}H_2O]^{3-}$ is indeed unlikely.

For this relatively simple simple uranyl ion the QM/MM approach can be carried out with a QM space of eight explicit solvent molecules. Using fewer QM solvent molecules does lead to artefacts whereas a larger number of QM water gives similar results. Energy minimization is rather difficult because structure optimizations are biased by the specified initial structure that is given. Part of the problem is of course that we tried to locate absolute minima, but it is expected that rather large QM spaces will also be necessary in finite-temperature simulations on this and other similar compounds.

7.6 Appendix

7.6.1 Setup for the QM/MM partitioning

The embedded tetrahydroxouranylate ion has various local minima that are related by rotations around the O-H bonds. This is due to a competition between the formation of two kind of hydrogen bonds: one with the oxygen atoms of the water cluster pointing to the positive hydogens of the hydroxo groups and the second with the hydrogen atoms of the water cluster pointing to the six negative oxygens of the complex ion. The number of possible configurations increases steeply upon addition of more explicit solvent molecules and makes the search for minima rather difficult. The precise form of the absolute minimum is not all that important, but we need to find comparable minima for the hexa and hepta-coordinated complex so that a representative analysis of the difference in bonding can be performed. In this search for suitable minima, we first determined the optimal division between the QM and MM regions. To study the effect of the size of the QM region we carried out geometry optimizations of a model system with a total of 12 water molecules taking 1, 4, 8 and 12 H_2O in the QM region, partitionings that will be denoted QM1, QM4, QM8, QM12, respectively. For all these partitionings, the search for the absolute minimum was started with the same initial structure. The QM1 model gives significantly different structures than

the other partitionings and was therefore not suitable. It might be possible to improve upon this by reparameterizing the MM force field but such a reparametrization was beyond the scope of the current paper. We therefore proceded with a partitioning in which a large fraction of the first layer of water molecules, including all hydrogen bonds to the OH units, is taken into the QM region. Given this criterium we had the choice between 8 or 12 water molecules in the QM layer. Analysis of the optimized hexa coordinated structures in both partitionings indicated that the final structures were slightly different but gave rise to similar interaction energies. Difference between the partionings are more prominent in the hepta coordination, because the coordinated water molecule breaks the symmetry of the complex, and gives more low-energy first shell conformations than in the hexa coordinated structure. Since the QM8 partitioning is computationally more efficient than the QM12 partitioning and also exhibits better convergence in the structure optimization we decided to choose the QM8 partitioning in the final calculations in which we included a second solvation shell.

With the second shell present it becomes even with the QM8 partitioning difficult to locate structures in which the hexa and hepta coordinated complexes can be reliably compared. We employed the efficient QM1 partition to perform a first scan of the different hepta coordinated structures (using a constraint to prevent the coordinating water molecule from rotating to the hexa coordinated structure) and selected the most stable structure as starting point for QM8 reoptimization of both the hepta and the hexa coordinated complexes. The hexa coordinated starting structure was thereby created out of the hepta structure by rotating the coordinated water molecule prior to the reoptimization. This approach gives comparable solvent layers for the hexa and hepta complexes.

Summary

Bela Lugosi: Pull the string ! Pull the string !

from the movie Ed Wood (1994)

To study the properties of molecules containing actinide elements relativistic quantum chemistry is required. The chemistry and the physics of these systems is very rich and complicated because the 5f, $7s$, $6d$ and $7p$ shells of an actinide atom are so close to each other that the electronic configuration of a molecule strongly depends on the atom to which the actinide is bonded. Furthermore, spin orbit coupling (SOC) can be large for these systems and affect the electronic structure as well.

Relativity and electron correlation are the two most important aspects of a calculation that need to be accurately described in order to have reliable results. The choice of the method which can account for both of them depends on whether we are interested in a qualitative or quantitative description of the system we are analyzing.

In line with these considerations, the purpose of this thesis is twofold. We first investigate the spectroscopy of small molecules using very precise methods, like the multi-reference Fock-space Coupled Cluster (FSCC) [1], which is a very powerful method that has been mainly used for atomic calculations. The main goal for this part of the thesis is to check the validity of this technique in order to study complicated and challenging systems. As second task we use DFT to evaluate the effect of the solvent on medium-sized actinide molecules. In particular, a qualitative analysis of the coordination number and short-range solute/solvent interactions using the hybrid QM/MM method is carried out.

Part I : The spectroscopy of small actinide molecules

The infrared spectrum of UO_2 in an argon matrix presents an intense band at 776 cm^{-1} that was assigned to the U-O asymmetric stretching [2]. In neon matrix, the asymmetric stretching vibration was found at the much lower frequency of 915 cm^{-1} [145]. To explain this behavior, Andrews et al. [145] argued that the trapped molecule interacts with the surrounding argon atoms, modifying the electronic structure, and switching the ground state between two different triplet states, $^3\Phi_u$ and ^3H_g [140]. In neon matrix, the interaction is so weak that the trapped molecule behaves as if it were in the gas-phase, keeping the $^3\Phi_u$ as the ground-state. The same unusual behavior was found for the CUO molecule [113], with a similar shift for the asymmetric stretch of the C-U and O-U bonds in argon matrix with respect to the neon matrix. In this case the ground state changes from a singlet $^1\Sigma_0^+$ (in neon) to a triplet $^3\Phi_u$ state (in argon) [113].

Our calculations, based on the DC-CCSD(T) approach, show undoubtedly that the singlet $^1\Sigma_0^+$ is the ground state in the gas-phase, being more stabilized by 40.6 kJ/mol than the triplet state, as pointed out in Chapter 3. Correlation stabilizes the more compact singlet by 100 kJ/mol, whereas the SOC term favors the triplet configuration, but not enough to make it the stablest configuration in the ground state. The basis-set plays a minor role, whereas the inclusion of sub-valence electrons in the correlated space tends to stabilize the singlet state. Our data support the suggestion of a switch of the ground state when the CUO molecules is trapped in the Ar matrix. However, explicit argon atoms have not been added and more theoretical calculations are needed to explain the effect of the matrix on the low-lying states. Our results contradict previous high-level CASPT2 data, that computed a triplet $^3\Phi_u$ ground state already in the gas-phase. However, a singlet-type ground state is also confirmed by a FSCC calculation, in which only a small model P space, for the computation of the non-dynamic correlation energy, is employed. This result, which can be considered as the most accurate, favors largely the singlet by 58.2 kJ.mol than the triplet $^3\Phi_u$.

In Chapter 4, the excitation spectrum of the UO_2 molecule is computed using the IH-FSCC method. It turns out that to describe with high precision the excited states that include the $7p$ shell, more diffuse functions need to be added to the basis set. The increase of the correlated space plays a minor role when more than 24 electrons are used, whereas the P_m space, in the intermediate Hamiltonian framework, has to be sufficiently large to include also the $7p$ shell.

The ground state is found to have a $^3\Phi_{2u}$ configuration, and this does not contradict the laser ablated spectroscopy measurement about the switching of the ground

state in the argon matrix. By taking for the first time the $6d$ shell into account, a metastable 4_u state composed by $5f^1 6d^1$ is found at about 5,000 cm^{-1}, which can be a suitable candidate for the re-intepretation of the old IP measurements that underestimate the IP value. The 4_g state lies at more than 10,000 cm^{-1}, at much larger values than previous CASPT2+SOC and GAS-CI calculations. This indicates that the 4_g can not be considered the ground-state when the molecule is trapped in the argon matrix.

The assignment of the excited states has turned to be an extremely complicated work, but a good agreement has been found between the calculations and the recent REMPI experiment that measured for the first time the absorption spectrum of the UO_2 molecule. More theoretical work is needed to study the effect of explicit Ar atoms bonded to the UO_2 molecule. The IH-FSCC approach represents a promising technique to analyze these larger systems, because it scales as N^6, like a standard CC approach, and yields accurate excitation energies.

In Chapter 5, the IHFSCC method is used to investigate the spectroscopy of NpO_2^+ and PuO_2^{2+} molecules, which are isoelectronic to UO_2. Theoretical attempts at interpreting these ions' experimental absorption spectra in water have been done previously with semi-empirical methods, followed by some more accurate ab initio methods. These calculations, however, were not sufficient to provide a quantitative and unambiguous assignment of the ordering and spacing between the transitions.

The IHFSCC approach has proven to be a cost–effective and accurate way to calculate the low-lying states of these ions. From the IHFSCC calculations it was possible to determine that both ions present a 4_g ground state, and all the excited states up to 20,000 cm^{-1} arise from excitations within the $5f^2$ configuration. Moreover, these calculations significantly improve the quantitative agreement with experiment in the region between 7,000 and 13,000 cm^{-1}. Errors now are of about 1,000-2,000 cm^{-1}, compared to more than 10,000 cm^{-1} in previous calculations.

In spite of these results, the IHFSCC method is not without drawbacks: for instance, it cannot be used in a black-box manner, and, at the time of writing, cannot be used for the evaluation of higher spin-states due to implementation issues. Thus, more applications and development work are needed to fully assess the reliability of the method.

Part II : DFT calculations on aqueous systems

The uranyl ion can be considered one of the most important molecules in actinide chemistry. Indeed this molecule has been studied both experimentally, due to its use in the recycling process of the nuclear waste, and theoretically, due to the rel-

ative simplicity to describe the closed-shell configuration. The aqueous solvation of this molecule has been object of debate in the last years. Unfortunately, for several different reasons, a clear method that determines the coordination number, and computes short-range interactions between the ion and the water surrounding has not been found yet. The purpose of the second part of this thesis is the assessment of the QM/MM method in studying solvated systems, in which the solute is treated at high-level of approximation using DFT and the water surrounding (or part of it) is treated using classical methods, like molecular mechanics.

In Chapter 6, we study the structure of the tetrafluorouranylate ion $[UO_2F_4]^{2-}$ that in water solution presents an unusual hepta-coordinated structure, in which the uranium atom forms an extra bond with one of the solvent water molecules. Geometry optimizations are carried out at QM/MM level, using different layering of the water shell. The best compromise is found by computing the tetrafluorouranylate ion and one water molecule in the QM region, and the remainder of the water cluster in the MM region. An analysis of the structural parameters shows a good agreement with the experiment. The increase of number of water molecules yields a significant change on the U-O_{ax} and U-O_{H_2O} bond distances. It is shown that a full first-shell is formed by 11 water molecules, and a water cluster of only 3 molecules, used in other works, is a too small ansatz to obtain even qualitative prediction.

A more quantitative analysis of the charge transfers between the solute and the solvent is provided by a full QM single point calculation on the optimized structure at QM/MM level of approximation. When a large number of water molecules is added to the system, the total energy is dominated by the water positions at the periphery of the solvent shell, yielding a severe limitation of the model. To overcome this problem we consider as total energy the sum of the QM region and the interaction energy of the solute with the solvent. A fragment decomposition scheme is used to divide such interaction energy in terms of steric and orbital contributions. In the gas-phase the hexa coordinated structure $[UO_2F_4(H_2O)]^{2-}$ is favored over the hepta, because the latter shows an unfavorable electrostatic interaction with the water surrounding that is reduced by charge transfer in the solvated complex. Such stabilization in the solvent is large enough that the hepta molecule results the most stable configuration by about 60 kJ/mol. In Chapter 7, the more challenging tetrahydroxouranylate ion $[UO_2(OH)_4]^{2-}$ is studied. In strong alkaline conditions, the EXAFS experiment on this molecule gives a coordination number with an uncertainty of ± 1, which is not definitive in assigning an hexa $[UO_2(OH)_4]^{2-}$ or hepta $[UO_2(OH)_5]^{3-}$ structure. Since the basic conditions are difficult to model using a static QM/MM approach, we verify

whether the $[UO_2(OH)_4 \cdot H_2O]^{2-}$ conformation is more favored than the hexa tetrahydroxouranylate ion when one water molecule is inserted in-between two oxygen atoms, since this ansatz represents a lower limit of the more complicated $[UO_2(OH)_5]^{3-}$ case, and does not change the total charge of the model system.

The same procedure used for the tetrafluorouranylate ion is employed here, with the difference that it is more difficult to sample a suitable first and second shells for both the hexa and hepta, because the presence of the hydroxyl units give rise to many more configurations. In the gas-phase, the hexa conformation is more favored than the hepta, but in this case the Pauli repulsion between a water molecule and the $[UO_2(OH)_4]^{2-}$ ion is much larger than in the$[UO_2F_4]^{2-}$ molecule. This term is sufficiently strong that for the hepta the more favorable charge transfer from the solvent does not allow an inversion of the stability, and the hexa structure remains the more stable structure in solution. With this assumption, it is highly unlikely that in alkaline condition the $[UO_2(OH)_4]^{2-}$ can insert an additional hydroxide.

Another aspect of the $[UO_2(OH)_4]^{2-}$ molecule is the large charge transfer from the hydroxo moieties to the non-bonding $5f$ orbitals localized on the less positive uranium atom, and to the anti-bonding $5f_\pi$ and $5f_\sigma$. This determines the formation of a less positive charge on the actinide atom and a stronger repulsion with the negative charged oxygen atoms, whichincrease the U-O_{ax} bond distance (1.88 Å) compared to the bare uranyl ion (1.72 Å).

A drawback of the QM/MM scheme is that only few configurations of the water surrounding can be chosen and a more realistic sampling of the system may be done using large scale molecular dynamics calculations. For technical reason, this latter path was not followed in this thesis.

Samenvatting

Bela Lugosi: Trek aan de snaar ! Trek aan de snaar !

uit de film Ed Wood (1994)

Titel: Computationele studies in actinidechemie

Om de eigenschappen van moleculen die actinide elementen bevatten te bestuderen is relativistische quantum chemie noodzakelijk. De chemie en fysica van deze systemen is erg veelzijdig en gecompliceerd, omdat de 5f, $7s$, $6d$ en $7p$ schillen van een actinide atoom zo dicht bij elkaar liggen dat de electronische configuratie van een molecuul sterk afhankelijk is van het atoom waaraan het actinide gebonden is. Bovendien kan spin-baan-koppeling (SOC) groot zijn voor dergelijke systemen en ook de electronsiche structuur beïnvloeden.

Relativiteit en electronencorrelatie zijn de meest belangrijke aspecten van een berekening die nauwkeurig dienen te worden beschreven om betrouwbare resultaten te krijgen. De keuze van de methode welke met beide effecten rekening houdt hangt af van waar we in genteresseerd zijn: een kwalitatieve of kwantitatieve beschrijving van het te analyseren systeem.

Dit beschouwend is het doel van dit proefschrift tweeledig. Ten eerste onderzoeken we de spectroscopie van kleine moleculen gebruik makend van hele nauwkeurige methodes, zoals multi-reference Fock-space Coupled Cluster (FSCC) [1], wat een erg krachtige methode is die voornamelijk voor atomaire berekening is gebruikt. Het hoofddoel voor dit deel van het proefschrift is de validering van deze techniek, zodat

gecompliceerde en uitdagende systemen kunnen worden bestudeerd. Het tweede doel is om met behulp van DFT het effect van het oplosmiddel op middelgrote actinide moleculen te onderzoeken. Er is met name aandacht besteed aan een kwalitatieve analyse van het coördinatie getal en korte-dracht interacties tussen het opgeloste en het oplosmiddel gebruik makend van de hybride QM/MM methode.

Deel I : De spectroscopie van kleine actinide moleculen

In het infrarood spectrum van UO_2 in een argon matrix is een intense band aanwezig bij 776 cm^{-1} die was toegekend aan de U-O asymmetrische strek-vibratie [2]. In een neon matrix, wordt de asymmetrische strek-vibratie gevonden bij een veel lagere frequentie van 915 cm^{-1} [145]. Om dit gedrag te verklaren beargumenteerde Andrews et al. [145] dat het ingevangen molecuul interactie heeft met de omliggende argon atomen, waardoor de electronenstructuur verandert, zodat de grondtoestand verschuift tussen twee verschillende triplettoestanden, $^3\Phi_u$ en ^3H_g [140]. In een neon matrix is de interactie dermate zwak dat het ingevangen molecuul zich gedraagt zoals in de gasfase, zodat de $^3\Phi_u$ de grondtoestand blijft. Hetzelfde ongebruikelijke gedrag is gevonden voor het CUO molecuul [113], met een vergelijkbare verschuiving voor de asymmetrische strek van de C-U en O-U bindingen in een argon matrix vergeleken met de neon matrix. In dit geval verandert de grondtoestand van een singlet $^1\Sigma_0^+$ (in neon) naar een triplet $^3\Phi_u$ state (in argon) [113]. Onze berekeningen, die zijn gebaseerd op de DC-CCSD(T) aanpak, laten zonder twijfel zien dat de singlet $^1\Sigma_0^+$ de grondtoestand is in de gasfase, welke 40.6 kJ/mol meer gestabiliseerd wordt dan de triplet toestand, zoals aangegeven in Hoofdstuk 3. Correlatie stabiliseert de meer compacte singlet met 100 kJ/mol, terwijl de SOC term de triplet configuratie prefereert, maar niet genoeg om de triplet stabieler te maken in de grondtoestand. De basis-set speelt een minimale rol, terwijl het in rekening nemen van de sub-valentie electronen in de correlatieruimte de neiging heeft de singlet toestand te stabiliseren. Onze data ondersteunen de suggestie van een verandering van de grondtoestand als het CUO molecuul is ingevangen in de Ar matrix. Echter expliciete argon atomen zijn niet toegevoegd en meer theoretische berekeningen zijn nodig om het effect van de matrix op de laagliggende toestanden te verklaren. Onze resultaten zijn in strijd met eerdere hoog-niveau CASPT2 data, die al een triplet $^3\Phi_u$ als grond toestand berekende in de gasfase. Echter, een singlet grondtoestand is ook bevestigd door een FSCC berekening, waarin slechts een klein model P ruimte is gebruikt voor de berekening van de niet-dynamische correlatie energie. Dit resultaat, welke als meest nauwkeurig kan worden beschouwd, prefereert in hoge mate de singlet met 58.2 kJ.mol boven de triplet $^3\Phi_u$.

In Hoofdstuk 4, wordt het middels de IH-FSCC methode berekende excitatie spectrum van het UO_2 molecuul beschreven. Het blijkt dat om aangeslagen toestanden die de $7p$ schil bevatten met hoge precisie te beschrijven, meer diffuse functies aan de basis set dienen te worden toegevoegd. De uitbreiding van de gecorreleerde ruimte speelt een minimale rol als meer dan 24 electronen worden gebruikt, terwijl de P_m ruimte, binnen de intermediaire Hamiltoniaan aanpak, voldoende groot moet zijn om ook de $7p$ schil te bevatten.

Het blijkt dat de grondtoestand een ${}^3\Phi_{2u}$ configuratie is, dit is niet in strijd met de laser ablatie spectroscopie metingen betreffende de verschuiving van de grondtoestand in de argon matrix. Door voor de eerste keer de $6d$ schil mee te nemen, is er een metastabiele 4_u toestand bestaande uit $5f^16d^1$ is gevonden rond 5,000 cm^{-1}, wat een geschikte kandidaat kan zijn voor de herinterpretatie van de oude IP metingen die de IP waarde onderschatten. De 4_g toestand ligt bij meer dan 10,000 cm^{-1}, wat een veel grotere waarde is dan bij voorgaande CASPT2+SOC en GAS-CI berekeningen. Dit geeft aan dat de 4_g niet als grondtoestand beschouwd kan worden als het molecuul ingevangen is in de argon matrix.

De toekenning van de aangeslagen toestanden bleek uitermate moeilijk te zijn, maar goede overeenkomst is gevonden tussen de berekeningen en het recente REMPI experiment, waarin experimentatoren voor het eerst het absorptie spectrum van het UO_2 hebben gemeten. Meer theoretisch werk is nodig om het effect van expliciet aan het UO_2 molecule gebonden Ar atomen te bestuderen. De IH-FSCC aanpak representeert een veelbelovende techniek om deze grotere systemen te analyseren, omdat het schaalt als N^6, net zoals een standaard CC aanpak, en nauwkeurige excitatie energieën oplevert.

In Hoofdstuk 5, is de IH-FSCC methode gebruikt om de spectroscopie te onderzoeken van NpO_2^+ en PuO_2^{2+} moleculen, welke isoelectronisch zijn aan UO_2. Theoretische pogingen om het experimentele absorptie spectrum van deze ionen in water te interpreteren zijn eerder gedaan met semi-empirische methoden, gevolgd door wat nauwkeurigere ab initio methoden. Deze berekeningen waren echter niet voldoende voor een kwantitatieve en onomstreden toekenning van de ordening en de uiteenligging van de overgangen.

De IHFSCC aanpak heeft bewezen een kost-effectieve en nauwkeurige methode te zijn om de laag liggende toestanden van deze ionen te berekenen. Met behulp van de IHFSCC berekeningen was het mogelijk te bepalen dat beide aanwezige ionen een 4_g grond toestand hebben en dat alle aangeslagen toestanden tot aan 20,000 cm^{-1} voortkomen uit excitaties binnen de $5f^2$ configuratie. Bovendien verbeteren

deze berekeningen de overeenkomst met het experiment in het gebied tussen 7,000 and 13,000 cm^{-1} aanzienlijk. De fouten zijn nu in de orde van 1,000-2,000 cm^{-1}, vergeleken met meer dan 10,000 cm^{-1} in voorgaande berekeningen.

Ondanks deze resultaten heeft de IHFSCC methode ook nadelen. Het kan bijvoorbeeld niet gebruikt worden op een 'black-box manier en, op het moment van schrijven, kan het niet gebruikt worden voor de berekening van hogere spin-toestanden dankzij implementatie problemen. Dus, meer applicaties en ontwikkeling zijn nodig om de betrouwbaarheid van de methode vast te stellen.

Deel II : DFT berekeningen aan systemen in water

Het uranyl ion kan beschouwd worden als een van de meest belangrijke moleculen in actinide chemie. Dit molecuul is zowel experimenteel vaak bestudeerd, vanwege zijn gebruik in het recycle proces van kernafval, als theoretisch, omdat het relatief eenvoudig is om de gesloten schil configuratie te beschrijven. Het oplossen van dit molecuul in water is de laatste jaren onderwerp van discussie geweest. Helaas, om verscheidene redenen, is er nog geen goede methode gevonden welke het coördinatie getal kan bepalen en korte-drachts interacties tussen het ion en de wateromgeving kan berekenen. Het doel van het tweede deel van het proefschrift is de bruikbaarheid testen van de QM/MM methode in het onderzoeken van opgeloste systemen, waarin het opgeloste beschreven wordt met behulp van een hoog-niveau benadering gebruik makend van DFT en de water omgeving (of een deel daarvan) door middel van klassieke methodes, zoals moleculaire mechanica.

In Hoofdstuk 6 hebben we de structuur van het tetrafluoroanylat ion $[UO_2F_4]^{2-}$ bestudeerd, welke opgelost in water een ongebruikelijke hepta-gecoördineerde structuur heeft, waarin het uranium atoom een extra binding vormt met een van de water moleculen. Geometrie optimalisaties zijn uitgevoerd met behulp van QM/MM, gebruik makend van verschillende gelaagdheid van de waterschil. Het beste compromis is gevonden door het tetrafluorouranylat ion en een water molecuul in het QM gebied te berekenen en the rest van het watercluster in het MM gebied. Analyse van de structurele parameters laat goed overeenkomsten zien met het experiment. De toename van het aantal water moleculen resulteert in een significante verandering van de U-O_{ax} en U-O_{H_2O} bindings afstanden. Het is aangetoond dat een volle eerste schil wordt gevormd door 11 water moleculen en dat een water cluster van slechts 3 moleculen, zoals gebruikt in ander werk, te klein is om zelfs kwalitatieve voorspellingen te doen.

Een meer kwantitatieve analyse van de ladingsoverdracht tussen het opgeloste molecuul en het oplosmiddel is verkregen door een volledige single point QM berekening op de geoptimaliseerde QM/MM structuur uit te voeren. Als een groot aantal

water moleculen wordt toegevoegd aan het systeem wordt het grootste gedeelte van de totale energie van het systeem bepaald door de water moleculen aan de buitenkant van de oplosmiddelschil. Dit is een serieuze beperking van dit model. Om dit probleem te omzeilen hebben we de totale energie beschouwd als de som van het QM gebied en de interactie energie van het opgeloste molecuul met het oplosmiddel. Er is gebruik gemaakt van een fragment decompositieschema om deze interactie energie op te delen in termen van sterische en orbitaal bijdragen. In de gasfase is de hexa gecoördineerde structuur $[UO_2F_4(H_2O)]^{2-}$ stabieler dan de hepta structuur, omdat de laatste een ongunstige electrostatische interactie met de wateromgeving vertoond, welke gereduceerd wordt door ladingsoverdracht in het opgeloste complex. Deze stabilisatie is dusdanig groot dat het hepta molecuul de meest stabiele configuratie wordt met 60 kJ/mol. In hoofdstuk 7, is het meer uitdagende tetrahydroxouranylat ion $[UO_2(OH)_4]^{2-}$ bestudeerd. In sterk basische omstandigheden geeft het EXAFS experiment aan dit molecuul een coördinatie getal met een onzekerheid van ± 1, wat niet afdoende is om een hexa $[UO_2(OH)_4]^{2-}$ of hepta $[UO_2(OH)_5]^{3-}$ structuur toe te kennen. Aangezien de basische omstandigheden moeilijk zijn te modelleren gebruik makend van een statische QM/MM benadering, zijn we nagegaan of de $[UO_2(OH)_4{\cdot}H_2O]^{2-}$ conformatie stabieler is dan het hexa tetrahydroxouranylat ion als een water molecuul wordt geïnserteerd tussen twee zuurstof atomen, omdat deze aanpak een uiterste representeert van het meer gecompliceerde $[UO_2(OH)_5]^{3-}$ geval, en de totale lading van het systeem niet verandert.

Dezelfde procedure die gebruikt is voor het tetrafluorouranylat ion is hier ook gebruikt, met het verschil dat het moeilijker is om een goede eerste en tweede schil voor zowel de hexa en hepta te beschrijven, omdat de aanwezigheid van de hydroxyl eenheden leidt tot veel meer configuraties. In de gasfase is de hexa conformatie stabieler dan de hepta conformatie, maar de Pauli repulsie tussen een water molecuul en het $[UO_2(OH)_4]^{2-}$ ion is veel groter dan in het $[UO_2F_4]^{2-}$ molecuul. Deze term is dusdanig sterk dat voor het hepta geval de gunstigere ladingsoverdracht vanuit het oplosmiddel niet voor een inversie van stabiliteit zorgt, en de hexa structuur de meest stabiele structuur in oplossing blijft. Met deze aanname is het hoogst onwaarschijnlijk dat in basische omstandigheden in het $[UO_2(OH)_4]^{2-}$ een extra hydroxide kan inserteren.

Een ander aspect van het $[UO_2(OH)_4]^{2-}$ molecuul is de grote ladingsoverdracht van de hydroxo-eenheden naar de niet-bindende $5f$ orbitalen gelokaliseerd op het minder positieve uranium atoom, en naar de anti-bindende $5f_\pi$ en $5f_\sigma$. Dit zorgt voor de vorming van een minder positieve lading op het actinide atoom en een sterkere

repulsie met de negatief geladen zuurstof atomen, wat resulteert in een toename van de U-O_{ax} bindingsafstand (1.88 Å) vergeleken met het kale uranyl ion (1.72 Å).

Een nadeel van dit QM/MM schema is dat slechts een paar configuraties van de water omgeving gekozen kunnen worden en dat een meer realistische modellering van het systeem gedaan kan worden door middel van moleculaire dynamica berekeningen. Vanwege technische redenen is deze aanpak in dit proefschrift niet uitgevoerd.

Acknowledgments

Shaun: As Bertrand Russell once said, "The only thing that will redeem mankind is cooperation". I think we can all appreciate the relevance of that now.
Liz: Was that written on a beer mat?
Shaun: Yeah, it was Guinness Extra Cold.
Liz: I won't say anything.
Shaun: Thanks.

from the movie Shaun of the Dead (1994)

In this space I would like to thank the people that have been involved directly and indirectly to the development of my research project.

Luuk, I am very grateful for the opportunity you have given me to study very intriguing and stimulating systems. Your knowledge and passion in this field of research have been valuable tools in helping me to grow scientifically. Your criticism and will of improvement has kept me in the right path, learning that research is about both the big picture and the tiny details. I will try to make mine this lesson in every moment of my scientific career. I am happy that we had also the possibility to spend some nice time outside the work environment, giving me the opportunity to meet your family. A deep thank also to Tineke, Bert, Klaas and Marika, your jewels.

Evert Jan, I would like to express my thanks for the chance to participate actively in one of the most influential Theoretical Chemistry group in the world. Thanks for reading critically the manuscript and for the freedom given to me in these four years of studies.

Joost, my nigga ! What can I say ? You certainly win the award for best officemate ever ! I deeply thank you for the friendship we have developed in these years,

hoping that we will keep it flourish in the coming years. I practically learned to bike during my time in Amsterdam, and thanks to you I could train constantly to climb the Alpe d'Huez in a reasonable time . Since there is always space for improvements, I challenge you on watching my back wheel, next time we bike on the Alpes. That's a promise ! I owe you my gratitude for the time we spent outside the office, and for learning new quotes from school of life movies. And when you have some doubts, remember... the Dude abides ! Thanks also for translating the Summary of this thesis to a Samenvatting and for being my paranimf at my defence.

Pina, grazie per essere un punto di riferimento costante degli ultimi quattro anni, come anche dei precedenti venti ! Non ho parole per esprimere la mia stima nei tuoi confronti e l'amicizia, che anche davanti a difficolta' evidenti come la distanza, trova sempre modo di rigenerarsi e trasformarsi in qualcosa di stabile e unico. Spero che gli anni a venire siano il massimo per te come persona e per la tua carriera scientifica, che sara' brillante, ne sono sicuro. Grazie anche per essere la mia paranimf. A big thank also to Arjan, for the nice time spent in Groningen, and in various conferences/schools.

André, when I think that we built such a nice friendship, I am always impressed that you come (almost) from the other side of the world, or more precisely, from the jungle, as you like to say (eheheheh). I have no doubts that light and deep conversations will keep going on also in the coming years. Thanks for the fruitful collaboration we had on the plutonyl/neptunyl paper, and I hope the article that came out was just the first of a long series. Thanks also for reading carefully the manuscript of my thesis and criticize it, when necessary.

Marc, without you the atmosphere at work would be less energizing. The funny moments and talks about lighthearted subjects during the breaks have been very valuable to cope more vigorously with the serious moments of my research. I will not forget the football matches we have seen together, with reciprocal respect and interest in the technical details. I will for ever remember that piece of your couch in which I have seen Italy winning the World Cup. Thank you, man ! My gratitude also for the translation of the Summary into a Samenvatting. A big thank to Floor and Tammy too !

I would like to express my acknowledgment and admiration for the people I met in the yearly DIRAC meeting in Odense. Each year, it was an enjoyable time following Luuk's traditions. Ephraim Eliav, I feel honored to have the possibility to collaborate with you and learn the advantages and flaws (if any!) of the Fock-Space Coupled-Cluster method. I am glad that you are member of the committee at my promotion. I equivalently thank Uzi Kaldor. Trond Saue, I thank you very much for being a perfect

host during my short visit in Strasbourg. I hope to have one more opportunity to cook another dinner together. I am glad to thank also the other members of the group in Strasbourg: Hélèn, Sebastian and Radovan. Timo Fleig, thanks for the funny discussions during meetings and conferences. Your knowledge about music and football is stimulating. Moreover, I hope we have the opportunity to discuss more about the intrigues of the UO_2 molecule ! Hans Jørgen Jensen, thanks for the hospitality during the DIRAC meetings.

Belén, quién hubiera imaginado que, tras conocernos en la conferencia de Niza, podríamos iniciar una amistad tan bonita como la que nos une hoy? Sólo espero que podamos seguir siempre así, quizá con algún que otro fin de semana en la playa, donde se que recargas pilas! Muchas gracias también a el fricchettone Fernando, quien me ha acogido siempre en su casa ofreciéndome hospitalidad y buen humor todas y cada una de las veces que aparecí por Madrid. Un cariñoso saludo también para David! Luis Seijo, podríamos haber tenido más suerte con los projectos, pero gracias por enseñarme la palabra honestidad, por inculcarme su significado incluso cuando las circunstancias te tientan en otra dirección más fácil. Mi agradecimiento va también para Zoila.

Lennard, thanks for the nice and funny evening outside in Alkmaar and Utrecht. Especially, I will remember the hate and love "vacation" in France with Joost. I hope we will climb again another "Mountain of Hell" without getting off the bike, and I wish you to become like King Arnault, an example.

Marcello e Myrta, sono contento che voi siete stati la sponda italiana nel gruppo. In particolare, ringrazio Myrta per le volte che siamo usciti e incontrati in conferenze varie. Grazie anche per avermi ospitato a San Sebastian e mostrato la citta'. Marcello, grazie per il tempo di spensieratezza e divertimento che abbiamo passato durante i break sul lavoro. Grazie per avermi disegnato la copertina e un salutone a Cristina e al Pupi.

Daniel Irimia and Laura Lipciuc, thanks for enduring me as a flat-mate for about two years. Daniel, I will not forget the nights spent in the kitchen talking about football and computer issues.

Christoph, thanks for being a very good housemate in these last months and for reading carefully my manuscript.

Patricia, Johannes (for friends, Prof. Neugebauer), Xana, Laura Orian, Simon & Soizic, Daniel Rohr, Filippo, Kasia, Paul, I thank all of you for the beautiful time we have spent inside and outside the group. We talked about almost everything, I wish we can meet from time to time in some other places. You will always be my special

guests, wherever I will be. Daniel, thanks for introducing me to the DAM experience. I hope to participate some other time ! Theodoor, thanks for the political discussions we had, sometimes it's nice to talk about less important things ;) . Pier, thanks for the chats about all kind of sports. Manuel, thanks for the discussions about chemistry. Matthias, I owe you my gratitude for being member of the committee at my promotion.

Drew, thanks for the computer assistance and for cleaning up my english in this manuscript and other projects I have written.

Leonardo Belpassi, grazie per avermi coinvolto nei tuoi progetti di ricerca. Spero di poter cominciare una lunga collaborazione con te. Sono sontento dell'amicizia che e' nata e ti ringrazio dell'invito a visitare la tua famiglia a Perugia. Non manchero' di certo !

Paula van Berkum, you have my gratitude for being the best secretary ever. Without you, most of my administrative stuff would get lost somewhere in the Kafka's Castle. A special thank to Fu-Wei too !

I also thank Paola Gori-Giorgi, Paola Belanzoni, Emanuel Fromager, which have been part of the group for some time.

Bas, thanks for the funny chats we had in the office and for the help in one of the articles. Two van Stralens are better than one, but more it is quite dangerous !!

I also thank the rest of the TC group. I do not try to write all the names, because if I miss someone I will be feeling guilty. But thanks to let me integrate rather easily.

Un ringraziamento speciale al Prof. Lelj, un supporto costante negli ultimi anni, sempre pronto ad una pizza al nostro rientro, nonostante gli impegni. Un grazie anche a Mario e ai suoi famosi dubbi del venerdi.

Ringrazio Guido per la fondamentale amicizia a distanze e alle chat su msn. Un saluto anche a Francesco, Mimmo, Gigia e alle famiglie di Guido e Pina (Maria, ti mando un ciaua).

Ho iniziato la tesi con una sola nipotina, Yasmin, e l'ho finita con tre, con l'aggiunta del piccolo Igor Jr. e la pacioccona Amira. Pertanto, un ringraziamento speciale alla mia famiglia, che non ha mai fatto mancare li suo supporto.

List of Publications

This thesis is a collection of the results achieved during my PhD studies at the Department of Theoretical Chemistry of the Vrije Universiteit Amsterdam. Only the published (or soon to be published) articles related to this thesis are listed.

I. Infante, L. Visscher
"QM/MM study of aqueous solvation of the uranyl fluoride $[UO_2F_4]^{2-}$ complex"
J. Comp. Chem., 25(3), 386-392, 2004

I. Infante, L. Visscher
"The importance of spin-orbit coupling and electron correlation in the rationalization of the ground state of the CUO molecule"
J. Chem. Phys., 121(12), 5783-5788, 2004

I. Infante, B. van Stralen, L. Visscher
"A QM/MM study on the aqueous solvation of the tetrahydroxouranylate $[UO_2(OH)_4]^{2-}$ complex ion"
J. Comp. Chem., 27(11), 1156-1162, 2006

I. Infante, A.S.P. Gomes, L. Visscher
"On the Performance of the Intermediate Hamiltonian Fock-Space Coupled–Cluster Method on Linear Triatomic Molecules: the Electronic Spectra of NpO_2^+, NpO_2^{2+} and PuO_2^{2+}"
accepted for publication on the J. Chem. Phys.

I. Infante, E. Eliav, L. Visscher, U. Kaldor
"The electronic structure of UO_2 revisited"
submitted to the J.Chem.Phys

BIBLIOGRAPHY

[1] D. Mukherjee and S. Pal, *Use of Cluster Expansion Methods in the Open–Shell Correlation Problem*, Academic Press, 1989.

[2] R. D. Hunt and L. Andrews, *J. Chem. Phys.*, **98**, 3690 (1993).

[3] R. G. Cochran and N. Tsoulfandis, *The Nuclear Fuel Cycle: Analysis and Managment*, American Nuclear Society, La Grange Park, IL, 1999.

[4] D. Bodansky, *Nuclear Energy: Principles, Practices and Prospects*, Springler-Verlag, New York, 2004.

[5] J. Burns, *Inorg. Chem.*, **22**, 1174 (1983).

[6] E. P. Horwitz, D. G. Kalina, H. Diamond, G. F. Vandegrift, and W. W. Schulz, *Solvent Extr. Ion Exch.*, **3**(1-2), 75 (1985).

[7] C. Madic, P. Blanc, N. Condamines, P. Baron, L. Berthon, C. Nicol, C. Pozo, M. Lecomte, M. Philippe, M. Masson, C. Hequet, and M. J. Hudson, *Actinide Partitioning from HLLW using the DIAMEX process*, 4th International Conference Nuclear Fuel Reprocessing and Waste Management, Record94, London, 1994.

[8] C. Hill, X. Heres, J. N. Calor, K. Romer, B. Guilanneux, B. Mauborgne, P. Rivalier, and P. Baron, *Trivalent actinides / lanthanides separation using bistrianyl-pyridines*, GLOBAL99, Jackson Hole, Wyoming, USA, 1999.

[9] C. Clavaguera-Sarrio, V. Brenner, S. Hoyau, C. Marsden, P. Millie, and D. J.P., *J. Phys. Chem. B*, **107**, 3051 (2003).

[10] S. Spencer, L. Gagliardi, N. C. Handy, A. G. Ioannou, C. K. Skylaris, A. Willetts, and A. M. Simper, *J. Phys. Chem. A*, **103**, 1831 (1999).

[11] V. Vallet, U. Wahlgren, B. Schimmelpfennig, Z. Szabo, and I. Grenthe, *J. Am. Chem. Soc.*, **123**, 11999 (2001).

[12] A. A. Michelson and E. W. Morley, *Am. J. Sci.*, **134**, 33 (1887).

[13] E. Schrödinger, *Ann. Physik*, **81**, 109 (1926).

[14] O. Klein, *Z. Physik*, **41**, 407 (1927).

[15] W. Gordon, *Z. Physik*, **40**, 117 (1926).

[16] W. Gordon, *Z. Physik*, **50**, 630 (1928).

[17] P. A. M. Dirac, *Proc. Roy. Soc. (London)*, **A117**, 610 (1928).

[18] P. A. M. Dirac, *Proc. Roy. Soc. (London)*, **A118**, 351 (1928).

[19] P. A. M. Dirac, *The Principles of Quantum Mechanics*, Clarendon Press, Oxford, 1958.

[20] P. A. M. Dirac, *Proc. Roy. Soc. (London)*, **A126**, 360 (1929).

[21] H. M. Quiney, H. Skaane, and I. P. Grant, *Adv. Quant. Chem.*, **32**, 1 (1999).

[22] J. Sapirstein, *Phys. Scr.*, **36**, 801 (1987).

[23] M. E. Rose, *Relativistic Electron Theory*, John Wiley, New York, 1961.

[24] L. Visscher and K. G. Dyall, *Atom. Data Nucl. Data Tabl.*, **67**, 207 (1997).

[25] M. Born and R. Oppenheimer, *Ann. Physik*, **84**, 457 (1927).

[26] J. A. Gaunt, *Proc. Roy. Soc. (London)*, **A122**, 513 (1929).

[27] T. Helgaker, P. Jørgensen, and J. Olsen, *Molecular Electronic Structure Theory*, Wiley, Chichester, 2000.

[28] J. D. Talman, *Phys. Rev. Lett.*, **57**, 10914 (1986).

[29] L. LaJohn and J. D. Talman, *Chem. Phys. Lett.*, **189**, 383 (1992).

[30] C. C. J. Roothaan, *Rev. Mod. Phys.*, **32**, 179 (1960).

[31] H. M. Quiney, I. Grant, and S. Wilson, *J. Phys. B - Atom. Mol. Opt. Phys.*, **20**, 1413 (1987).

[32] L. Visscher PhD thesis, Rijksuniversiteit Groningen, (1993).

[33] T. Saue, K. Fægri, Jr., T. Helgaker, and O. Gropen, *Mol. Phys.*, **91**, 937 (1997).

[34] T. Saue PhD thesis, University of Oslo, (1996).

[35] R. McWeeny, *Methods of molecular quantum mechanics,* 2nd edition, Academic Press, London, 1989.

[36] J. Thyssen PhD thesis, University of Southern Denmark, (2001).

[37] H. A. Bethe and E. E. Salpeter, *Quantum Mechanics of One- and Two-electron atoms*, Springer, Berlin, 1957.

[38] C. J. Bradley and A. P. Cracknell, *The mathematical theory of symmetries in solids*, Clarendon Press, Oxford, 1972.

[39] T. Saue and H. J. A. Jensen, *J. Chem. Phys.*, **111**, 6211 (1999).

[40] I. P. Grant and H. M. Quiney, *Adv. Phys.*, **19**, 747 (1970).

[41] R. E. Stanton and S. Havrilak, *J. Chem. Phys.*, **81**, 1910 (1984).

[42] K. G. Dyall, I. P. Grant, and S. Wilson, *J. Phys. B*, **17**, 493 (1984).

[43] K. G. Dyall and K. Faegri, *Introduction to Relativistic Quantum Chemistry.*

[44] L. Visscher, *Theor. Chem. Acc.*, **98**, 68 (1997).

[45] G. T. de Jong and L. Visscher, *Theor. Chem. Acc.*, **107**, 304 (2002).

[46] K. G. Dyall, *J. Chem. Phys.*, **100**, 2118 (1994).

[47] J. M. Lévy-Leblond, *Commun. Math. Phys.*, **6**, 286 (1967).

[48] T. Saue, T. Enevoldsen, T. Helgaker, H. J. A. Jensen, J. K. Laerdahl, K. Ruud, J. Thyssen, and L. Visscher, Dirac04, a relativistic ab initio electronic structure program, release 4.1, 2000.

[49] M. Dolg In *Relativistic Electronic Structure Theory – Part 1: Fundamentals*, P. Schwerdtfeger, Ed.; Elsevier, Amsterdam, 2002; page 793.

[50] M. Douglas and N. M. Kroll, *Ann. Phys.*, **82**, 89 (1974).

[51] B. A. Hess, *Phys. Rev. A*, **33**, 3742 (1986).

[52] B. A. Hess, *Phys. Rev. A*, **32**, 756 (1985).

[53] C. Chang, M. Pelissier, and P. Durand, *Phys. Scr.*, **34**, 394 (1986).

[54] E. van Lenthe, E. Baerends, and J. Snijders, *J. Chem. Phys.*, **99**, 4597 (1993).

[55] E. van Lenthe, E. Baerends, and J. Snijders, *J.Chem. Phys.*, **101**(11), 9783 (1994).

[56] E. van Lenthe, A. Ehlers, and E. Baerends, *J. Chem. Phys.*, **110**, 8943 (1999).

[57] E. van Lenthe, J. Snijders, and E. Baerends, *J. Chem. Phys.*, **105**(15), 6505 (1996).

[58] L. L. Foldy and S. A. Wouthuysen, *Phys. Rev.*, **78**, 29 (1950).

[59] A. Szabo and N. S. Ostlund, *Modern Quantum Chemistry*, McGraw-Hill, New York, 1989.

[60] B. O. Roos and P.-O. Widmark, *European Summerschool in Quantum Chemistry 2003*, Lund University, Lund, 2003.

[61] P. E. M. Siegbahn In *Methods in Computational Molecular Physics*, G. H. F. Diercksen and S. Wilson, Eds.; Reidel, 1982.

[62] R. J. Bartlett, *Ann. Rev. Phys. Chem.*, **32**, 359 (1981).

[63] J. K. Laerdahl, T. Saue, and K. Fægri, Jr., *Theor. Chem. Acc.*, **97**, 177 (1997).

[64] J. N. P. van Stralen, L. Visscher, C. V. Larsen, and H. J. A. Jensen, *Chem. Phys.*, **311**, 81 (2005).

[65] J. N. P. van Stralen PhD thesis, Vrije Universiteit Amsterdam, (2004).

[66] B. O. Roos, P. R. Taylor, and E. M. Siegbahn, *Chem. Phys.*, **48**, 157 (1980).

[67] J. Olsen, B. O. Roos, P. Jørgensen, and H. J. A. Jensen, *J. Chem. Phys.*, **89**, 2185 (1988).

[68] K. Andersson, P.-A. Malmqvist, B. O. Roos, A. J. Sadlej, and K. Wolinski, *J. Phys. Chem.*, **94**, 5483 (1990).

[69] K. Andersson, P.-A. Malmqvist, and Roos, *J. Chem. Phys.*, **96**, 1218 (1992).

[70] K. Raghavachari, G. W. Trucks, and J. A. Pople, *Chem. Phys. Lett.*, **157**, 479 (1989).

[71] H. Koch, O. Christiansen, R. Kobayashi, P. Jørgensen, and T. Helgaker, *Chem. Phys. Lett.*, **228**, 233 (1994).

[72] A. Koch, H.and Sanchez de Meras, T. Helgaker, and O. Christiansen, *J. Chem. Phys.*, **104**, 4157 (1996).

[73] L. Visscher, T. J. Lee, and K. G. Dyall, *J. Chem. Phys.*, **105**, 8769 (1996).

[74] L. Visscher, *J. Comp. Chem.*, **23**, 759 (2002).

[75] M. Pernpointner and L. Visscher, *J. Comp. Chem.*, **24**, 754 (2003).

[76] E. Ilyabaev and U. Kaldor, *Chem. Phys. Lett.*, **194**, 95 (1992).

[77] E. Ilyabaev and U. Kaldor, *Phys. Rev. A*, **47**, 137 (1993).

[78] E. Eliav, U. Kaldor, and Y. Ishikawa, *Phys. Rev. A*, **50**, 1121 (1994).

[79] U. Kaldor, E. Eliav, and A. Landau In *Relativistic Electronic Structure Theory – Part 1: Fundamentals*, P. Schwerdtfeger, Ed.; Elsevier, Amsterdam, 2002.

[80] I. Lindgren and J. Morrison, *Atomic Many-Body Theory*, Springer Series in Chemical Physics: vol. 13, Berlin, 1982.

[81] J. P. Malrieu, P. Durand, and J. P. Daudey, *J. Phys. A*, **18**, 809 (1985).

[82] A. Landau, E. Eliav, and U. Kaldor, *Chem. Phys. Lett.*, **313**, 399 (1999).

[83] A. Landau, E. Eliav, Y. Ishikawa, and U. Kaldor, *J. Chem. Phys.*, **113**, 9905 (2000).

[84] A. Landau, E. Eliav, Y. Ishikawa, and U. Kaldor, *J. Chem. Phys.*, **115**, 6862 (2001).

[85] A. Landau, E. Eliav, Y. Ishikawa, and U. Kaldor, *J. Chem. Phys.*, **121**, 6634 (2004).

[86] P. Hohenberg and W. Kohn, *Phys. Rev. B*, **136**, 864 (1964).

[87] A. K. Rajagopal, *J. Phys. C*, **11**, 943 (1978).

[88] A. H. Mac Donald and S. H. Vosko, *J. Comp. Chem.*, **23**, 814 (2002).

[89] E. Engel, H. Muller, C. Speicher, and R. M. Dreizler In *Density Functional Theory*, E. K. U. Gross and R. M. Dreizler, Eds.; Plenum Press, New York, 1995.

[90] W. Kohn and L. J. Sham, *Phys. Rev. A*, **140**, 1133 (1965).

[91] S. H. Vosko, L. Wilk, and M. Nusair, *Can. J. Phys.*, **58**, 1200 (1980).

[92] A. D. Becke, *Phys. Rev. A*, **38**, 3098 (1988).

[93] C. T. Lee, W. T. Yang, and R. G. Parr, *Phys. Rev. B.*, **37**, 785 (1988).

[94] J. P. Perdew and Y. Wang, *Phys. Rev. B.*, **33**, 8800 (1986).

[95] J. P. Perdew, *Phys. Rev. B*, **33**, 8822 (1986).

[96] J. P. Perdew, K. Burke, and M. Ernzerhof, *Phys. Rev. Lett.*, **77**(18), 3865 (1996).

[97] A. D. Becke, *J. Chem. Phys.*, **98**, 1372 (1993).

[98] A. Klamt, *J. Phys. Chem.*, **99**(7), 2224 (1995).

[99] A. Klamt, *J. Phys. Chem.*, **100**(9), 3349 (1996).

[100] A. Klamt and V. Jonas, *J. Chem. Phys.*, **105**(22), 9972 (1996).

[101] R. Car and M. Parrinello, *Phys. Rev. Lett.*, **55**, 2471 (1985).

[102] T. A. Wesolowski and A. Warshel, *J. Phys. Chem.*, **97**, 8050 (1993).

[103] J. Neugebauer, M. J. Louwerse, E. J. Baerends, and T. A. Wesolowski, *J. Chem. Phys.*, **122**, 094115 (2005).

[104] J. Neugebauer, Ch. R. Jacob, T. A. Wesolowski, and E. J. Baerends, *J. Phys. Chem. A*, **109**, 7805 (2005).

[105] Ch. R. Jacob, T. A. Wesolowski, and L. Visscher, *J. Chem. Phys.*, **123**, 174104 (2005).

[106] T. Woo, L. Cavallo, and T. Ziegler, *Theo. Chem. Acc.*, **100**, 307 (1998).

[107] W. Cornell et al, *J. Am. Chem. Soc.*, **117**, 5179 (1995).

[108] R. M. Badger, *J. Comp. Phys.*, **2**, 2128 (1934).

[109] M. Swart, P. van Duijnen, and J. Snijders, *J. Comp. Chem.*, **22**, 79 (2001).

[110] M. F. Zhou, L. Andrews, J. Li, and B. E. Bursten, *J. Am. Chem. Soc.*, **121**(41), 9712 (1999).

[111] L. Andrews, M. F. Zhou, B. Y. Liang, J. Li, and B. E. Bursten, *J. Am. Chem. Soc.*, **122**, 11440 (2000).

[112] B. Y. Liang, L. Andrews, J. Li, and B. E. Bursten, *J. Am. Chem. Soc.*, **124**(31), 9016 (2002).

[113] J. Li, B. E. Bursten, B. Y. Liang, and L. Andrews, *Science*, **295**(5563), 2242 (2002).

[114] L. Andrews, B. Y. Liang, J. Li, and B. E. Bursten, *New J. Chem.*, **28**(2), 289 (2004).

[115] L. Andrews, B. Y. Liang, J. Li, and B. E. Bursten, *J. Am. Chem. Soc.*, **125**(10), 3126 (2003).

[116] B. E. Bursten, J. Li, B. Y. Liang, and L. Andrews, *Abstracts of Papers - Am. Chem. Soc.*, **226**, U721 (2003).

[117] B. O. Roos, P. O. Widmark, and L. Gagliardi, *Farad. Discus.*, **124**, 57 (2003).

[118] L. Visscher, E. Eliav, and U. Kaldor, *J. Chem. Phys.*, **115**, 9720 (2001).

[119] C. F. Guerra, J. Snijders, G. te Velde, and E. J. Baerends, *Theo. Chem. Acc.*, **99**, 391 (1998).

[120] G. te Velde, F. M. Bickelhaupt, E. J. Baerends, C. Fonseca Guerra, S. J. A. van Gisbergen, J. G. Snijders, and T. Ziegler, *J. Comp. Chem.*, **22**(9), 931 (2001).

[121] L. Visscher and T. Saue, *J. Chem. Phys.*, **113** (2000).

[122] T. H. Dunning, *J. Chem. Phys.*, **90**(2), 1007 (1989).

[123] A. K. Wilson, D. E. Woon, K. A. Peterson, and T. H. Dunning, *J. Chem. Phys.*, **110**(16), 7667 (1999).

[124] D. E. Woon and T. H. Dunning, *J. Chem. Phys.*, **98**(2), 1358 (1993).

[125] W. A. de Jong, L. Visscher, and W. C. Nieuwpoort, *J. Mol. Struct.*, **458**(1-2), 41 (1999).

[126] K. Faegri, *Chem. Phys.*, **311**(1-2), 25 (2005).

[127] J. P. Perdew, J. A. Chevary, S. H. Vosko, K. A. Jackson, M. R. Pederson, D. J. Singh, and C. Fiolhais, *Phys. Rev. B*, **46**(11), 6671 (1992).

[128] M. E. Casida, *Recent Advances in Density Functional Methods*, World Scientific, Singapore, 1995.

[129] L. Andrews, B. Y. Liang, J. Li, and B. E. Bursten, *Angew. Chem. Int. Ed.*, **39**(24), 4565 (2000).

[130] Y. Zhang and W. Yang, *Phys. Rev. Lett.*, **80**, 890 (1998).

[131] A. D. Boese and N. C. Handy, *J. Chm. Phys.*, **114**, 5497 (2001).

[132] A. D. Boese, N. L. Doltsinis, N. C. Handy, and M. Sprik, *J. Chm. Phys.*, **112**, 1670 (2000).

[133] F. A. Hamprecht, A. J. Cohen, D. J. Tozer, and N. C. Handy, *J. Chm. Phys.*, **109**, 6264 (1998).

[134] F. Capone, Y. Colle, J. P. Hiernaut, and C. Ronchi, *J. Phys. Chem. A*, **103**(50), 10899 (1999).

[135] M. F. Zhou, L. Andrews, N. Ismail, and C. Marsden, *J. Phys. Chem. A*, **104**(23), 5495 (2000).

[136] L. Gagliardi, B. O. Roos, P. A. Malmqvist, and J. M. Dyke, *J. Phys. Chem. A*, **105**(46), 10602 (2001).

[137] J. D. Han, V. Goncharov, L. A. Kaledin, A. V. Komissarov, and M. C. Heaven, *J. Chem. Phys.*, **120**(11), 5155 (2004).

[138] B. Y. Liang, L. Andrews, J. Li, and B. E. Bursten, *Chem. Eur. J.*, **9**(19), 4781 (2003).

[139] B. Y. Liang, L. Andrews, J. Li, and B. E. Bursten, *Inorg. Chem.*, **43**(3), 882 (2004).

[140] J. Li, B. E. Bursten, L. Andrews, and C. J. Marsden, *J. Am. Chem. Soc.*, **126**(11), 3424 (2004).

[141] L. A. Gagliardi and B. O. Roos, *Chem. Phys. Lett.*, **331**(2-4), 229 (2000).

[142] L. Gagliardi, M. C. Heaven, J. W. Krogh, and B. O. Roos, *J. Am. Chem. Soc.*, **127**(1), 86 (2005).

[143] I. Infante and L. Visscher, *J. Chem. Phys.*, **121**(12), 5783 (2004).

[144] V. Vallet, *Very Heavy Metal 2006 (VHM2006) Conference*, 2006.

[145] M. Zhou, L. Andrews, N. Ismail, and C. Marsden, *J. Phys. Chem. A*, **104**, 5495 (2000).

[146] J. D. Han, L. A. Kaledin, V. Goncharov, A. V. Komissarov, and M. C. Heaven, *J. Am. Chem. Soc.*, **125**(24), 7176 (2003).

[147] M. C. Heaven, V. Goncharov, J. D. Han, and L. Kaledin, *Abstracts of Papers - Am. Chem. Soc.*, **227**, U319 (2004).

[148] C. J. Lue, J. J., M. J. Ortiz, J. C. Rienstra-Kiracofe, and M. Heaven, *J. Am. Chem. Soc.*, **126**, 1812 (2004).

[149] Q. Chang, *Master Thesis, Ohio State University* (2002).

[150] T. Fleig, H. J. A. Jensen, J. Olsen, and L. Visscher, *J. Chem. Phys.*, **124**, 104106 (2006).

[151] A. Landau, E. Eliav, and U. Kaldor, *Int. J. Mod Phys B*, **17**(28), 5335 (2003).

[152] K. G. Dyall, *J. Chem. Phys.*, **100**, 2118 (1994).

[153] L. Visscher, K. G. Dyall, and T. J. Lee, *Int. J. Quantum Chem*, **29**, 411 (1995).

[154] E. Eliav, M. J. Vilkas, Y. Ishikawa, and U. Kaldor, *J. Chem. Phys.*, **122**, 224113 (2005).

[155] T. Koren, E. Eliav, Y. Ishikawa, and U. Kaldor, *Theochem in press* (2006).

[156] D. Majumdar, K. Balusubramanian, and H. Nitsche, *Chem. Phys. Lett.*, **361**, 143 (2002).

[157] H. H. Cornehl, C. Heinemann, J. Marcalo, A. P. de Matos, and H. Schwarz, *Angew. Chem.*, **108**, 950 (1996).

[158] S. D. Gabelnick, G. T. Reedy, and M. G. Chasanov, *Chem. Phys. Lett.*, **19**, 90 (1973).

[159] K. L. Nash, *Solvent Extr. Ion Exch.*, **11**, 729 (1993).

[160] K. L. Nash, R. E. Barrans, R. Chiarizia, M. L. Dietz, M. Jensen, and P. G. Rickert, *Solvent Extr. Ion Exch.*, **18**, 605 (2000).

[161] N. C. Rasmussen, *Technologies for separations and transmutations*, National Academy Press, Washington, 1996.

[162] J. P. Bladeau, S. A. Zygmunt, L. A. Curtiss, D. T. Reed, and B. E. Bursten, *Chem. Phys. Lett.*, **310**, 347 (1999).

[163] S. Matsika and R. M. Pitzer, *J. Phys. Chem. A*, **104**, 4064 (2000).

[164] S. Matsika, Z. Zhang, S. R. Brozell, J. P. Bladeau, and R. M. Pitzer, *J. Phys. Chem. A*, **105**, 3825 (2001).

[165] C. Clavaguera-Sarrio, V. Vallet, D. Maynau, and C. J. Marsden, *J. Chem. Phys.*, **121**, 5312 (2004).

[166] M. Musial, L. Meissner, S. A. Kucharski, and R. J. Bartlett, *J. Chem. Phys.*, **122**, 224110 (2005).

[167] O. Visser, P. J. C. Aerts, D. Hegarty, and W. C. Nieuwpoort, *Chem. Phys. Lett.*, **134**, 34 (1987).

[168] J. P. Descalaux, *Atomic Data Nuclear Data Tables*, **12**, 311 (1973).

[169] I. Infante, E. Eliav, L. Visscher, and U. Kaldor, *to be published.*

[170] K. G. Dyall, *in preparation. Basis sets are available from the DIRAC website, http://dirac.chem.sdu.dk.*

[171] S. Matsika, R. M. Pitzer, and D. T. Reed, *J. Phys. Chem. A*, **104**, 11983 (2000).

[172] D. Cohen and B. Taylor, *J. Inorg. Nucl. Chem.*, **22**, 151 (1962).

[173] H. A. C. McKay, J. S. Nairn, and M. B. Waldron, *J. Inorg. Nucl. Chem.*, **7**, 167 (1958).

[174] R. G. Denning, J. O. Norris, and W. Brown, *Mol. Phys.*, **46**, 325 (1982).

[175] R. G. Denning, J. O. Norris, and W. Brown, *Mol. Phys.*, **46**, 287 (1982).

[176] J. C. Eisenstein and M. H. L. Pryce, *J. Res. Nat. Bur. Stand. - A.*, **70**, 165 (1966).

[177] J. C. Eisenstein and M. H. L. Pryce, *Proc. Roy. Soc. A*, **229**, 20 (1965).

[178] J. C. Eisenstein and M. H. L. Pryce, *J. Res. Nat. Bur. Stand. - A.*, **69**, 217 (1965).

[179] *Gmelin Handbooks of Inorganic Chemistry, Transuranium Elements, A2, 8th ed.*, 1973.

[180] R. Sjoblom and J. C. Hindman, *J. Am. Chem. Soc.*, **73**, 1744 (1951).

[181] W. C. Waggener, *J. Phys. Chem.*, **62**, 382 (1958).

[182] T. W. Newton and F. B. Baker, *J. Phys. Chem.*, **61**, 934 (1957).

[183] R. H. Betts and B. G. Harvey, *J. Chem. Phys.*, **16**, 1089 (1948).

[184] L. Maron, T. Leininger, B. Schimmelpfennig, V. Vallet, J. L. Heully, C. Teichteil, O. Gropen, and U. Wahlgren, *Chem. Phys.*, **244**, 195 (1999).

[185] G. S. Groenewold, A. K. Gianotto, K. C. Cossel, M. J. van Stipdonk, D. T. Moore, N. Polfer, J. Oomens, W. de Jong, and V. L, *J. Am. Chem. Soc.*, **128**, 4802 (2006).

[186] C. Madic, G. M. Begun, D. E. Hobart, and R. L. Hahn, *Inorg. Chem.*, **23**, 1914 (1984).

[187] F. A. Cotton, C. A. Wilkinson, and M. Bochmann, *Advanced Inorganic Chemistry*, Wiley, New York, 1999.

[188] P. Schwerdtfeger, *Relativistic Electronic Structure Theory – Part 1: Fundamentals*, Elsevier, Amsterdam, 2002.

[189] P. Schwerdtfeger, *Relativistic Electronic Structure Theory – Part 2: Applications*, Elsevier, Amsterdam, 2004.

[190] B. Allard, U. Olofsson, and B. Torstenfelt, *Inorg. Chim. Acta*, **94**, 205 (1984).

[191] K. N. Raymond, G. E. Freeman, and M. J. Kappel, *Inorg. Chim. Acta*, **94**, 193 (1984).

[192] H. Eccles, *Solv. Extr. Ion. Exch.*, **18**, 633 (2000).

[193] D. L. Clark, S. D. Conradson, R. J. Donohoe, D. W. Keogh, D. E. Morris, P. D. Palmer, R. D. Rogers, and C. D. Tait, *Inorg. Chem.*, **38**(7), 1456 (1999).

[194] L. Gagliardi and B. O. Roos, *Chem. Phys. Lett.*, **331**, 229 (2000).

[195] E. M. van Wezenbeek, E. J. Baerends, and J. G. Snijders, *Theor. Chim. Acta*, **81**, 139 (1991).

[196] R. G. Denning, *Struct. Bond.*, **79**, 215 (1992).

[197] K. Tatsumi and R. Hoffmann, *Inorg. Chem.*, **19**, 2656 (1980).

[198] W. R. Wadt, *J. Am. Chem. Soc.*, **103**, 6053 (1981).

[199] G. Schreckenbach, J. Hay, and R. Martin, *Inorg. Chem.*, **37**, 4442 (1998).

[200] G. Schreckenbach, J. Hay, and R. Martin, *Comp. Chem.*, **20**, 70 (1999).

[201] V. Vallet, U. Wahlgren, B. Schimmelpfennig, H. Moll, Z. Szabo, and I. Grenthe, *Inorg. Chem.*, **40**, 3516 (2001).

[202] R. G. Parr and W. Yang, *Density-Functional Theory of Atoms and Molecules*, Oxford University Press, Oxford, 1989.

[203] J. P. Perdew, J. A. Chevary, S. H. Vosko, K. A. Jackson, M. R. Pederson, D. J. Singh, and C. Fiolhais, *Phys. Rev. B*, **46**(11), 6671 (1992).

[204] J. C. Slater, *Quantum Theory of Molecular and Solids*, McGraw-Hill, New York, 1974.

[205] P. Guilbaud and G. J. Wipff, *J. Phys. Chem.*, **97**, 5685 (1993).

[206] T. Ziegler and A. Rauk, *Theo. Chim. Acta*, **46**(1), 1 (1977).

[207] T. Ziegler and A. Rauk, *Inorg. Chem.*, **18**(6), 1558 (1979).

[208] B. T. Thole and P. T. van Duijnen, *Theor. Chim. Acta*, **63**, 209 (1983).

[209] M. Baaden, M. Burgard, and G. Wipff, *J. Phys. Chem. B*, **105**(45), 11131 (2001).

[210] C. Clavaguera-Sarrio, V. Brenner, S. Hoyau, C. J. Marsden, P. Millie, and J. P. Dognon, *J. Phys. Chem. B*, **107**(13), 3051 (2003).

[211] M. Buhl, R. Diss, and G. Wipff, *J. Am. Chem. Soc.*, **127**(39), 13506 (2005).

[212] I. Infante and L. Visscher, *J. Comp. Chem.*, **25**(3), 386 (2004).

[213] C. Den Auwer, E. Simoni, S. Conradson, and C. Madic, *Eur. J. Inorg. Chem.*, (21), 3843 (2003).

[214] A. Navaza, F. Villain, and P. Charpin, *Polyhedron*, **3**(2), 143 (1984).

[215] B. Viossat, N. H. Dung, and C. Soye, *Acta Crystallogr., Sect. C: Cryst. Struct. Commun.*, **39**(MAY), 573 (1983).

[216] J. Toivonen and R. Laitinen, *Acta Crystallogr., Sect. C: Cryst. Struct. Commun.*, **40**(JAN), 7 (1984).

[217] J. L. Sonnenberg, P. J. Hay, R. L. Martin, and B. E. Bursten, *Inorg. Chem.*, **44**(7), 2255 (2005).

[218] U. Wahlgren, H. Moll, I. Grenthe, B. Schimmelpfennig, L. Maron, V. Vallet, and O. Gropen, *J. Phys. Chem. A*, **103**(41), 8257 (1999).

[219] A. Becke, *Phys. Rev. A*, **38**, 3098 (1988).

[220] C. F. Guerra, J. W. Handgraaf, E. J. Baerends, and F. M. Bickelhaupt, *J. Comp. Chem.*, **25**(2), 189 (2004).

[221] F. L. Hirshfeld, *Theor. Chim. Acta*, **44**, 129 (1977).

[222] *ADF2004.01*, SCM, Theoretical Chemistry Amsterdam, Vrije Universiteit, The Netherlands, http://www.scm.com.

[223] S. P. McGlynn, J. K. Smith, and W. C. Neely, *J. Chem. Phys.*, **35**(1), 105 (1961).

[224] W. A. de Jong, R. J. Harrison, J. A. Nichols, and D. A. Dixon, *Theor. Chem. Acc.*, **107**, 22 (2001).

[225] C. Kritayakornupong, K. Plankensteiner, and B. M. Rode, *J. Comput. Chem.*, **25**(13), 1576 (2004).